UNIVERSITY OF APPLIED SCIENCES ZURICH

DEPARTMENT OF LIFE SCIENCES AND FACILITY MANAGEMENT

INSTITUTE FOR ENVIRONMENT AND NATURAL RESOURCES

Incremental Capacity Analysis (ICA) as a diagnostic tool for the State of Health (SoH) estimation of second Life Batteries

Master Thesis

by
Kaja Mona Kristensen
Master in Environment and Natural Resources 2018
Submission date: 23.12.2020
Field of Study: Renewable Energies

Correction:

Prof. Jürg Rohrer

Leader of Research Group Renewable Energies

Zurich University of Applied Sciences (ZHAW)

CH - 8820 Wädenswil

Prof. Daniel-Ioan Stroe

Leader of Battery Storage Systems Research Program

Aalborg University (AAU)

DK – 9220 Aalborg

Life Sciences und Facility Management

IUNR Institut für Umwelt und Natürliche Ressourcen

This master thesis was conducted in an exchange semester in the Department of Energy Technology at Aalborg University as a completion of the Master education in Environment and Natural Resources at the University of applied science in Zurich. The project was proceeded as a single project between 09.08.2020 and 23.12.2020.
At this point, I would like to express my gratitude to my supervisor, Prof. Daniel-Ioan Stroe and Prof. Jürg Rohrer, for their valuable input and support during this project.

Keywords: Battery, Lithium-Titanate-Oxide (LTO), Second Life, State of health (SoH), Diagnostic tool, Remaining capacity, Incremental capacity analysis (ICA)

Citation:

Kristensen, K. (2021). Incremental Capacity Analysis (ICA) as a diagnostic tool for the State of Health (SoH) estimation of second Life Batteries [Master thesis]. Department of Energy Technology at Aalborg University (AAU) in Aalborg.

Faculty: Energy and Science

Energy Technology
Aalborg University
http://www.aau.dk

AALBORG UNIVERSITY

Title:
Incremental Capacity Analysis (ICA) as a diagnostic tool for the State of Health (SoH) estimation of Second Life Batteries

Theme:
Advanced Project in Electrical Power Systems and High Voltage Systems

Project Period:
Autumn Semester 2020

Project Group:
EPSH3-934

Participant:
Kaja Mona Kristensen

Supervisor:
Prof. Daniel-Ioan Stroe

Page Numbers: 79

Date of Completion:
December 23, 2020

Abstract:

The climate crisis has an impact on almost every sector in our life, including the transportation sector. A positive trend of electric vehicles could be registered. With the increase of electric vehicles, also the amount of lithium-ion batteries increased. Studies showed that the batteries are not free from environmental pollution, which is why it is proposed to keep the batteries as long as possible in use. In the transportation sector, batteries are declared to be at end of life (EoL) when they reach 80 % remaining capacity. Even though those batteries are no longer used in a vehicle, they could be used in a stationary application – as a so-called second life application. To design a second life application, the state of health (SoH) of the battery, in other words, the remaining capacity needs to be known, among other parameters. Today, the SoH is estimated by the car manufacturer or calculated by the car mechanic. So far, there is no commercialised procedure to estimate the SoH in a standardised way. Therefore, it is worthwhile to develop a procedure to estimate the remaining capacity of not only one, but multiple battery cells in a fast but nonetheless accurate way. This is where this master thesis takes up. With an experimental study including aged lithium-titanate-oxide (LTO) battery cells, it was tested whether a well-known and validated SoH estimation method could also be applied on batteries that already reached 80 % remaining capacity. This thesis also discusses the feasibility of real application and the possibility of reducing the application time by reducing the measurement interval.

Summary

The climate crisis has an impact on almost every sector in our life, including the transportation sector. A positive trend of electric vehicles could be registered. With the increase of electric vehicles, also the amount of lithium-ion batteries increased. Studies showed that the batteries are not free from environmental pollution, which is why it is proposed to keep the batteries as long as possible in use. In the trans-portation sector, batteries are declared to be at end of life (EoL) when they reach 80 % remaining capacity. Even though those batteries are no longer used in a vehicle, they could be used in a stationary application – as a so-called second life application. To design a second life application, the state of health (SoH) of the battery, in other words, the remaining capacity needs to be known, among other param-eters. Today, the SoH is estimated by the car manufacturer or calculated by the car mechanic. So far, there is no com-mercialised procedure to estimate the SoH in a standardised way. Therefore, it is worth-while to develop a procedure to estimate the remaining capacity of not only one, but multiple battery cells in a fast but nonetheless accurate way. This is where this master thesis takes up. With an experimental study including aged lithium-titanate-oxide (LTO) battery cells, it was tested whether a well-known and validated SoH estimation method could also be applied on batteries that already reached 80 % remaining capacity. This thesis also discusses the feasi-bility of real application and the possibility of reducing the application time by reducing the measure-ment interval.

The results of the study have shown that an application on aged batteries is possible. However, as the charging behaviour changes after falling below 80 % remaining capacity, the application range changes. Depending on the training of the ICA curve, accurate results could be obtained with a deviation of less than 5 %. In particular, the feature “peak location” gave a promising result. Nonetheless, only a partial charging curve was applied. However, it is rec-ommended, that further research should be conducted in order to define the ideal charging interval. Hence, the charging procedure could be reduced, which would save a lot of time.

Zusammenfassung

Auf Grund der Klimakriese treten in fast allen Sektoren Veränderungen auf, unter anderem auch im Mobilitätssektor. Es konnte ein Positivtrend in den Absatzzahlen der Elektroautos vermerkt werden, was die Dekarbonisierung in diesem Sektor begünstigt. Mit diesem Anstieg wuchs auch die Nachfrage an Lithium-Ionen-Batterien. Studien haben jedoch gezeigt, dass diese Batterien nicht ohne negative Umwelteinwirkungen daherkommen, weshalb empfohlen wird diese so lange wie möglich im Umlauf zu behalten. Die Mobilitätssektor deklariert Batterien ab 80 % Restkapazität als Batterien am Ender der Lebenszeit. Aber nur weil sie nicht mehr in der Mobilitätssektor eingesetzt werden können, bedeutet dies nicht, dass sie nicht in anderen Sektoren für einen zweiten Lebenszyklus eingesetzt werden können. Um einen solchen zweiten Lebenszyklus anzustreben, muss unter anderem der Zustand der Batterie und vor allem die restlich zur Verfügung stehende Kapazität bekannt sein. Aktuell wird die Lebensdauer vom Autohersteller geschätzt oder vom Automechaniker evaluiert. Es existiert noch kein Prozess, der den Zustand der Batteriezelle auf einem kommerzialisierten Weg erschliessen würde. Deshalb ist es von Interesse einen Prozess zu entwickeln, mit welchem eine schnelle und auch genaue Restkapazitätsbestimmung von mehreren Zellen ermitteln kann. An diesem Punkt setzt die Studentin mit dieser Masterarbeit an. Es wurde mit einer experimentellen Studie überprüft wie sich die bisher bekannten und validierten Methoden zur Ermittlung der Restkapazität verhalten, wenn sie bei gealterten Batterien angewendet werden. Die Studie wurde mit gealterten Lithium-Titanat-Oxide (LTO) Batterie durchgeführt.

Die Ergebnisse der Studie haben gezeigt, dass eine Anwendung an gealterten Batterien durchaus möglich ist, diese sich aber von der herkömmlichen Anwendung unterscheidet. Der Grund dafür ist, dass sich das Ladeverhalten verändert nach unterschreiten dieser 80 % Restkapazität und somit auch die ICA-Kurve. Je nach Training des ICA-Models, können mit einer Abweichung von weniger als 5 % auch weit unter 80 % Restkapazität genaue Resultate erzielt werden. Insbesondere das ICA-Merkmal «*peak location*» weisst in dieser Studie eine genaue Abschätzung auf, auch mit einer partiellen Ladekurve. Es wird jedoch empfohlen, dass weitere Forschung bei der Bestimmung des Ladeintervalls angesetzt werden. Somit könnte die Messung der notwendigen Informationen zur Durchführung der ICA-Methode verkürzt werden.

Table of content

List of Abbreviations 8
1 Introduction 9
1.1 The role of the battery to mitigate climate change 9
1.2 Second life concept 10
1.3 State of the art SoH estimation methods 12
1.4 Problem formulation and objectives 15
1.4.1 Scope and limitations of the project 15
1.5 Content of the Report 16
2 Basics about Batteries 17
2.1 Lithium-ion Batteries 17
2.2 Battery degradation 18
3 Material and Method 21
3.1 State of health (SoH) estimation method 21
3.1.1 Fundamentals 23
3.1.2 Incremental capacity (IC) feature as a State of health (SoH) indicator 24
3.2 Procedure to test the chosen SoH estimation method 26
3.3 Experimental Study 27
3.3.1 Overview 27
3.3.2 Battery cell under test 28
3.3.3 Experimental set-up 29
3.4 State of health (SoH) estimation algorithm 33
3.4.1 Overview 33
3.4.2 Incremental capacity (IC) algorithm in MATLAB 34
3.4.3 Model diagnostic 38
3.5 Model validation 40
4 Results and Discussion 41
4.1 Applying the incremental capacity (IC) algorithm on the output of the reference performance tests (RPT) 41
4.2 Model based on the incremental capacity (IC) algorithm 44
4.2.1 Model and model diagnostic 44
4.2.2 Validation of the model 45

4.2.3 Applicability of the method 46

5 Conclusion 47

5.1 Findings 47

5.2 Future work 48

Bibliography 49

List of Figures 54

List of Tables 55

Attachments 58

Attachment A: Declaration of plagiarism 58

Attachment B: Technical Data Sheets 59

Attachment C: Models according to the three scenarios 61

Attachment D: Model diagnostic 64

Attachment E: Model validation 73

Attachment F: Poster 79

List of Abbreviations

BAT	Best Available Technology
BoL	Begin of Life
C	Graphite
CC	Constant Current
C-rate	Current rate
CV	Constant Voltage
DoD	Depth of Discharge
DVA	Differential Voltage Analysis
ECHM	Electrochemical Model
ECM	Equivalent Circuit Model
EIS	Electrochemical Impedance Spectroscopy
EPR	Extended Producer Responsibility
EV	Electric Vehicle
FL	Fuzzy Logic
HPPC	Hybrid Pulse Power Characterisation
ICA	Incremental Capacity Analysis
IC	Incremental Capacity
KF	Kalman Filter
LCO	Lithium-Cobalt-Oxide
LFP	Lithium-Iron-Phosphate
LMO	Lithium-Manganese-Oxide
LNCA	Lithium-Nickel-Cobalt-Aluminum-Oxide
LNMC	Lithium-Nickel-Manganese-Cobalt-Oxide
LTO	Lithium-Titanate-Oxide
NMC	Nickel-Manganese-Cobalt
RPT	Reference Performance Test
SoC	State of Charge
SoH	State of Health

1 Introduction

1.1 The role of the battery to mitigate climate change

The energy sector is shifting towards renewable energies due to the climate crisis. A similar trend could also be seen in the transportation sector, which shifts towards electric mobility. In 2018 the transportation sector represented 30 % of the global, final energy consumption, being the biggest of all energy consumption sectors at that time (IEA, 2019b). In 2018 the global stock of electric passenger cars was about 5 million and recorded an increase of 63 % compared to 2017 (IEA, 2019a). Because of this increasing trend of electric vehicles (EV), batteries - especially lithium-ion batteries - face a positive trend, as shown in Figure 1. It can be seen that lithium-ion batteries (red) are not the market leader, but they register the highest market growth from 2015 to 18, as visualised with the steepness of the two arrows (Pillot, 2019).

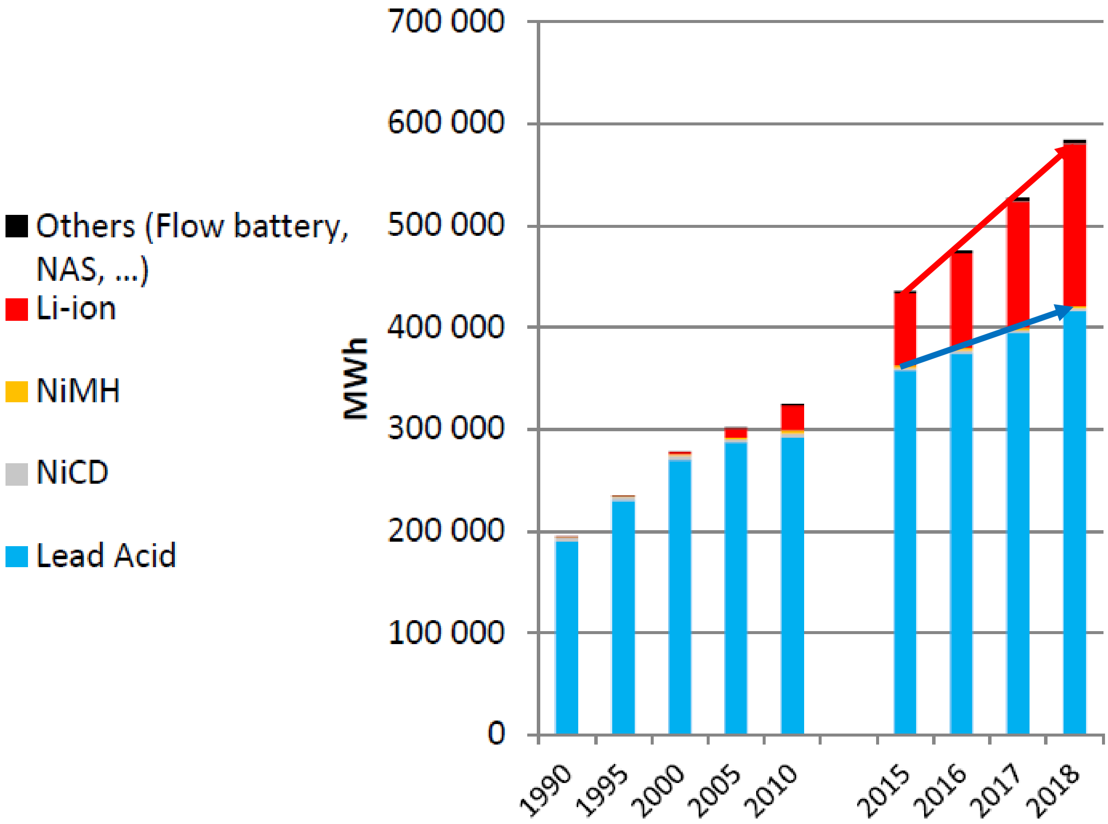

Figure 1 Market share of different battery types, where lithium-ions show the biggest market growth (Pillot, 2019). Lead Acid stands for Lead Acid batteries; NiCD stands for nickel-cadmium battery; NiMH stands for nickel-metal hybride battery; Li-ion stands for Lithium-ion batteries; others stands for all other batterie types as for example Flow batteries and NAS, which stands for Sodium-sulfur battery. The two arrows show the slope of the market growth.

As the importance of batteries in the transportation sector is increasing, it makes sense to take a closer look at the batteries' impact on the environment. According to Dai et al. (2019), the most severe environmental impacts over the whole life cycle are coming from the production of the active material of the positive electrode and the aluminium, as well as the energy use for the cell production. A long-term goal could be, to ensure that the cell factory produces with more renewable energy. But this does not solve the problem for the already produced battery cell. For them it would make sense, to ensure that the whole lifecycle of the battery is closed. The complete recycling of the lithium-ion batteries would technically already be possible, but is not proceeded, as it is economically not profitable. Also, with the increasing request of lithium-ion batteries, it is not expected to be in the near future. As lithium is richly distributed on earth, it is predicted that the mining of lithium is cheaper than recycling it from the batteries, as stated from Offenhalter D. (2019) and Wäger P. (2019). Therefore, expanding their life with a second purpose could be an appealing alternative, in order to reduce their environmental footprint (Stolz, 2019).

In the transportation sector, the battery end of life (EoL) is mostly defined at 80 % remaining capacity (Nagpure et al., 2011), as then the vehicle manufacturer cannot ensure the promised driving range anymore. To expand the lifetime of the batteries, a new purpose must be found. Either where a smaller range is required, or in another sector, where weight and size do not play an important role. The lack of capacity could then be compensated with the amount of batteries. One suitable sector for that could be the energy sector, as this sector is stationary and does not rely as much on weight and size of the battery as the transportation sector.

As mentioned before, there is an increase of renewable energies in the energy sector, due to the climate crisis. The production of renewable energy is weather dependent, which requires batteries to ensure that the produced energy can be used when needed. Because of that, these so-called second life batteries could contribute a part towards sustainable energy consumption (Sterner & Stadler, 2014, p. 619).

In addition, these waste batteries are subject to a directive from the European Parliament, which introduces the extended producer responsibility (EPR). This means that the producer or third parties, who act on their behalf, have to ensure that the waste batteries are being collected and disposed according to best available technology (BAT) in order to protect the health and the environment (DIRECTIVE 2006/66/EC, 2013). As the complete recycling of lithium-ion batteries is not state of the art yet, the question arises, what to do with those batteries, when there is no environmentally friendly solution? The 2030+ roadmap, a large scale European research initiative, founded by the European Union, proposes to apply this second life approach whenever possible in order to keep the battery as long as possible on the market. That way, there might be an environmentally friendly recycling process, when those second life batteries have to be disposed (Edström & Perraud, 2019).

1.2 Second life concept

The second life concept from Montoya-Bedoya et al, (2020) proposes to use the batteries which are declared to be at end of life in the transportation sector, in a stationary application. Figure 2 visualizes this concept, where 1) represents the first life of the battery. Based on the warranty - given by the manufacturer - or the information from the workshop, the vehicle owner decides, if he wants to replace the battery or not. As illustrated in 2), the old battery is going to be tested with a state of health (SoH) estimation method. For that, the battery is disassembled from the vehicle. The SoH value is an indication of the condition of the battery (Li et al., 2019). The estimation method is one among other tools, which enables to decide if the battery can be used in a second application 3a) or if the battery must be disposed 3b). Before the battery could be reused in the second life, it must be reassembled to fit the new requirements of the second life, as represented in 4). The second use phase is illustrated in 5). Some example for second life applications could be to support the grid stability, emergency power supply, provide uninterruptable power supplies or off-grid systems (Fischhaber et al., 2016). There are already prototypes of second life applications installed, for example *Sunbatt* in Spain, which is a living lab to study the behaviour of second life electric vehicle (EV) batteries (Canals Casals et al., 2018; *SUNBATT*, 2015) and *Second Life Battery* in Germany, which is a flexible energy storage system and ensures the grid stability (Hustadt, 2018). Collecting and processing of the second life batteries, after the use in the second life, is represented in 6). The disposal of the battery is illustrated as the recycling of the raw materials in 7). One important role in this second life process is the SoH estimation, as accentuated in Figure 2. It helps to decide, whether a battery could be used for a second purpose or if it must be scrapped. However, it must be mentioned, that there are also other aspects which have to be considered, besides the SoH estimation. Nowadays, there are already accurate SoH estimation methods available. However, they need a lot of time to apply, which is why they would not be favourable for an economically bearable second life product (Martinez-Laserna et al., 2018). More about the state of the art of SoH estimation methods, can be found in the next section.

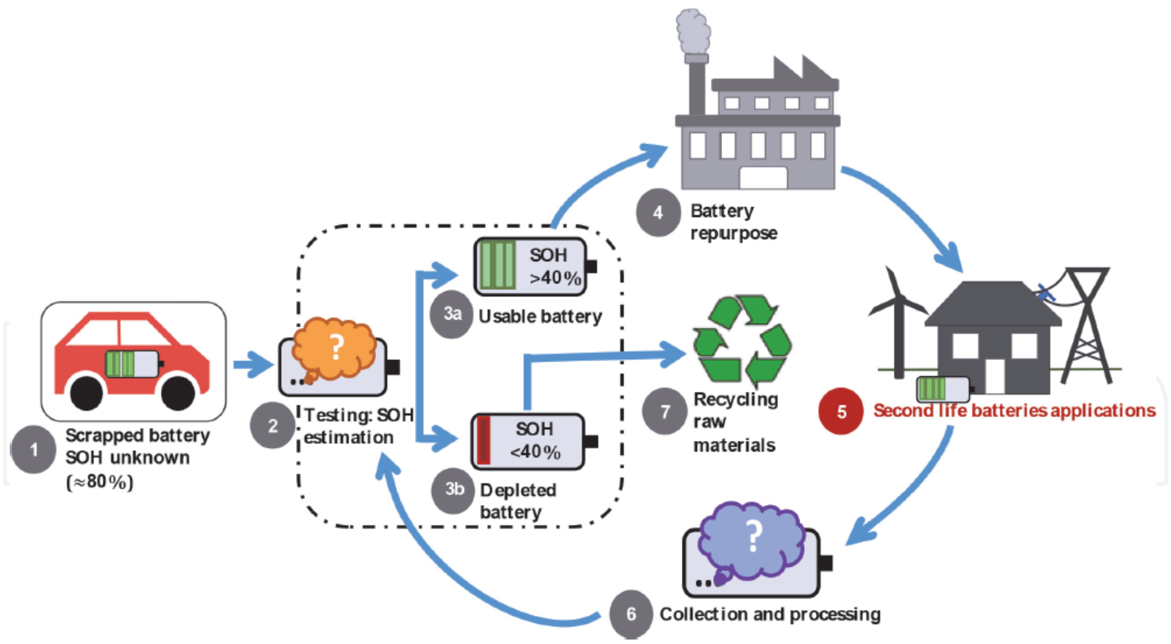

Figure 2 Overview of the second life concept (Montoya-Bedoya et al., 2020). The dashed box indicates the importance of the state of health estimation.

1.3 State of the art SoH estimation methods

The battery SoH can be related to various battery performance parameters. Nevertheless, most of the proposed methods are focusing on only two parameters. Either the SoH is estimated by analysing the internal resistance, which increases over time through irreversible, chemical processes. Alternatively, the SoH is related to capacity fading, which occurs through the loss of ions during long-term operation (Birkl et al., 2016). For more information about the degradation, see section 2.2. As the limiting factor in the transportation sector is the remaining capacity, the definition of SoH is focused on capacity fading. See equation (1), where Q_i represents the current Capacity and $Q_{nominal}$ the nominal capacity.

$$SoH = \frac{\mathrm{Qi}}{Qnominal} \tag{1}$$

The simplest procedure of measuring the (remaining) capacity is to discharge and charge the battery completely and calculate the capacity by integrating either the charging or the discharging current. This method is called Coulomb counting method, as given in equation (2), where *i* is the current and dt is the time difference of the interval in seconds.

$$Q = \frac{1}{3600}\int i\,dt\,, [Ah] \tag{2}$$

This is a very accurate but time-consuming procedure, as it requires the full discharge and charge of the battery. Furthermore, it is not very practical to apply the method at module level, as the different capacity level of the cells in the module have to be balanced. This result in a long charging time. To achieve a trustworthy result, the method is usually applied only on cell level (Quinard et al., 2019). There is a wide spectrum of methods for the SoH estimation in general. Mainly they can be divided into experimental techniques and adaptive models (5) (Berecibar et al., 2014). Out of those two approaches, there are different methodologies, as indicated in Figure 3, where the adaptive models estimate the SoH based on either battery models (4) or on parameters which are sensitive to the SoH, as for example impedance or capacity. The experimental techniques rely on the cycling behaviour of the battery. This technique can be divided further into two categories. One is the estimation based on the battery impedance (1) – which is the combination of the resistance and the reactance of the battery - or on the battery capacity. In the capacity-based methods, there are two further differentiations, one is the current-based (2) and the voltage-based method (3). The before mentioned Coulomb counting method belongs to the current-based method, as demonstrated in Figure 3. Battery models (4) are built based on the information of impedance and capacity (Berecibar et al., 2014).

In order to gather information about the different methods, a literature research was conducted. This research was focusing on the five different categories of the methods, which are shown in Figure 3: Impedance-based (1), current-based (2), voltage-based (3) methods, as well as battery (4) and adaptive (5) models. The difference of model and method is, that the method also defines how to gather the needed information, where the models only define the in- and output. The summary of the literature research presented in Table 1 was focussed on the information about the application time, the accuracy and the feasibility of either the method or the model.

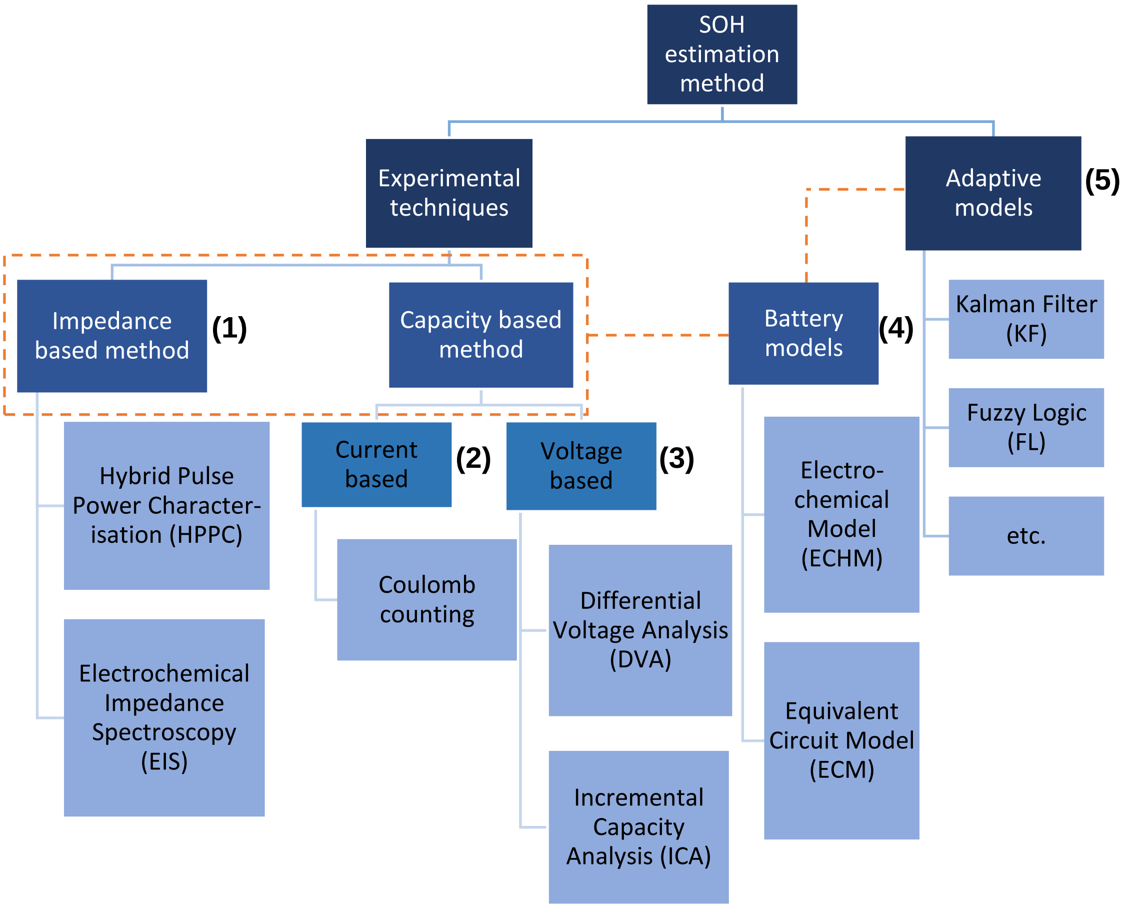

Figure 3 Visualization of the most common SOH estimation methods, based on (Berecibar et al., 2014; Pastor-Fernández et al., 2019; Tian et al., 2019; Venugopal & Vigneswaran, 2019; Xia et al., 2019). The orange dashed lines indicate an indirect connection between the impedance-based and capacity-based method and the battery models. As well as the indirect connection between the battery models and the adaptive models. The different blue brightness indicates the level in the hierarchy.

Table 1 Advantages and Disadvantages of the five defined SoH estimation categories based on literature research.

Categories of Meth-ods	Characteristics
1) Impedance-based methods	• Can take up to one hour (i.e. EIS) • Sometimes special equipment is needed (i.e. EIS) • Accurate method (≤ 5 %) • Historical data required to compare with • To implement it on the vehicle, further methods are needed (i.e. battery models) (Berecibar et al., 2014; Grandjean et al., 2018; Klotz & Schönleber, 2010)
2) Current-based methods	• Long measurement time for battery modules • Accurate method (≤ 5 %) for one cell • Not practical to apply on module level (Quinard et al., 2019)
3) Voltage-based methods	• Fast method, as the charge- or discharge interval can be re-duced (partial charging/discharging) • Applicable on modules • Accurate method (≤ 5 %) • Sensitive to the environment, i.e. temperature (Berecibar et al., 2014; Lee et al., 2019; Nemeth et al., 2020; Qu et al., 2019; Riviere et al., 2019)
4) Battery model	• Mostly applied in combination with other methods, i.e. adap-tive models • Too complex for online parameter identification • Dependent on the resistance and the capacity of the cell • Accurate method (≤ 5 %) (Wei et al., 2018; Xia et al., 2019)
5) Adaptive models	• Complex method to apply, which needs a lot of knowledge to maintain • Needs a lot of training data • Accurate method (≤ 5 %) (Huang et al., 2018; Zhao et al., 2019)

1.4 Problem formulation and objectives

Based on the literature research summarised in Table 1, most of the presented methods are well developed and deliver an accurate result in a controlled environment. The average of the SoH estimation methods has a percentage error of 5 %. Nevertheless, this cannot be confirmed for practical applications (Dubarry & Liaw, 2009). However, according to Montoya-Bedoya et al. (2020), there is a lack of literature for validation below 80 % remaining capacity. Therefore, it is proposed to test whether a specific SoH estimation method can be applied on already aged battery cells and keep the expected accuracy, or not. According to Martinez-Laserna (2018) the SoH estimation method should be a fast, easy and accurate method which is also practical to use while operating the battery. Therefore, the incremental capacity analysis (ICA) estimation method was chosen to be tested (please find further explanation in chapter 3.1). The ICA has multiple indicators to estimate the SoH, which is why it would be worthwhile to test which one of those delivers the most accurate outcome for battery cells with a SoH of less than 80 %. Based on this information, the following research questions were formulated:

1. **Can the ICA method still deliver an estimation with a percentage error below the average estimation error of 5 %, if only a partial charging or discharging is performed?**
2. **Is the ICA method applicable for batteries with a capacity below 80 %?**
3. **Which SoH indicator of the ICA method deliver the most accurate outcome for batteries with a capacity below 80 %?**

1.4.1 Scope and limitations of the project

In order to contribute a part towards commercialising the second life concept, this master thesis focus on the application of the SoH estimation method for batteries below 80 % SoH. By providing a method that allows the fast determination of the remaining capacity on battery pack level, it is expected that this could contribute a part to keep the battery longer in the lifecycle. Therefore, as an output of this master thesis, it is expected to have a validated model, which can determine the remaining capacity on already aged battery cells. It shall be possible to estimate the battery capacity, without a full discharge and a subsequent charge of the battery. Furthermore, it will be decided which of the inspected indicators of this method deliver the most accurate SoH estimation for cells below 80 % remaining capacity.

Due to time limitations, the master thesis focuses only on one method, other methods were not investigated. The experimental study was conducted only on one cell chemistry, i.e. lithium-titanate-oxide (LTO) battery cells and from one manufacturer, which means, that it is not expected, that the outcome can be transferred to other manufacturer or technologies. Tests will be conducted on each single cell and not on all of them together, in order to keep the tests as simple as possible. There will be no chemical analysis, which means, that the degradation mechanism will not be studied in detail.

1.5 Content of the Report

The master thesis is structured in the following 4 chapters, with each include several sections:

- **Chapter 2** describes the basic know how of the lithium-ion batteries and presents a short overview of some different technologies, with their characters. It touches briefly the process of battery degradation, where the focus lies more in how the degradation is affected by external influences.
- **Chapter 3** describes the method of this master thesis, which includes how the ICA as the SoH estimation method was chosen, what was used in experimental study and what the content of it was. Also, the input, the function and the output of the ICA algorithm is described in this chapter. Finally, it is described with which scenarios the models were built and how they were validated.
- **Chapter 4** presents and simultaneously discusses the output of this master thesis. This includes the output of the experimental study, which were basically measurements of voltage, current and time, as well as the capacity calculation. It presents the output of the ICA algorithm, which results in ICA curves. Then, the different models with their diagnostics are presented whereupon the validation of the model follows. In addition, the application of this ICA method is discussed in this chapter.
- **Chapter 5** answers all three research questions and presents an outlook for possible future work.

2 Basics about Batteries

2.1 Lithium-ion Batteries

Figure 4 visualizes the basic information about the working principle of a conventional lithium-ion battery cell. The example shows a battery with lithium-manganese-oxide (LMO) as cathode material and graphite as anode material. The procedure presented is the discharge procedure, which means that the anode is the negative electrode and the cathode is the positive electrode. In the charging procedure, the nomenclature is the opposite way around. The anode is the term which is used to describe the electrode where the oxidation procedure is happening, which means, where the positive ions are provided. When the battery is fully charged, the lithium-ions are inserted in the graphite structure. Through electrochemical reactions, current is induced. As soon as the current flows, the active material provides ions, which deintercalate from the anode, move by diffusion through the electrolyte and intercalate into the cathode. On electrical level, the energy efficiency of this procedure is dependent on the internal resistance. This means, the higher the internal resistance, the less efficient it is. The battery is fully discharged, as soon as the equilibrium in the battery is reached. (Chiasserini, & Rao, 2001; Meuser, 2011; Rahimzei et al., 2015; Reddy, 2011).

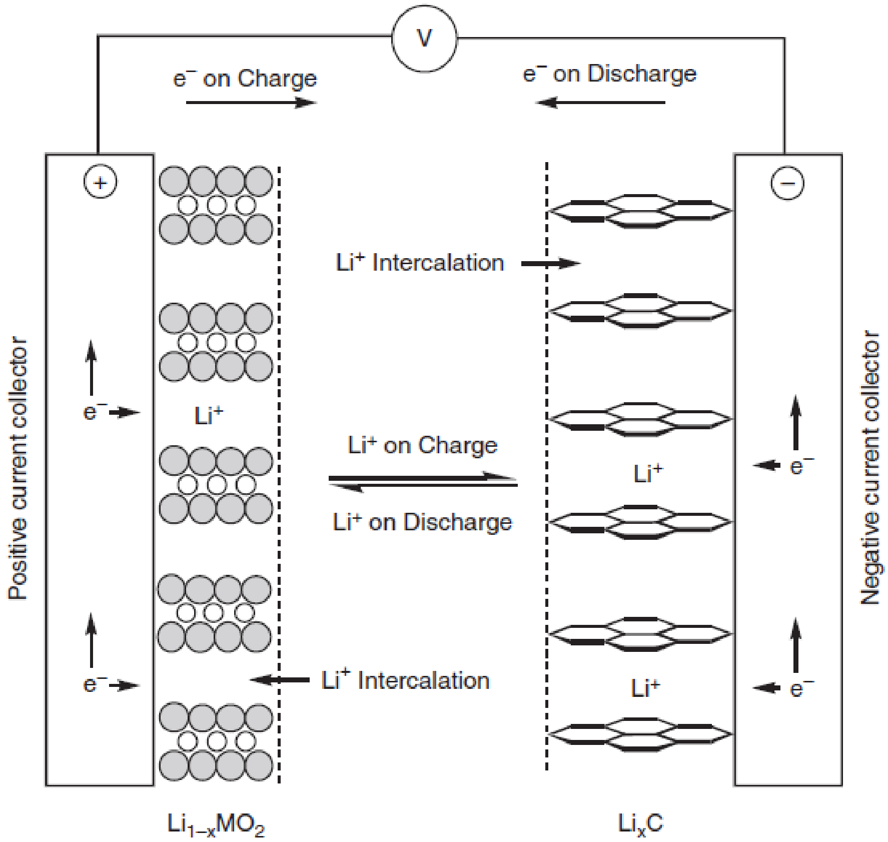

Figure 4 Design and working principle of a commercial Lithium-ion battery (Reddy, 2011). $LiMO_2$-Electrode is also called LMO-electrode and means lithium-manganese-oxide-electrode, Li_xC is the graphite structure with inserted Lithium-ions. Li^+ stands for the positive Lithium-ions and e^- for the electrons.

In Table 2 some common lithium-ion technologies are listed. As it can be seen, these technologies have different nominal voltage values. This is because of their different elements, which each have different potentials. In this master thesis, the second listed technology is used for the experimental study. This technology differs from the others, as the negative electrode is lithium-titanate-oxide (LTO) instead of graphite. Based on literature, LTO shows an excellent charge-discharge performance and has therefore a longer cycle life, compared to graphite. For further information about this cell technology, as for example about the specific energy, see section 3.3.2. For more details about the other technologies, the reader is referred to Linden's Handbook of Batteries (Meuser, 2011; Rahimzei et al., 2015; Reddy, 2011).

*Table 2 Overview of the most common lithium-ion technologies (*BU-205: Types of Lithium-Ion*, 2020; Meuser, 2011). LNMC stands for lithium-nickel-manganese-cobalt-oxide; LFP stands for lithium-iron-phosphate; LMO stands for lithium-manganese-oxide; LCO stands for lithium-cobalt-oxide; LNCA stands for lithium-nickel-cobalt-aluminum-oxide; C stands for graphite.*

Positive electrode	Negative electrode	Nominal voltage [V]	Specific Energy [Wh/kg]
LNMC	C	3.6	150-220
LNMC	**LTO**	**2.4**	**50-80**
LFP	C	3.3	90-120
LMO	C	3.7	100-150
LCO	C	3.6	150-200
LNCA	C	3.6	200-260

2.2 Battery degradation

As soon as the charging-/discharging processes are not reversable anymore, the degradation of the battery has started. This degradation leads to a gradual loss of performance and happens in all parts of the batteries. The degradation is influenced by the condition of the battery, the load cycle or from environmental conditions, also called stress factors. These strass factors have different influences when they occur at different time intervals. In this section, the long-time effects are presented. Usually, the degradation is divided into two categories, calendar and cycle ageing. The calendar ageing describes the degradation of the cell over time and the cycle ageing the degradation of the cell over cycle numbers. In calendar aging, temperature and state of charge (SoC) have an impact, where in cycle aging additionally the depth of discharge (DoD) and the current rate (C-rate) have an influence, as presented in Table 3. (Birkl et al., 2016; Sterner & Stadler, 2014).

Table 3 Stress factors for cell ageing (Sterner & Stadler, 2014).

Category	Stress factor
Calendar	**Temperature,** state of charge (SoC)
Cycle	**Temperature, depth of discharge (DoD),** state of charge (SoC), current rate (C-rate)

In this master thesis the focus is not on the degradation of the battery cell, but on the estimation of the remaining capacity, which decreases with increasing degradation. Therefore, only the stress factors which are relevant for this work are going to be explained below. The first relevant stress factor is the temperature, as this is used to influence the ageing in the experimental study, see section 3.3.3 for further information. Figure 5 presents the long-term impact of the temperature on the capacity on the example of an LCO/graphite cell. It is shown, that the cell aged with 23°C retains more capacity after the same amount of time, than the cell aged at 43°C. This indicates, that if the battery is exposed to higher temperature, it ages faster. Depth of discharge (DoD) defines how much the battery is discharged and charged in one cycle. In Figure 6 the influence of this DoD on the capacity is introduced on the example of an LNMC/carbon cell. Six different cycles are shown, of which each has its own DoD, but all cycles have the same state of charge (SoC) at 50 %. There is a remarkable gap between 20 and 50 % DoD, which results in the conclusion that the capacity fade is accelerated by a DoD of 50 %. However, the study does not show the DoD of 30 and 40 %.

For more information about the long-term impact on the capacity based on temperature and current rate the reader is referred to Linden's Handbook of Batteries (Reddy, 2011, p. 869 + 883). For more information about DoD and SoC the reader is referred to Eckert et al.'s paper about calendar and cycle life study of Li(NiMnCo)O_2-based 18650 lithium-ion batteries (2013, p. 8 + 9).

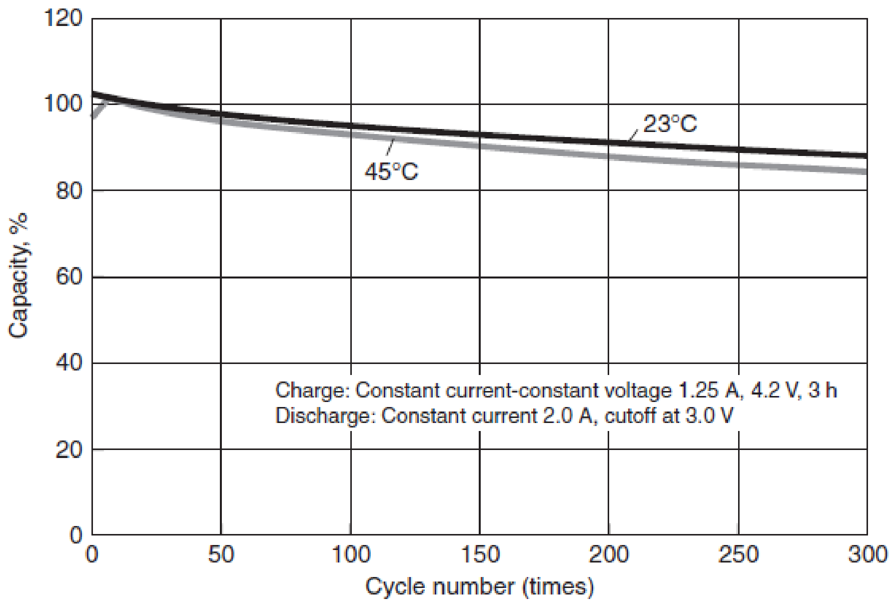

Figure 5 Long term impact of temperature on capacity on the example of an LCO/graphite cell (Reddy, 2011, p. 869).

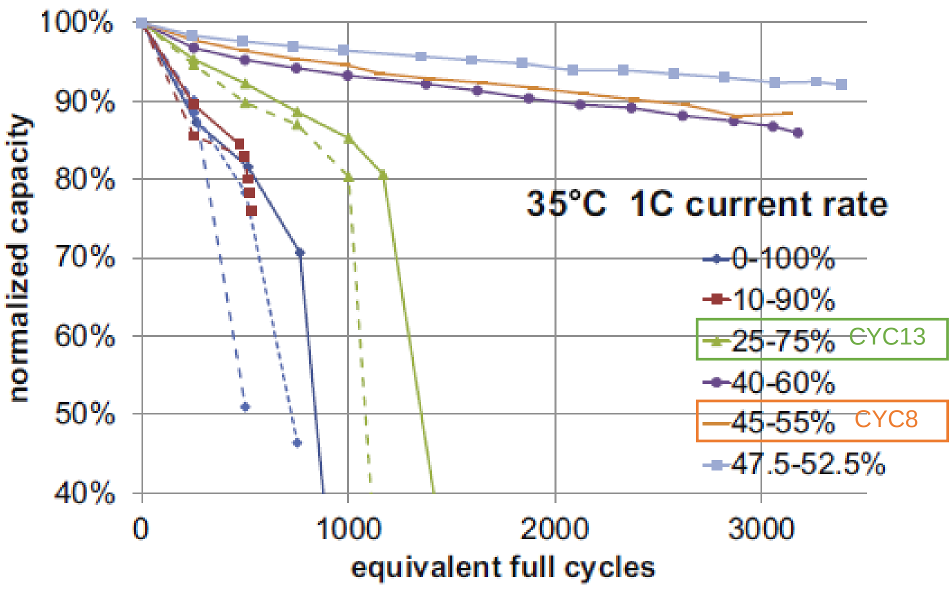

Figure 6 Long term impact of depth of discharge (DoD) on capacity (Eckert et al., 2013, p. 8). The green box highlights the DoD of the cell CYC13 and the orange box the DoD of cell CYC8.

3 Material and Method

3.1 State of health (SoH) estimation method

Based on the literature research in section 1.3 the voltage-based methods fulfilled the requirements for second life batteries the best, as they can reduce the estimation time by reducing the charging interval and are suitable for the application on modular level. The voltage-based methods classify two methods, the incremental capacity analysis (ICA) and the differential voltage analysis (DVA). Those two methods use the same information to estimate the SoH. The only difference is that the DVA derives the voltage by the capacity, see equation (3), and the ICA derives the capacity by the voltage, see equation (4). Finally, it was decided to choose the ICA method, as this is the more intuitive procedure and further studies confirm, that this method represents a promising method to estimate the SoH on the vehicle and also for batteries with a remaining capacity below 80 % (Fly & Chen, 2020; Han, et al., 2014). Equation (4) defines the ICA mathematically, where *dQ* is the step difference between the charge and *dV* is the step difference of the voltage.

$$DVA = \frac{dV}{dQ}, \left[\frac{V}{Ah}\right] \tag{3}$$

$$ICA = \frac{dQ}{dV}, \left[\frac{Ah}{V}\right] \tag{4}$$

Figure 7 visualizes the procedure of creating the ICA curve. Three information are needed, the voltage, the current and the time. The part where constant current (CC) applies is used to create the ICA curve. Only this part delivers the needed information to shape the characteristic ICA curve (Lin et al., 2020). For more information about the CC part, please see chapter 3.3. In order to create the ICA Curve, the CC current curve a) is integrated by the time, as described in equation (2). This leads to the capacity curve presented in c). The capacity curve c) is then plotted against the voltage curve b), which results in the curve d). Thereafter, this curve is derived by the voltage, as described in equation (4). The output represents the characteristic ICA curve, as presented in e).

Figure 7 shows also the impact of a partial charging. If the charging would be reduced to a voltage interval between 2.2 and 2.4 V, the charging time could theoretically be reduction by 20 minutes. However, this was not tested nor proved in this master thesis.

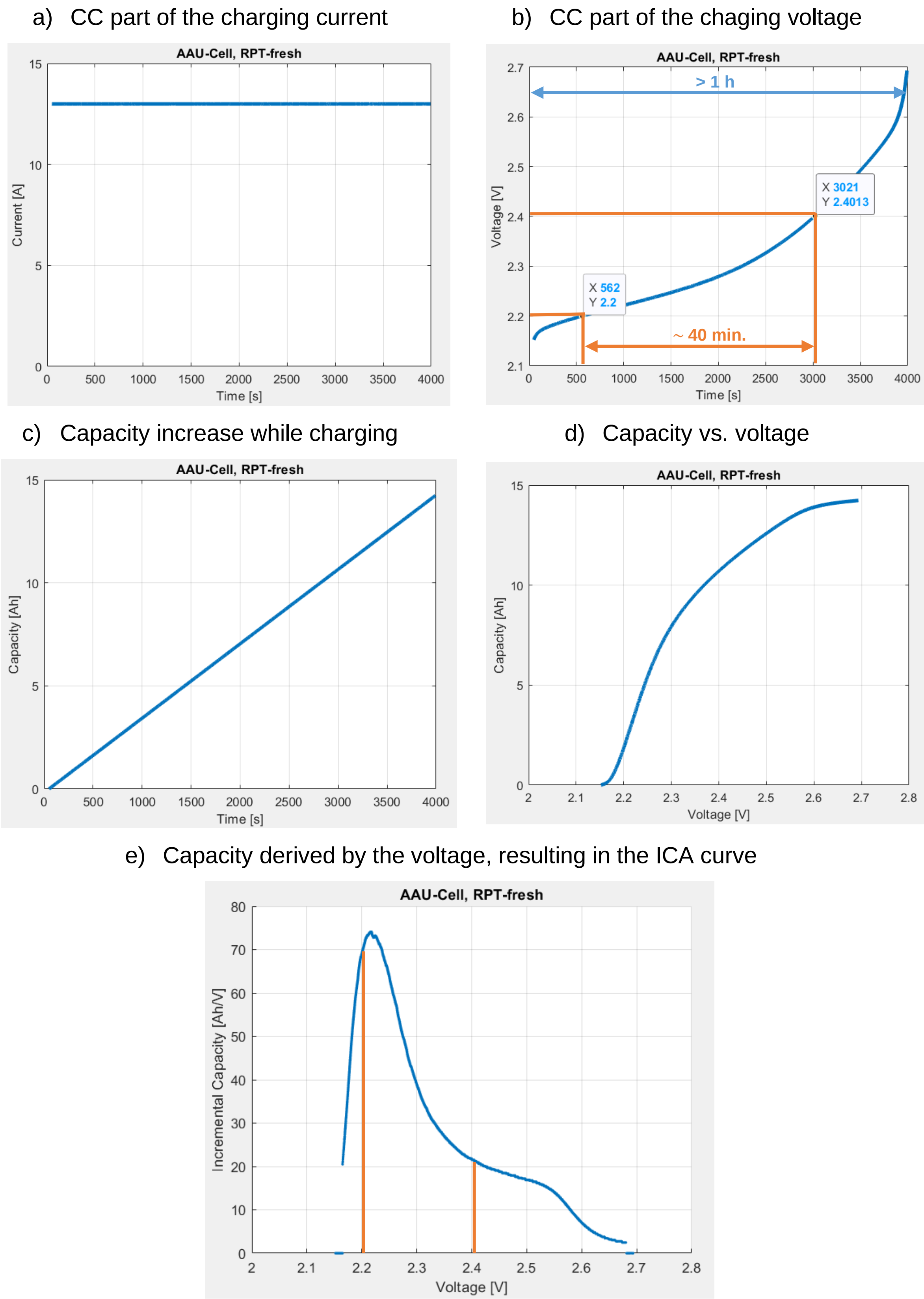

Figure 7 Demonstrative incremental capacity analysis (ICA) procedure with a LTO/LNMC cell, where a) shows the CC charging current, b) the CC charging voltage, c) the capacity increase, d) the capacity vs. voltage and e) the capacity derived by the voltage, resulting in the ICA curve. The orange lines indicate the voltage level in the range between 2.2 and 2.4 V. The blue arrow indicates the time to measure the whole charging curve in order to create the ICA curve. The green arrow indicates the time needed for a partial charging.

3.1.1 Fundamentals

The Incremental capacity curve was initially used to exhibit electrochemical interactions, which are taking place within the cell. It delivers indirect information about the degradation of the battery cell. This means, that without opening the cell, the electrochemical behaviour can be visualised. Each ICA curve has its own shape, depending on the electrochemical processes taking place withing the cell (Dubarry & Liaw, 2009; Lin et al., 2020). Figure 16 and Figure 17 show, that the trend of the ICA curves from the cell used in this master thesis is mostly decreasing and in some cases also moving to the right with increased degradation (ageing). But this behaviour can also be influenced by parameters i.e. temperature or current rate (C-rate). In comparison to the long-term influences presented in section 2.2, these parameters are influencing the cell in short-term. Figure 8 demonstrates different ICA curves at different C-rates, although with the same SoH. It can be seen that the higher the charging current, the smaller the amplitude of the peak. Also, that there is a right shift of the ICA curves the higher the C-rates is. This however can be explained due to the internal resistance of the battery. As the ohmic law states, that with constant resistance and increasing current, the voltage increases as well, see equation (5), where U stands for the voltage, R for the resistance and I for the current. Figure 9 shows the integration of Figure 8, but with other C-rates, in discharge procedure and for another battery cell. It shows that with increasing C-rate the available discharge capacity is decreasing. The red arrow in Figure 9 shows the same short-term trend as the red arrow in Figure 8 with increasing current. (Fly & Chen, 2020; Reddy, 2011; Riviere et al., 2019).

$$U = R * I \tag{5}$$

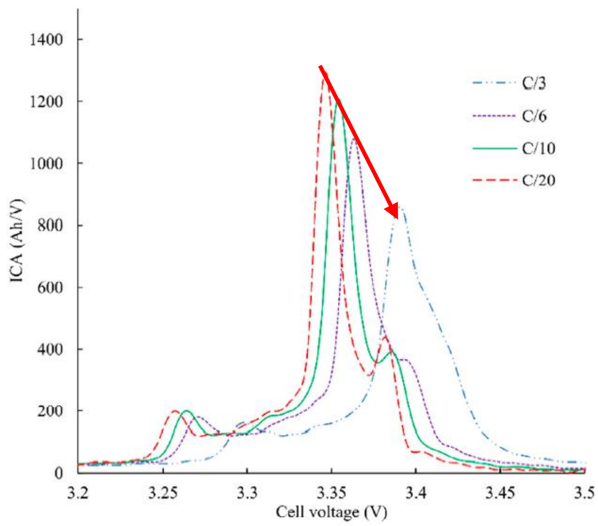

Figure 8 Incremental capacity curve with same state of health (SoH) but different current rates (C-rate) (Riviere et al., 2019). Here at the example of a C/LFP cell. The red arrow indicates the change with increasing current rate.

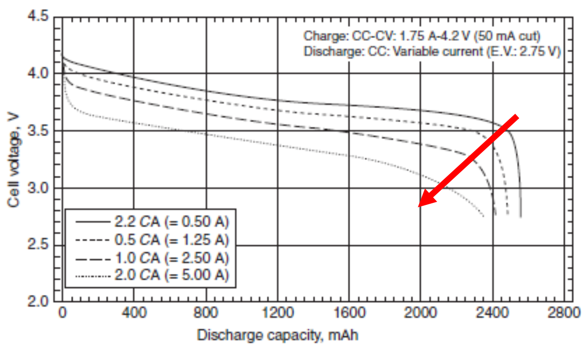

Figure 9 Short term impact of the current rate (C-rate) on the capacity (Reddy, 2011, p. 867). The red arrow indicates the increase of the capacity with increasing current rate (C-rate).

Furthermore, it is well known that the battery capacity depends on the temperature, due to the changes in the ionic conductivity of the electrolyte, which is confirmed by Figure 11. Thus, the ICA plot also changes depending on the temperature at which the current curve was extracted. As presented in Figure 10, the trend of the ICA curves moves to the left and in some cases the amplitude increases as well. The left shift can also be explained with equation (5). However, in this case, the current is constant, and the resistance is reducing with increasing temperature, as the conductivity of the electrolyte is increased. The two red arrows in Figure 10 and Figure 11 show both the short term increase of the capacity with increasing temperature.

Subsequently, in order to track the battery degradation and to predict the battery's SoH, the capacity must always be measured at the same conditions (i.e., the temperature or current rate). Otherwise, the changes in the results could be misinterpreted as degradation, whereat they are actually transformations coming from changing the measurement conditions.

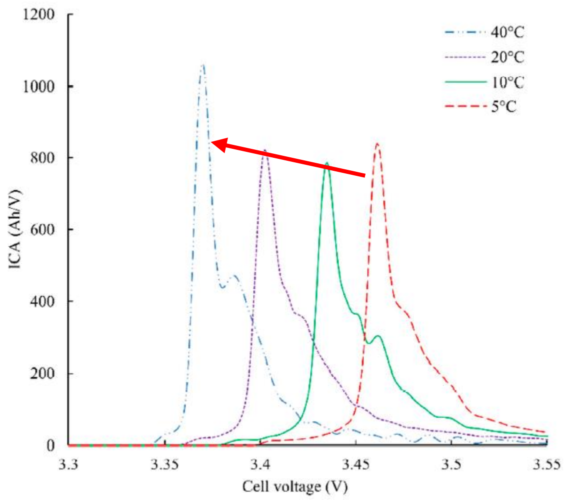

Figure 10 ICA curve with the dependency of temperature (Riviere et al., 2019). Here at the example of a C/LFP cell. The red arrow indicates the change with increasing temperature.

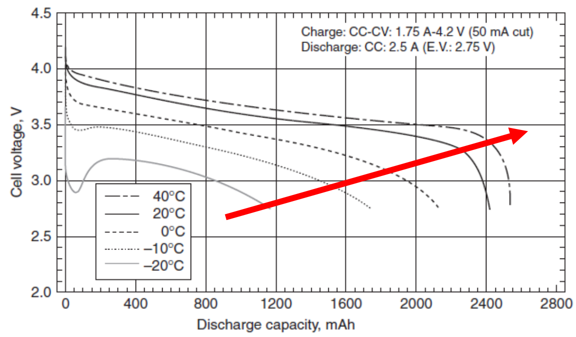

Figure 11 Short term impact of the temperature on the capacity (Reddy, 2011, p. 868). The red arrow indicates the change with increasing temperature.

3.1.2 Incremental capacity (IC) feature as a State of health (SoH) indicator

In order to predict the SoH with the ICA curve, an indicator is used to predict the SoH. There are many different indicators in the ICA curve, but mainly the peak coordinates (amplitude and location) or the area below the peak are used (Fly & Chen, 2020; Lin et al., 2020). These indicators are called features and are introduced below. See Figure 12 in order to get an overview of how these features are extracted from the ICA curves in order to relate them with the remaining capacity of the cell.

Peak location (green arrow)

Han, et al., (2014) observed that the ICA curve changes its position and shape while the battery ages. One feature of this behaviour is the location of the peak. In order to compare the peak location with the remaining capacity, the X-value of the peak value has to be determined. In the example in Figure 12 the X-value is the voltage.

Peak amplitude (orange arrow)

Same as with the peak location, also the peak amplitude is a feature of the cell age. For the peak amplitude, the Y-value must be determined, in order to compare it with the capacity. In the example in Figure 12, the maximum ICA value has to be determined.

Area below the peak (blue area)

Besides the peak location and the peak amplitude, the area below the peak can be calculated. A segmented peak curve is integrated by the voltage step difference, see equation (6), where *u* stands for the voltage, *du* for the voltage difference, u_1 and u_2 define the voltage interval, *dQ* the capacity difference, $Q(u_1)$ the capacity at u_1 and $Q(u_2)$ the capacity at u_2. This outcome represents the area below this peak curve.

$$\int_{u1}^{u2} ICA(u)du = \int_{u1}^{u2} \frac{dQ(u)}{du} du = Q(u2) - Q(u1)\,, [Ah] \tag{6}$$

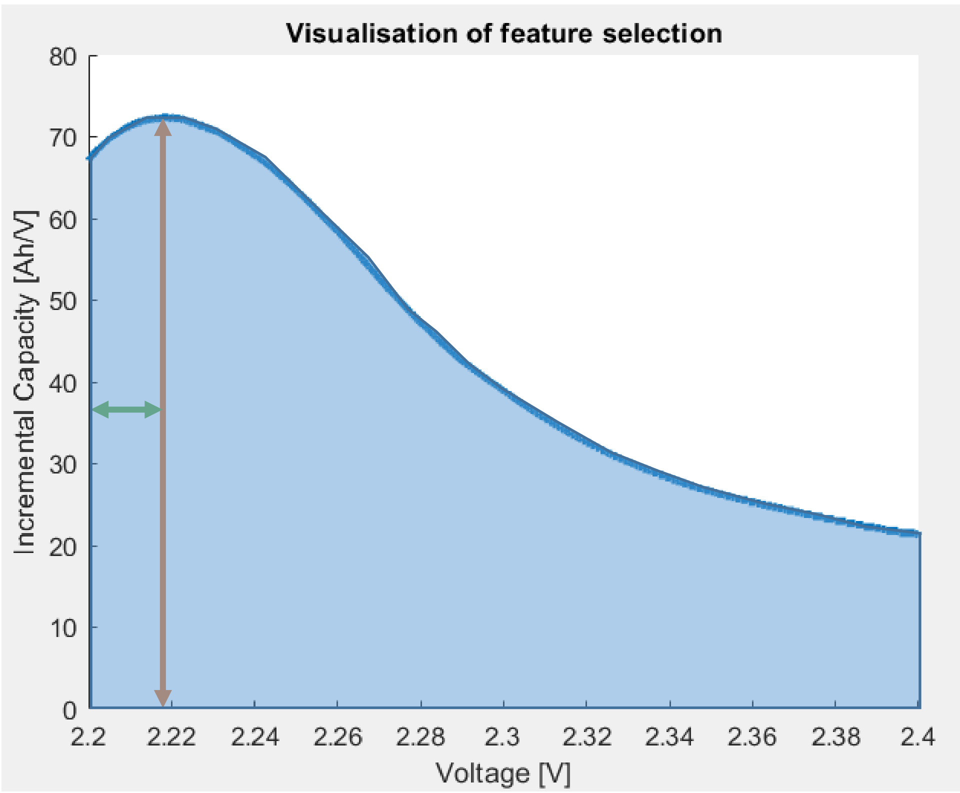

Figure 12 A partial ICA curve on an example of an LTO/LNMC cell, where the voltage interval between 2.2 and 2.4 V is chosen. The area [Ah] is indicated in blue; the peak amplitude [Ah/V] is indicated with the orange arrow and the peak location [V] is indicated with the green arrow.

3.2 Procedure to test the chosen SoH estimation method

Figure 13 visualizes the structure of how to test the chosen SoH estimation method. First, the experimental study (ES) was performed, which was needed to determine the SoH conventionally – in order to compare it with the result of the chose method. In addition, to extract the charging curve, which was used as an input for the ICA algorithm. See section 3.3 for more information about how this charging curve was extracted and how the cells were aged in order to extract more of those charging curves. By applying the ICA algorithm on all the extracted charging curves, the ICA feature values were extracted. Those feature values and the capacity calculated in the ES were used to create the models. This procedure is described in section 3.4. The last step, the validation of the model, is presented in section 3.5, for which three different scenarios were chosen.

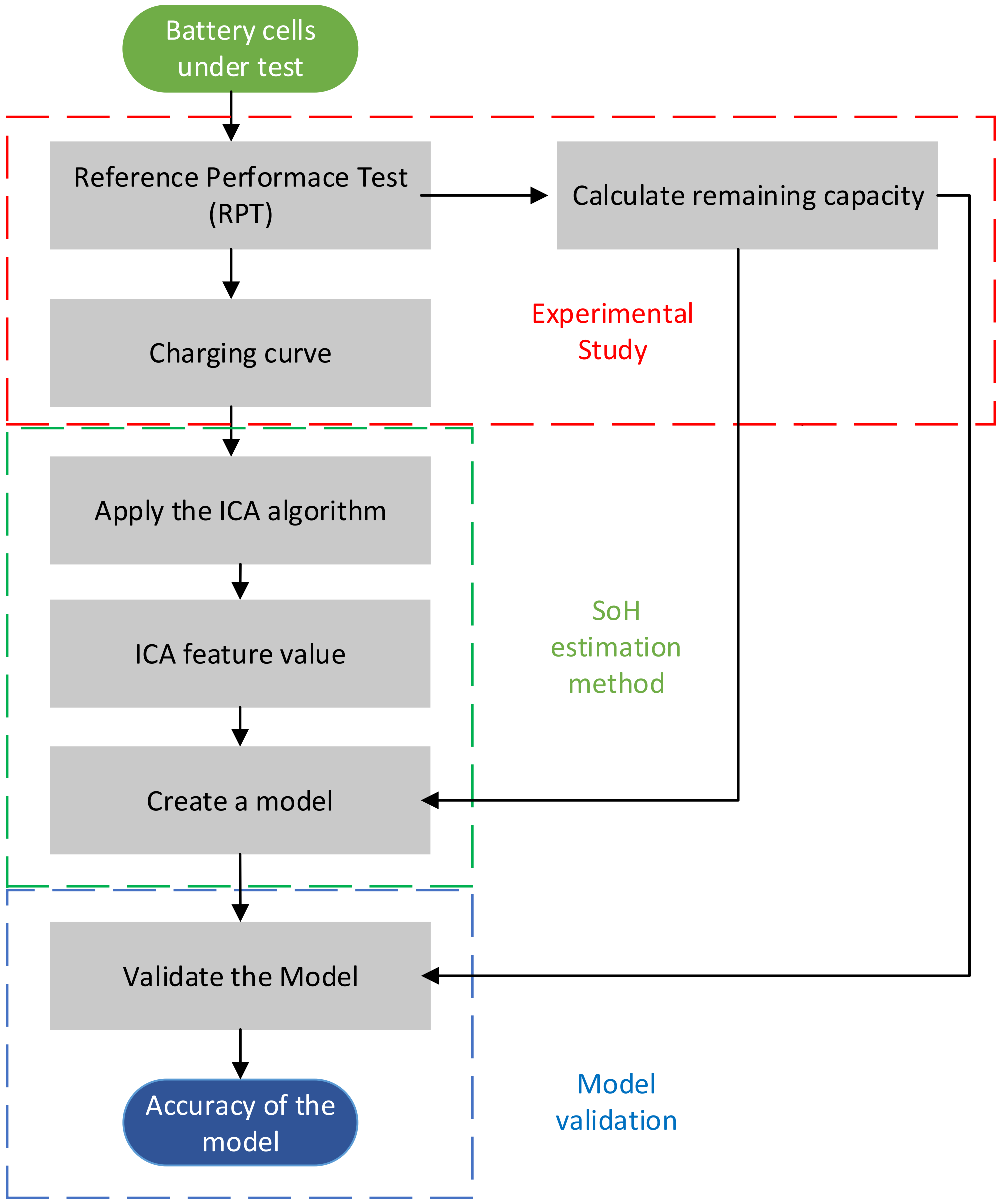

Figure 13 Overview of the procedure in order to create a SoH estimation model. Green indicates an input, blue an output and grey stands for a process. The three different borders visualize in which chapter the processes are described in detail.

3.3 Experimental Study

3.3.1 Overview

In order to answer the research questions, the proposed ICA method was tested with three battery cells; two cells which were previously aged and one fresh cell. In the beginning of the experimental study, a reference performance test (RPT) was performed to define the (remaining) capacity of the battery cells. This procedure includes the complete discharge and charge of the battery, which allows to determine the capacity of the cell by the Coulomb counting method. After the first RPT, the battery was aged with a predefined load cycle, whereupon another RPT was performed. As indicated in Figure 14, this procedure was repeated four times. The number of iterations is due to the time frame of this master thesis. Figure 15 gives an idea of how and when the data was collected and labelled. The historical data of the previously aged cells were also available. In order to separate the historical from the experimental study, the historical data was labelled with an "H" and the experimental data was labelled with "ES". The output from the first RPT was labelled "BOL", which stands for beginning of life. After each RPT, the data was labelled with "Eo1stL", "Eo2ndL" etc., which stands for end of first and end of second life, respectively.

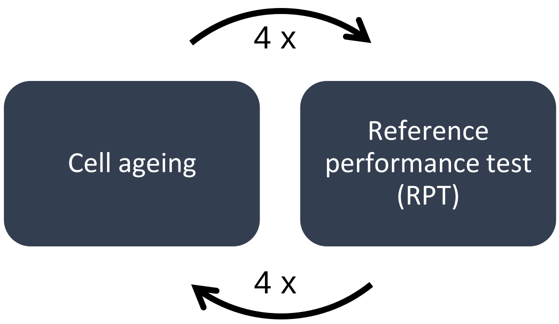

Figure 14 Experimental study - the procedure was repeated four times.

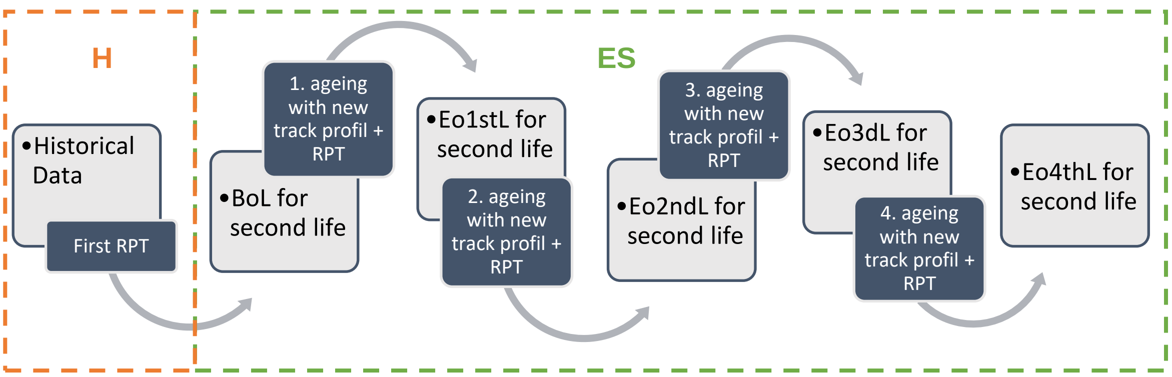

Figure 15 Organisation of the data collection. Light grey indicates the labeling of the data and dark blue indicates the procedure between two data sets. RPT stands for reference performance test; BoL stands for begin of life; EoL stands for end of life, where the number 1^{st}, 2^{nd}, 3d and 4^{th} are added to it.

3.3.2 Battery cell under test

The batteries in the transportation sector are assembled in packs, which is why it is meaningful to know the behaviour of the whole battery pack. But, since Lee et al. (2019) and Schalz et al. (2019) both state, that the characteristics of ICA on pack level are very similar to the ones at cell level, it was decided to keep the test as simple as possible and apply the method only on cell level.

The purpose of this master thesis is to support the second life concept for batteries from the transportation sector. Therefore, lithium-titanate-oxide (LTO) battery cells were used for this experimental study. Because LTO battery cells have a long calendrical lifetime, a long cycle lifetime, and a high-power capability, they are used in transportation applications, especially for electric trains and busses (Han, et al., 2014; Nemeth et al., 2020). The basic information about the LTO battery cell can be found in Table 4. For more information, please find the datasheet in the Attachment B: Technical Data Sheets.

Table 4 Nominal information of LTO battery cells

Negative electrode	Lithium-Titanate-Oxide (LTO)
Positive electrode	Nickel-Manganese-Cobalt (NMC)
Nominal Voltage	2.26 V
Nominal Capacity	13.4 Ah
Discharge cut off voltage at 20°C	1.5 V
Charge cut off voltage at 20°C	2.8 V

As a difference to batteries using a conventional negative electrode, i.e. graphite, LTO cells have a different voltage range, higher temperature range, longer lifetime, and higher rate capability. But, they have also a lower specific energy and a lower specific capacity. This is why they are more used in power specific applications, as for example in electric trains or busses (Nemeth et al., 2020).

In this master thesis, three LTO battery cells were used to test the ICA method. Two of those cells were already aged before, whereupon the third one was not cycled before this study. The condition at BoL, as well as the historical aging procedure of the three LTO batteries is presented in Table 5. The historical data of the two aged cells is presented in Figure 16 and Figure 17. The fresh one was used as a reference to differentiate between ageing behaviour and possible errors in the measurement equipment.

As it can be seen in Table 5, the battery cells CYC8 and the fresh one have more than 13.4 Ah capacity, which is according to the datasheet the nominal capacity. As this would result in more than 100 % SoH, it was decided to compare the remaining capacity in Ampere hours instead of the SoH in percentage.

Table 5 Introduction of the battery cells under test. Cycle interval in State of charge (SoC), 2 C means that the throughput of the nominal capacity of 13.4 Ah is conducted twice as fast as nominal – in this case, in a half an hour.

	CYC 8	CYC 13	Fresh cell
Historical ageing procedure	Temperature: 42.5 °C, Cycle interval: 45-55% SoC, 2 C charging, 2 C discharging	Temperature: 42.5 °C, Cycle interval: 25-75% SoC, 2 C charging, 2 C discharging	No cycle ageing
Remaining capacity at BoL	14 Ah	8 Ah	15 Ah

CYC8_H

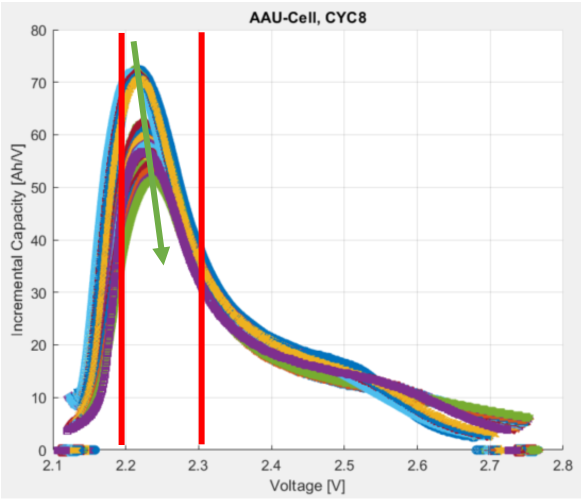

Figure 16 ICA curves of the historical data from cell CYC8, conducted with 1 C. The red lines indicate the voltage interval. The green arrow indicated the ageing direction.

CYC13_H

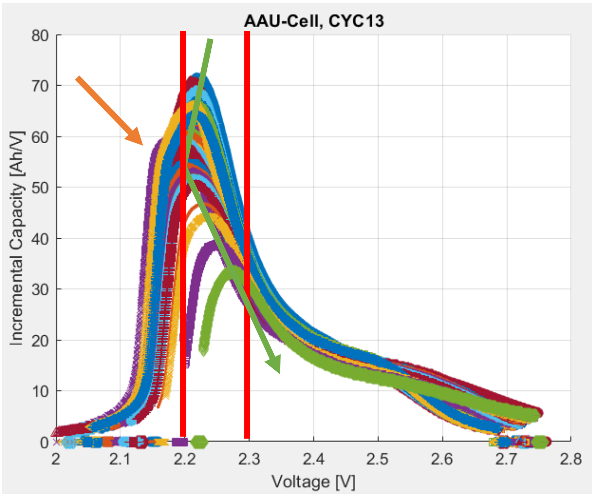

Figure 17 ICA curves of the cell historical data from cell CYC13, conducted with 1 C. The red lines indicate the voltage interval, the green arrow indicated the ageing direction, the orange arrow highlights an outlier.

3.3.3 Experimental set-up

As presented in Figure 18, the battery was placed in a thermal chamber for the ageing and the RPT, in order to control the cell temperature. The battery cell was connected to a battery test station, which defined the operation of the battery and recorded the main parameters such as voltage, current and temperature of the cell. The equipment used to perform the test and the ageing is presented in Table 6. More information about the equipment can be found in Attachment B: Technical Data Sheets.

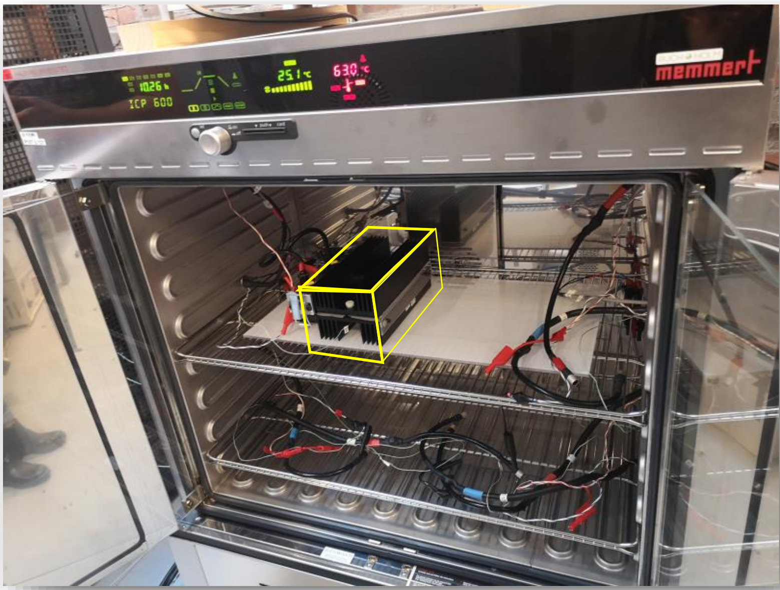

Figure 18 Battery cell in thermal chamber connected to the battery cycler, which demands the specified load cycle from the battery cell and measures the voltage, the current and the temperature.

Table 6 Used equipment for the experimental study and its accuracy.

Equipment name	Function	Accuracy
BTS600 (Digatron)	Battery test station	± 0.1 %
• Voltage sensor	Voltage measurement	
• Current sensor	Current measurement	
PT100	Temperature measurement	± 0.1°C
Memmert	Climatic chamber	± 0.1°C

Preparation test

The preparation test included five battery cycles, executed with 1 C. This was applied in order to remove any passivation to which the battery cell was exposed between manufacturing and the first use or the last use and the first test, when it was stored for a long time. The test was conducted to verify that the cell shows a stable capacity, and a stable thermal behaviour, as stated by D.-I. Stroe (2020). According to the ISO standard 12405-4:2018, the cell has passed the preparation test, if the capacity does not change by more than 3 % within two consecutive cycles (Electrically Propelled Road Vehicle - Test Specification for Lithium-Ion Traction Battery Packs and Systems - Part 4: Performance Testing, 2018).

Reference performance test (RPT)

The RPT test was the main part of the experimental study. It was executed to extract the charging curves and to define the remaining capacity. In order to charge and discharge the cell completely, the constant current (CC) and the constant voltage (CV) procedure was applied, see Figure 19. At first, a CC was induced until the CV was reached. While the CV was applying, the current was slowly reduced. With the output of this CC-CV method, the remaining capacity of the battery cell was computed based on Coulomb counting method, as presented in equation (2).

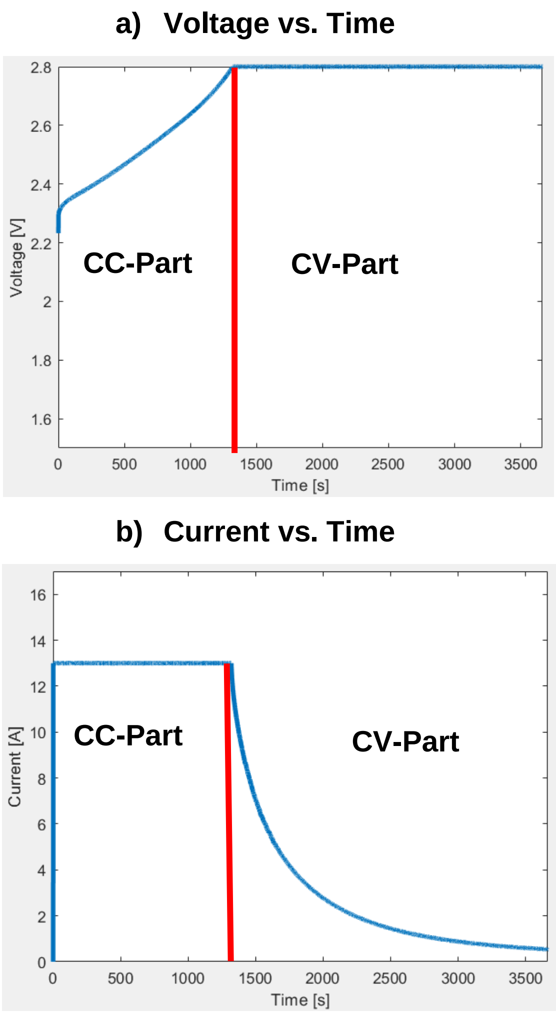

Figure 19 Constant current (CC) and constant voltage (CV) procedure on the example of a LTO/LNMC cell. The red lines highlight the shift from CC to CV.

Current rate (C-rate) for RPT

The charging procedure in the RPT could be performed with different current rates (C-rates), which results in different lengths of the test procedure. 1 C has a throughput of the nominal capacity within an hour and 2 C one of a half an hour. In this experimental study 1 C was chosen to be applied due to historical reasons, as 1 C was used for the previous RPTs of the two already aged batteries. As Han, et al. (2014) states that a C-rate which is close to the use-cycle should be selected, an additional C-rate was applied, in order to compare the output with the 1 C curves. An analysis showed that 1.6 C occurs frequently within the used load cycle, see equation (7), where 13.4 Ah is the nominal capacity and 21.35 A is the maximum current of the load cycle, see the green line in Figure 20 a). For further application of the ICA algorithm, although only the 1 C was used.

$$C - rate = \frac{21.35\ A}{13.4\ Ah} = 1.6\ h^{-1} \tag{7}$$

Ageing of the battery cells

After the RPT test, the cells were aged by a specific cycling profile, in a period of 14 days. The presented ageing profile in Figure 20 is a demanding cycle which is used for mass transport vehicles. This profile was received from a confidential industry partner. As the three used cells have a typical cell technology for the transportation sector, it was decided to age them further with a demanding cycle from the transportation sector. In Figure 20 a), the current profile is shown. After 4000 seconds, a constant current is used to charge the battery completely. In Figure 20 b), the state of charge (SoC) status of the battery is shown. In order to achieve the current change in Figure 20 a), the state of charge (SoC) profile in b) is followed, which is determined by using equation (8). Where *SoC(t)* is the SoC at time *t*, *SoC(t-1)* is the initial SoC, *I* the current in ampere, C_{bat} the battery capacity in Ampere hours and *dt* the time difference in hours. The ageing procedure was applied with the same equipment as the RPT. However, in order to age the cells faster, the ageing was proceeded at 50°C instead of 25 °C, see chapter 2.2 for further explanation.

$$SoC(t) = SoC(t-1) + \int_0^t \frac{I}{Cbat} dt \tag{8}$$

a) Current development of the battery used in a mass transport vehicle

b) SoC of the battery used in a mass transport vehicle

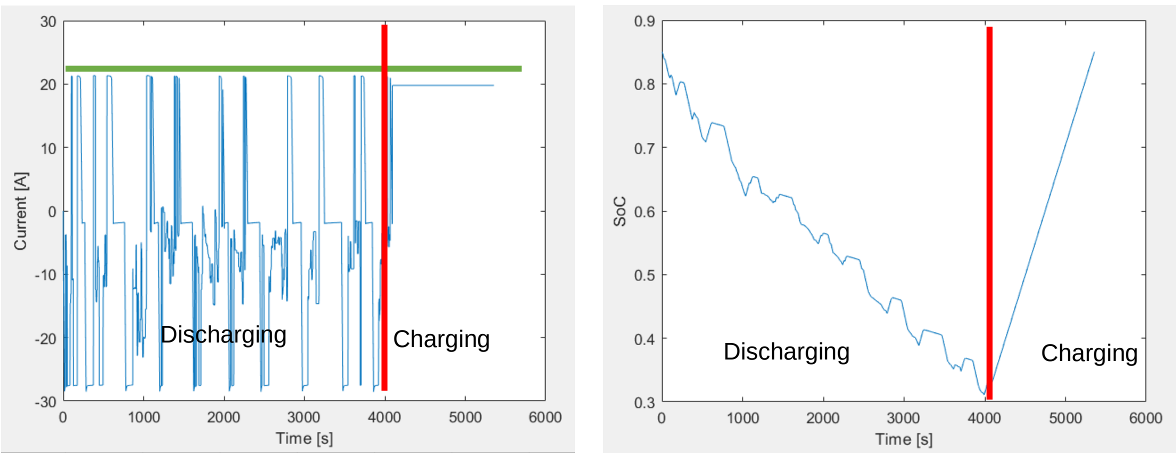

Figure 20 Track profile used to age the batteries in the experimental study.

3.4 State of health (SoH) estimation algorithm

3.4.1 Overview

After fulfilling all RPTs, only the charging curve was used for further procedure. The charging curves were used as an input of the ICA algorithm, where they were derived into ICA curves. This procedure is described in chapter 3.1. In this master thesis, the ICA algorithm is on MATLAB. After creating the ICA curves, they were reduced to a specified charging range, see section 3.4.2. The ICA feature values were extracted within this range. The feature values and the remaining capacity were set in relation with each other based on a regression analysis. Out of the regression analysis the model was defined. The whole procedure is visualised in Figure 21.

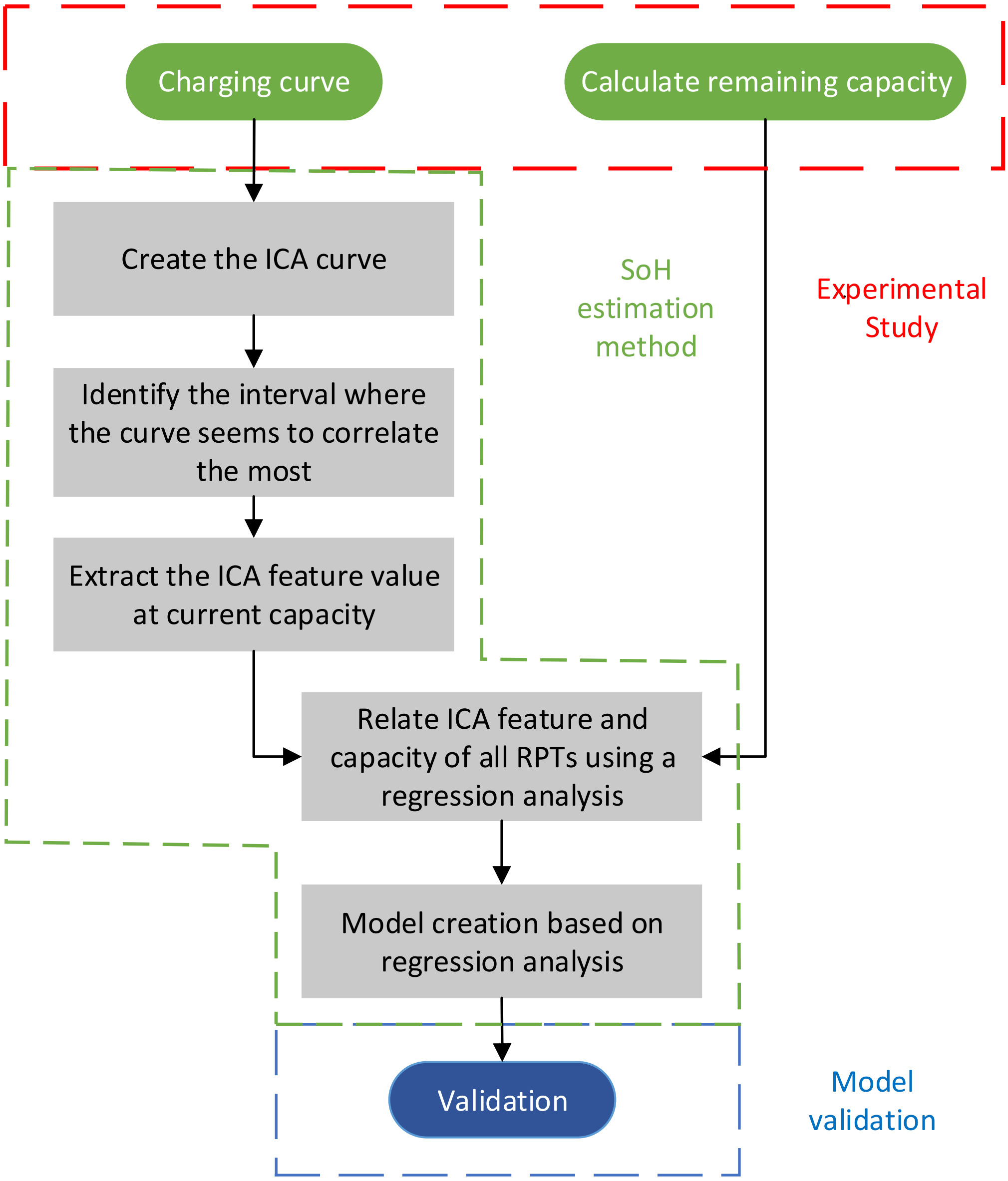

Figure 21 Flowchart of the ICA method. Green indicates an input, blue an output and grey stand for a process. The three different borders visualize in which chapter the processes are described in detail.

3.4.2 Incremental capacity (IC) algorithm in MATLAB

After having the input data created with the RPT, the IC algorithm was applied. Table 7 presents the starting condition of the algorithm. This information is relevant for the shape of the ICA curve and was not changed for the whole study. In Figure 22 the procedure of the IC algorithm is presented. The different colours indicate different stages of the algorithm, which are going to be explained below. The algorithm is based on MATLAB and was amplified during this master thesis.

Table 7 Pre-definitions in the ICA algorithm.

Lower voltage limit	1.5 V
Higher voltage limit	2.8 V
Constant current for 1 C	13 A
Constant current for 1.6 C	20.8 A
Sample time for ICA calculations	50 s
Voltage step for ICA calculations	0.025 V
Capacity step for ICA calculations	1 Ah

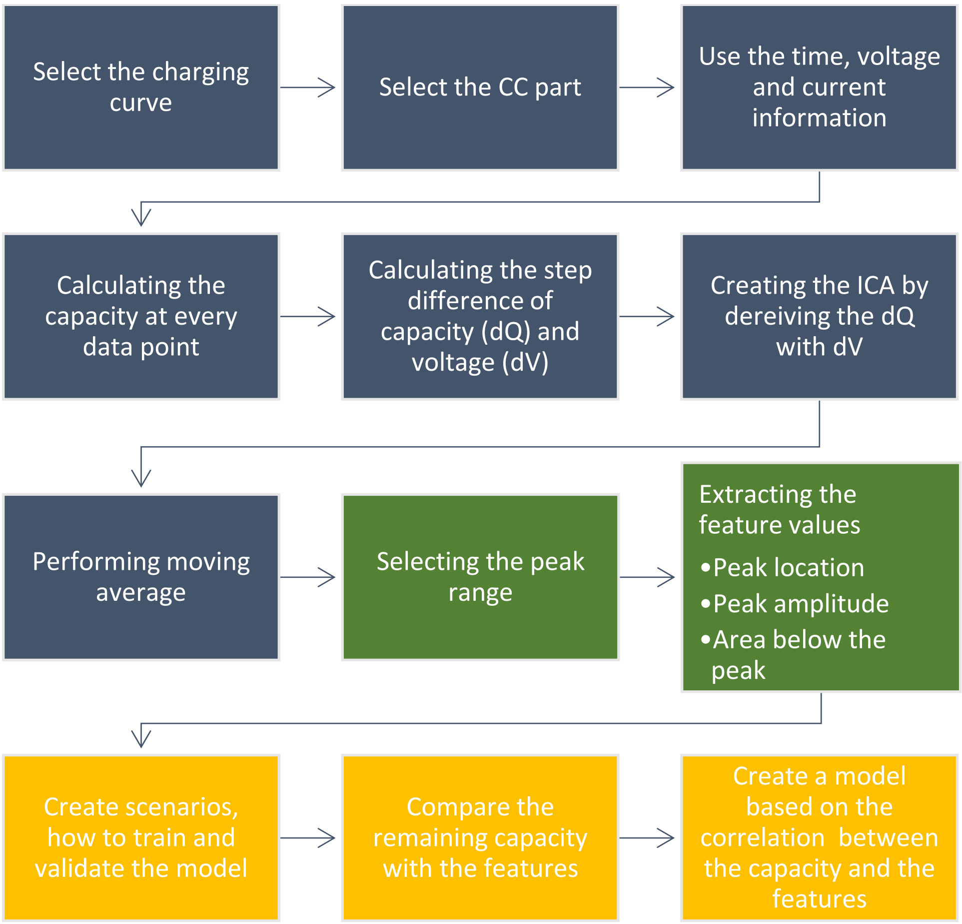

Figure 22 Flowchart describing the ICA algorithm. Dark blue shows the different steps which had to be considered while uploading the data and to prepare before creating the ICA curve. Dark green describes how the feature values were extracted. Yellow represents the model building procedure.

Explanation of the blue part of the flowchart in Figure 22

The charging curves from the RPTs were used as an input of the ICA algorithm. The RPT delivered a lot of different information, of which only the time, the current and the voltage information of the CC charging curve was used. Based on this information, the capacity and the voltage step difference were defined, out of which the ICA curve could be created by deriving the step difference of the capacity by the voltage step difference. Based on moving average, the ICA curve was smoothed. As an output the ICA curves were created.

Explanation of the green part of the flowchart in Figure 22

To define the peak range, the historical data was analysed. CYC8 and CYC13 were already aged before they were used in the experimental study. The historical data from those cells were also available and are presented in Figure 16 and Figure 17. Cell CYC13 was with 8 Ah more aged as cell CYC8 with 14 Ah. It also shows a more unstable behaviour than CYC8, as indicated with the green arrows in Figure 16 and Figure 17. The peak range from 2.2 to 2.3 V was chosen based on the peak distribution of the historical data. This range was plotted in Figure 16, where every peak could be covered with the voltage interval. Also in Figure 17 the range was plotted, but shows at least one outlier within this specified range, as indicated with the orange arrow in Figure 17. This interval was then compared with the data from the experimental study, where it appeared that with the chosen interval, not every peak of the CYC13 ICA curve could be covered. Therefore, the interval was expanded to 2.4 V (see the green line in Table 12). Figure 23 presents an example of this interval for the cell CYC13. After selecting the interval, the three feature values "location", "peak amplitude" and "area" were extracted of all ICA curves from the historical data and on all the ICA curves from the experimental study. These values where then used to define the models.

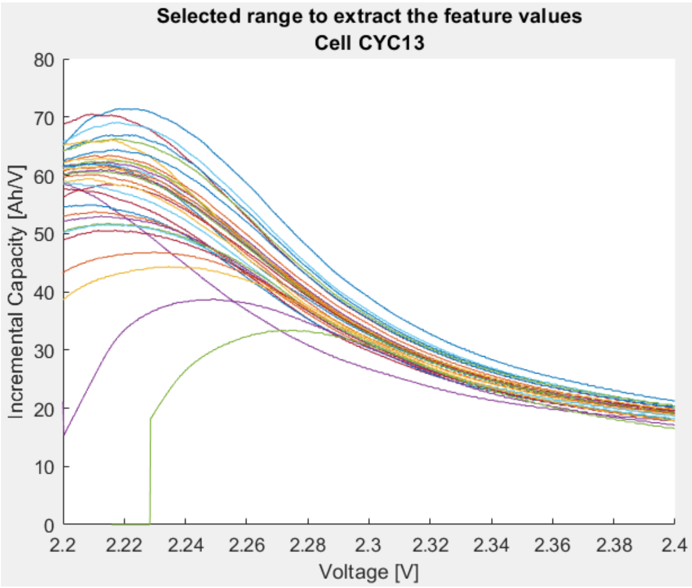

Figure 23 ICA curves in a selected range to extract the feature values on the example of cell CYC13.

Explanation of the yellow part of the flowchart in Figure 22

For each feature, one model was created. Three different scenarios were defined to train and validate the models, as summarizes in Table 8. The scenarios were defined based on the information presented in Figure 24. Scenario 1 uses the historical data from $CYC8_H$ (blue circles) and $CYC13_H$ (red circles) to train the model. To validate scenario 1 uses the cell $CYC8_{ES}$ (red stars) and cell CYC 13_{ES} (blue stars). Scenario 2 uses the same strategy, although the opposite way around. The five samples of each cell from the ES were used to train the model and seven out of 30 samples were chosen randomly to validate the model. As the training samples only had ten data points and the other two scenarios had also either ten or even five samples to validate the model, seven values were considered to be comparable. Scenario 3 uses another strategy, i.e. use the data available above 80 % SoH to train the model and the remaining data (below 80 % SoH) to validate it. In each scenario, the remaining capacity was related to the three different features, extracted from the ICA curves. This was done with a regression analysis, based on which the model was defined. As an example, the three models based on scenario 1 are presented in Table 9, where for each ICA feature of each RPT a data point is displayed. The models of the other scenarios can be found in the Attachment C: Models according to the three scenarios.

Table 8 Definition of the scenarios, where H stands for the historical data and ES for the data established in the experimental study.

Scenario:	1	2	3
Training	$CYC8_H$&$CYC13_H$	$CYC8_{ES}$&$CYC13_{ES}$	SoH > 80 %
Validation	$CYC8_{ES}$&$CYC13_{ES}$	$CYC8_H$&$CYC13_H$	SoH < 80 %

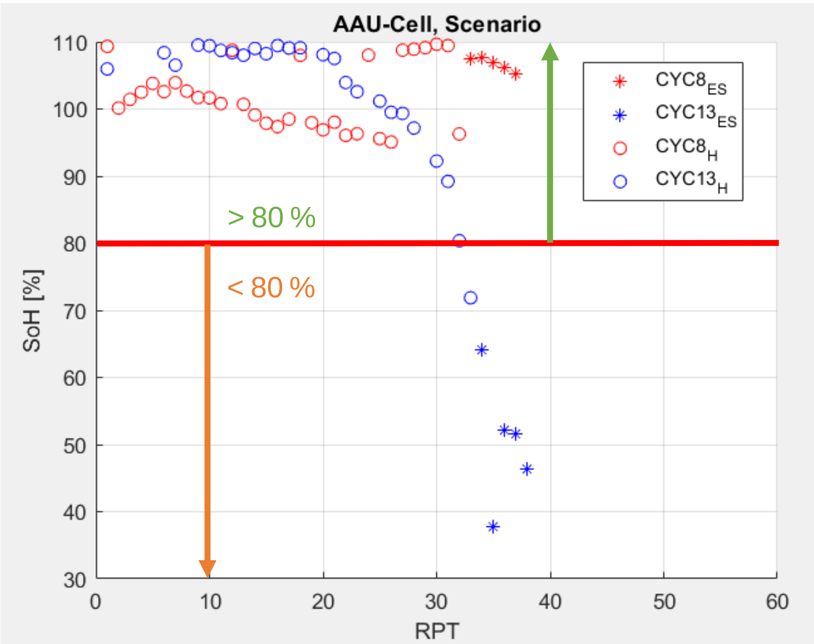

Figure 24 State of health at each RPT, divided into the two battery cells CYC8 & CYC13 and also into historical data (H) and the data created in the experimental study (ES). The red line shows the 80 % SoH.

Table 9 The data of the three different features plotted against the capacity in order to create a linear regression model.

Feature	Scenario 1
Peak locaion	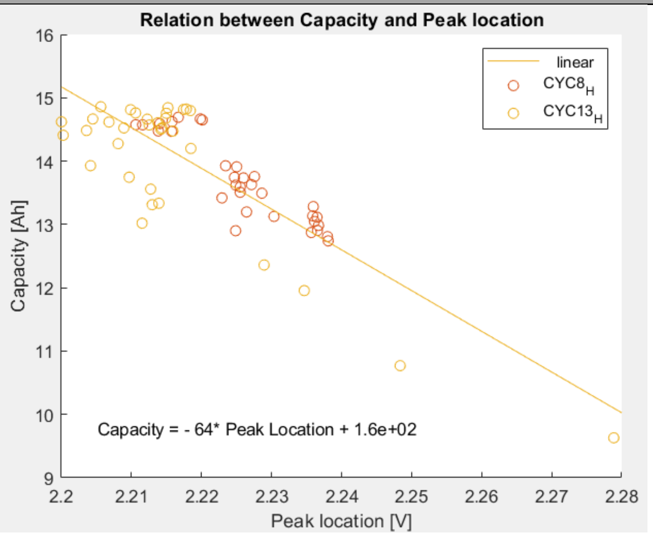
Peak height	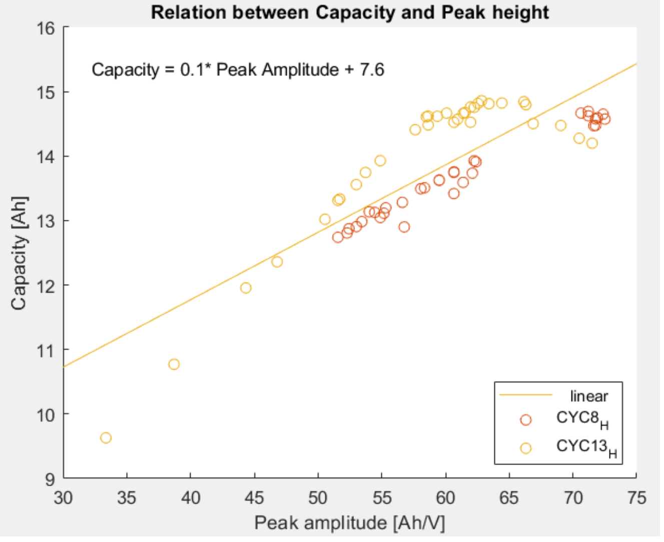
Area	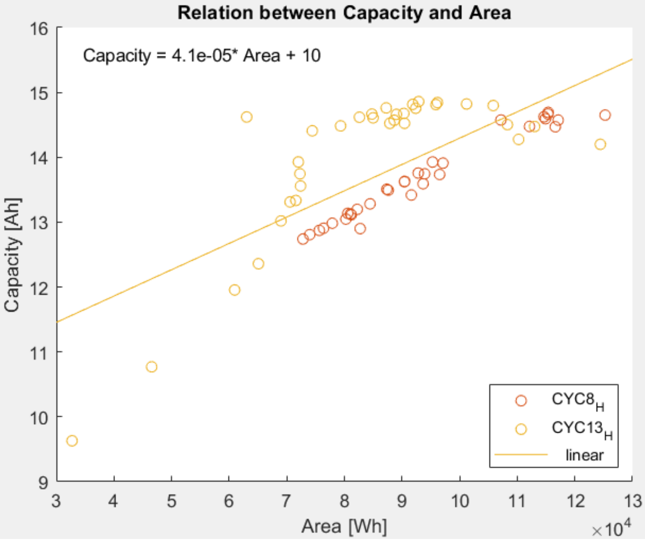

3.4.3 Model diagnostic

As soon as the model was defined, it had to be diagnosed, in order to define its stability. The model diagnostic was divided into five steps, of which each step represents another diagnostic method, see Table 10. Step one shows the adjusted data for the feature “peak location” and the model (red line), similar to the one in Table 9. However, it shows additional a confidence interval of 95 % (dotted line). Adjusted data means that the data was calculated based on the model. This plot indicates how representative the model will be. In the example presented in Table 10 it is expected that this model will have difficulties delivering an accurate output for ICA curves with the peak location in higher voltage ranges. Step two visualizes where the discrepancy of the residuals lies in regard to the peak location. However, with the value of one or less, the model is still expected to be accurate. Step three presents the probability of those residuals, where an accurate model would require that the data points would follow the diagonal line. If the data points drift apart from this line, it is expected, that the model in this area is not accurate enough. Step four shows the residuals plotted against the fitted values. An accurate model would show no trend in the plot. In this example, a small cluster can be seen. However, this trend is not valid for all the data points. The last step analyses the model by numbers. It shows the values of the model intercept (b0) and the steepness (b1) of the linear model, see equation (9). In order to test the model, there is a hypothesis for each of those parts (b0 & b1), which are tested by the t-test. The whole model (f(Y)) is tested by the F-ratio, which represents the t^2. Other important values of the model are the R^2, which should be as close as possible to one, in order to show a linear trend and the p-value, which should be as small as possible, in order to prove that the outcome is no coincidence. All in all, the model diagnostic is an assessment considering all information to make a statement about the stability of the model.

$$Y = b0 + b1 * X \tag{9}$$

Table 10 Model diagnostic for Scenario 1 – Peak location

Step 1. Confidence interval

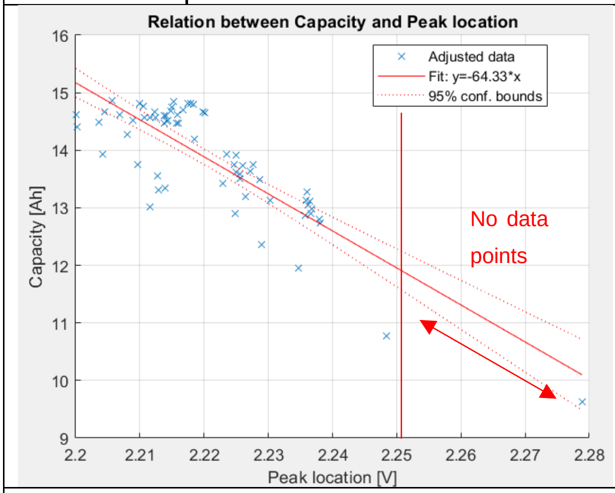

Step 3. Normal probability of residuals

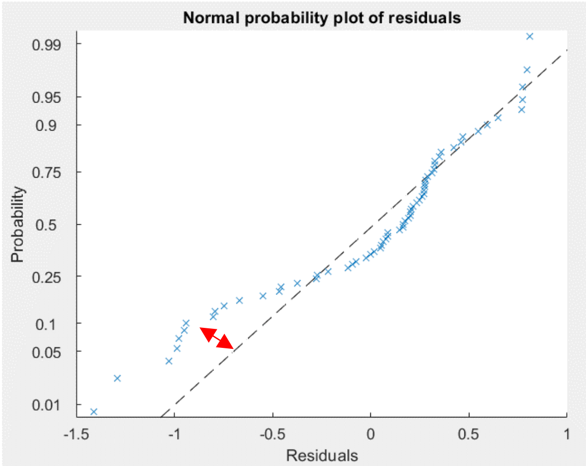

Step 2. Residuals distributed on feature value

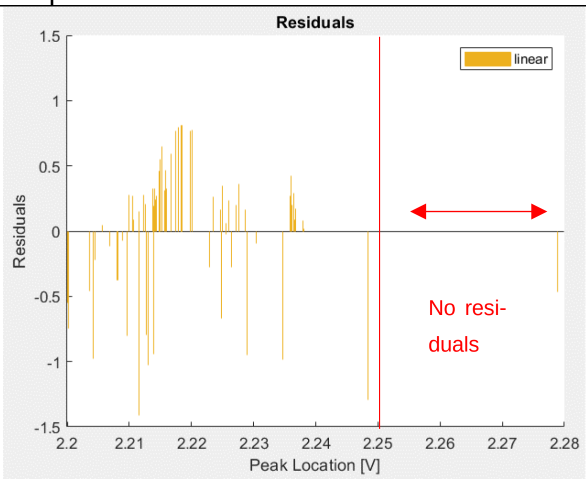

Step 4. Residuals vs. fitted values

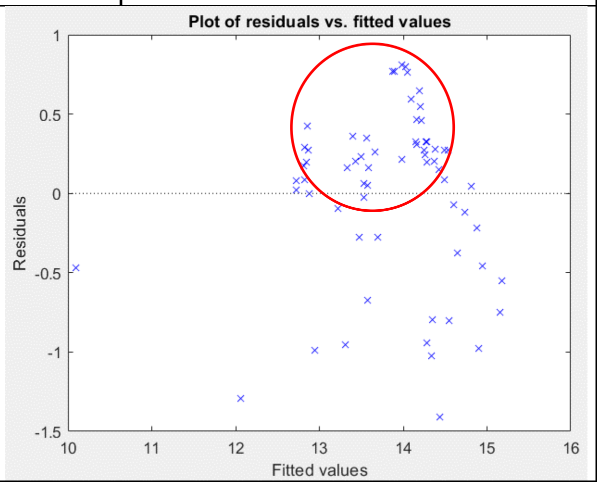

Step 5. Statistical data

Location	Estimate	Standard error	t-value	p-value
Intercept	156.7	11.45	13.69	1.54e-20
Steepness	-64.33	5.16	-12.48	1.11e-18

Number of observations	65
Error degrees of freedom	63
Root Mean Squared Error	0.54
R-squares	**0.71**
Adjusted R-Squared	0.71
F-statistic vs. constant model	156
p-value	**1.11e-18**

3.5 Model validation

After defining the model, it must be tested in order to prove its applicability. This procedure is also called validation. Figure 25 visualises this procedure. As presented in Table 8, the training data and the validation data differ for each scenario. The feature values from both data sets were extracted, whereupon the model was built with the training values. Based on this model, the capacity was estimated with the feature values from the validation data. The outcome from this model was set in reference to the remaining capacity, calculated based on Coulomb counting. Out of this reference, the estimation error was calculated. The estimation error was calculated based on equation (10), where model capacity stands for the capacity estimated with the model and the CC Capacity stands for the capacity calculated with the Coulomb counting method.

$$Estimation\ error = \frac{|\ Cc\ Capacity - \ model\ capacity\ |}{Cc\ Capacity} * 100 \tag{10}$$

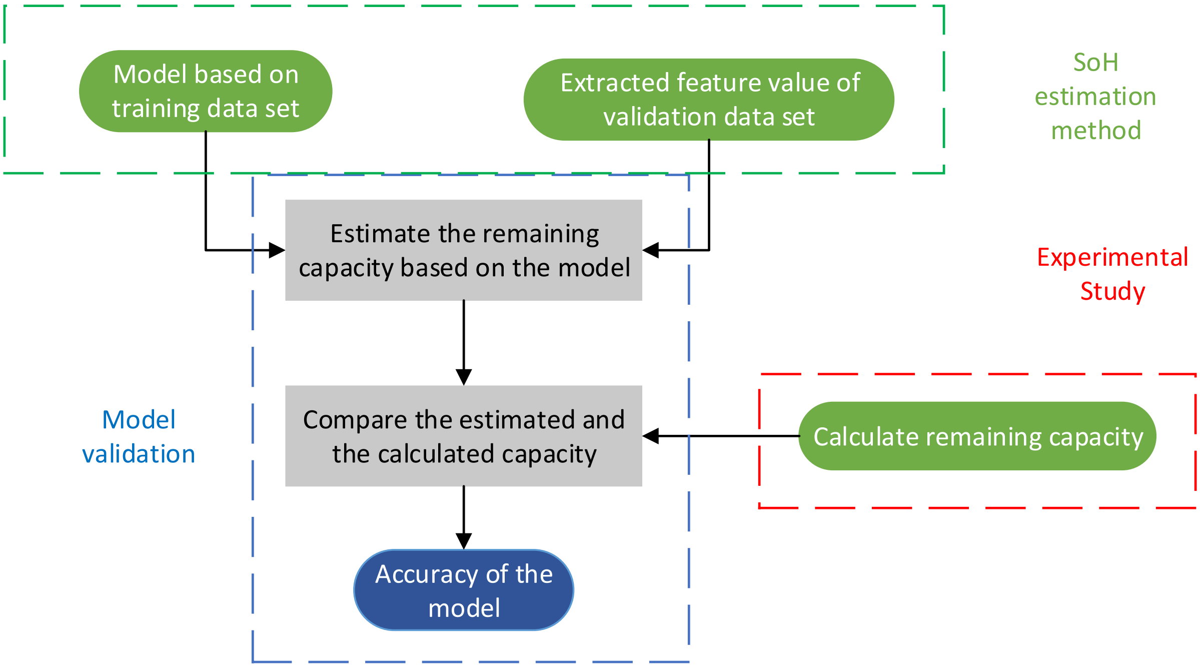

Figure 25 Flowchart of the model validation. Green indicates an input, blue an output and grey stand for a process. The three different borders visualize in which chapter the processes are described in detail.

4 Results and Discussion

4.1 Applying the incremental capacity (IC) algorithm on the output of the reference performance tests (RPT)

As the preparation test, mentioned in section 3.3.3, did not show any inconveniences, the experimental study (ES) was continued as planned. Table 11 summarizes the measured capacity and the SoH obtained after the five RPTs from the ES. It can be seen, that the SoH (see equation (1)) of the cell CYC8 is not falling below 100 %. Neither does the SoH of the fresh cell, it rather shows an increase of the capacity. At beginning of life (BoL) of the cell CYC13, the capacity is 8.6 Ah, which corresponds to a SoH of 64 %. After the first round of ageing with the profile presented in Figure 20, the SoH drops to 38 % and recovers then suddenly at 52 %. According to Chiasserini et. al, (2001) this recovery effect could be explained by a compensation of the active material, by a diffusion process within the battery. This means, that the ions which were deposited in a passive layer could be reused (Eddahech et al., 2013). Figure 26 visualises the capacity development over the five RPTs.

Table 11 Capacity value in [Ah] and the SoH in [%] after each reference performance test (RPT) of the aged battery cells.

Cells		BoL	Eo1stL	Eo2ndL	Eo3dL	Eo4thL
CYC8	Capacity [Ah]	14.40	14.42	14.32	14.22	14.01
	SoH [%]	> 100	> 100	> 100	> 100	> 100
CYC13	Capacity [Ah]	8.60	5.06	6.99	6.92	6.2
	SoH [%]	64	38	52	52	48
fresh	Capacity [Ah]	14.67	14.79	14.8	14.84	14.9
	SoH [%]	> 100	> 100	> 100	> 100	> 100

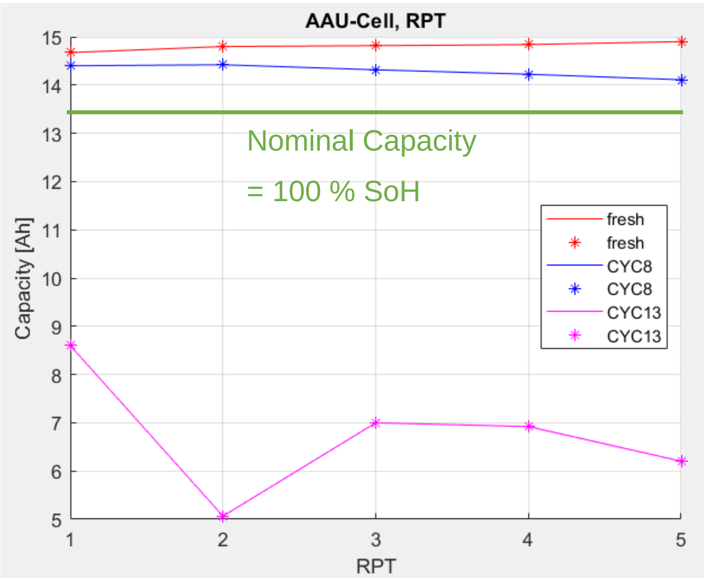

Figure 26 Capacity development of the battery cell CYC8, CYC13 and the fresh cell.

The cell CYC13 seems different to the other batteries, as the capacity development does not follow the same trend. In Figure 24 a noticeable decrease after reaching 90 % SoH can be observed. A similar behaviour was found in Figure 6. The information about the historical ageing procedure listed in Table 5 show that the cell CYC13 was aged from 25-75 % SoC and the cell CYC8 which was aged from 45-55 % SoC. This is in corresponds with the conclusion made by Eckert et al. (2013). Both cells show a similar behaviour in regard to their DoD, as presented in Figure 6. However, the cell CYC13 with a DoD of 50 % shows already a fast degradation after reaching 90 % SoH, where the corresponding curve in Figure 6 shows a fast degradation after reaching 80 %. This could either have something to do with the different cell technology or with the environmental conditions, as the cell in Figure 6 was cycled at 35°C and the cell CYC13 at 42.5°C.

Table 12 presents the ICA plots of the RPT's of this experimental study. It can be seen that there is a difference in the cells above 80 % remaining capacity (CYC8 and fresh) and the one below (CYC13). The ICA curves move faster further away from each other below 80 % SoH. For the 1 C curve of the CYC13, the development has a completely different trend as the others, this is highlighted with the red circle. Also, between the 1 C and 1.6 C curves is a difference noticeable, where it seems, that the amplitude of the ICA curves for 1.6 C are smaller than the one for 1C and also the location of the peak moves more to the right. This confirms the behaviour shown in Figure 8, where the change of the ICA curve, dependent on the C-rate is presented. The one cell not following the same trend is the CYC13 with the 1 C PRT-procedure. Similar findings could be found in Liu et al.'s (2019) paper about the analysis of cyclic ageing performance of commercial LTO cells, although this experiment was proceed with different positive electrode. Their conclusion is that this behaviour is caused by the capacity increase of the cell. Which would also be aligned with the findings described before. According to Liu et al.'s (2019), the reason for the capacity increase is that the degradation changed from losing active material from the positive electrode to an additional degradation of the negative electrode. Which would be a different clarification for the capacity regeneration. However, the battery cells in the mentioned literature were not aged as far as the CYC13 in this experimental study and were also tested with a different current rate. This would lead to the assumption, that the observed behaviour can either occur despites of the cell age or current rate. To draw a conclusion about this behaviour, further investigations are needed, which are out of the scope of this master thesis. Furthermore, it was expected that the same trend could also be seen for 1.6 C, which it does not, see the green circle in Table 12. A behaviour like this was not found in literature.

Table 12 ICA curves of the output from the reference performance tests (RPT) in the experimental study. The red lines indicate the previous mentioned ideal voltage interval. The green lines indicate the adapted voltage range for the cell CYC13.

<table>
<tr><th></th><th>1 C</th><th>1.6 C</th></tr>
<tr><td>CYC8</td><td>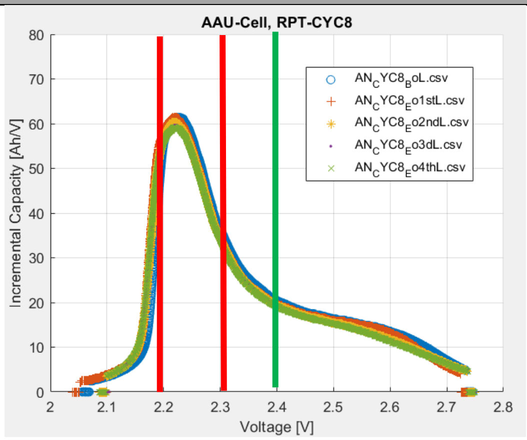
</td><td>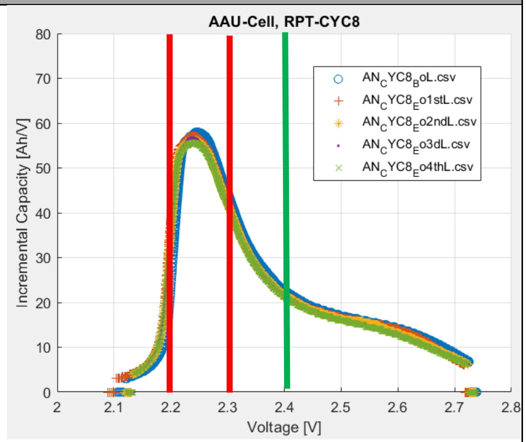
</td></tr>
<tr><td>CYC13</td><td>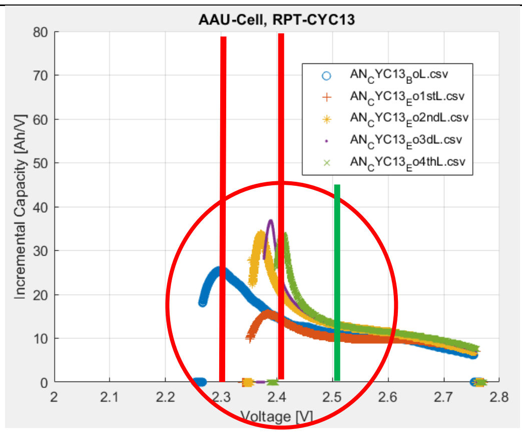
</td><td>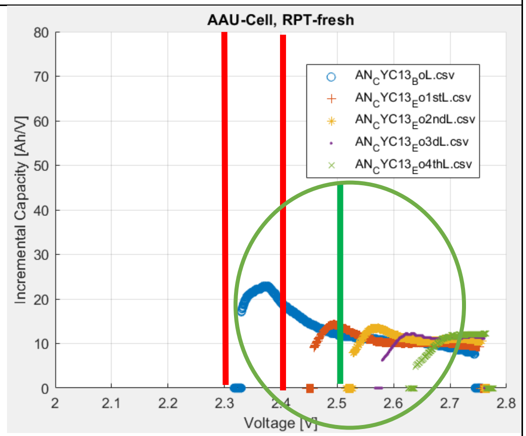
</td></tr>
<tr><td>Fresh cell</td><td>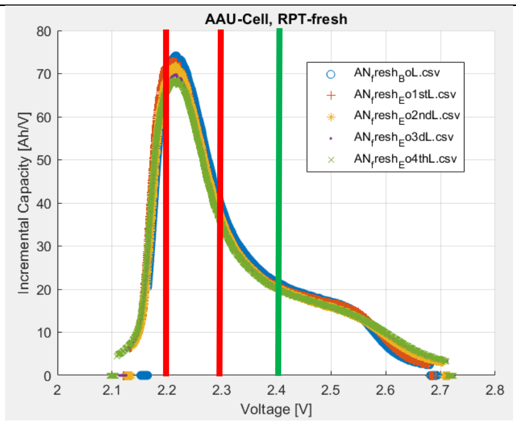
</td><td>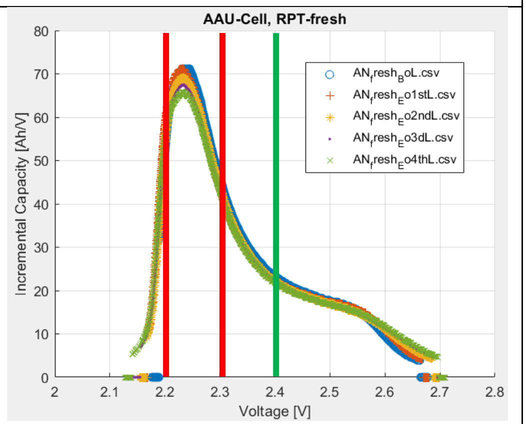
</td></tr>
</table>

4.2 Model based on the incremental capacity (IC) algorithm

4.2.1 Model and model diagnostic

In order to create the models, only the part of the ICA curves between 2.2 and 2.4 V was used, as presented in Figure 23 on the example of the historical data from cell CYC13. According to Table 8 three scenarios were defined, in which for each ICA feature (“location”, “peak amplitude” and “area”) a model was created. In Table 13 to Table 15, the models, together with the corresponding R^2 and the p-value, are presented. In Attachment C: Models according to the three scenarios, those models are visualised as a figure. The R^2 and the p-value are extracted from the model diagnostic, which can be found in Attachment D: Model diagnostic. The model diagnostic supported the validity of the models, based on which the model validation in section 4.2.2 is presented. Table 10 shows the model diagnostic of the feature “location” of the scenario 1.It can be seen that the model provides a reliable model in a lower voltage range, but not for a range with higher voltage values. As it is most likely that the voltage range will increase, when the battery cell ages, it is not expected, that this model can provide an accurate output for battery cells below 80 % capacity. The diagnostic of the model based on the feature “peak amplitude” (see Attachment D: Model diagnostic) shows a similar outcome, although with more samples at lower amplitudes, which would be favourable for cells below 80 % remaining capacity. The model based on the feature “area” (see Attachment D: Model diagnostic) shows a not so promising model diagnostic. It has a much smaller R^2 value, which means that it is not linear in comparison to the other two models. Based on this finding, in scenario 1 the model with the feature “peak amplitude” is considered to be the most accurate model for cells above 80 % remaining capacity. All of the models in scenario 2 show a high R^2, an acceptable p-value and also good diagnostic plots in the attachment. However, it must be taken into account that only five samples were available to train the model. Nevertheless, all three models are considered to be accurate according to the model diagnostic. Scenario 3 shows no promising R^2 values, compared to the other models. Therefore, none of those models are expected to be accurate.

Table 13 ICA models based on the different ICA features from scenario 1

Models	Based on scenario 1	R^2	p-value
Location	Q = -64.33 * U + 156.7	0.71	1.11e-18
Peak amplitude	**Q = 0.10 * ICA + 7.59**	**0.71**	**6.67e-19**
Area	Q = 0.00004 * A + 10.24	0.53	5.08e-12

Table 14 ICA models based on the different ICA features from scenario 2

Models	Based on scenario 2	R^2	p-value
Location	***Q = -49 * U + 123***	***0.96***	***7.84e-07***

Peak amplitude	***Q = 0.22 * ICA + 1.03***	***0.92***	***9.77e-06***
Area	**Q = 0.00009 * A + 6.06**	**0.98**	**4.94e-08**

Table 15 ICA models based on the different ICA features from scenario 3

Models	Based on scenario 3	R^2	p-value
Location	Q = -52.7 * U + 131	0.52	4.05e-12
Peak amplitude	Q = 0.085 * ICA + 8.8	0.59	1.17e-14
Area	Q = 0.00003 * A + 11.29	0.38	2.16e-08

4.2.2 Validation of the model

The models were validated based on equation (10). The outcome of all models can be found in Attachment E: Model validation. In Table 16 the average value of the models with the best model diagnostic are presented. In scenario 1 the model is more accurate for cell CYC8 then for cell CYC13. It is assumed, that this is because the model was trained with the historical data, which are mostly above 80 % SoH, as presented in Figure 24. The models in scenario 2 have a much more equal outcome for both cells. Here the models were trained with the data from the experimental study and were validated with the historical data.

One research question asked for an estimation error below 5 %. This could be achieved for all cases of the cell CYC8, but not for the cell CYC13. However, in scenario 2, the model based on the feature “location” could also achieve a value below 5% for cell CYC13. Therefore, it is assumed, that the feature “location” correlates the best with the remaining capacity, at any SoH level. Based on the validation with the fresh cell, an accurate outcome is also expected for newer cells.

Table 16 Average estimation error between the estimated capacity and the calculated remaining capacity.

Scenario	Model	Validation data	Estimation error
1	Peak amplitude	CYC8_ES	5%
1	Peak amplitude	CYC13_ES	57%
2	**Location**	**CYC8_H**	**3%**
2	**Location**	**CYC13_H**	**4%**
2	Peak amplitude	CYC8_H	5%
2	Peak amplitude	CYC13_H	9%
2	Area	CYC8_H	5%
2	Area	CYC13_H	8%
2	**Location**	**Fresh cell_ES**	**2.3%**

4.2.3 Applicability of the method

The ICA method refers to how to measure the voltage, the current and the time, which are needed to derive the ICA plot and then to apply the ICA algorithm. In order to provide a fast and accurate method, the goal would be to measure those values only on a certain voltage range, as illustrated in Figure 7. In this master thesis the voltage range was chosen to be from 2.2 to 2.4 V. It is expected that this already could save up to 20 minutes of the charging procedure. An advantage of limiting the voltage in comparison to other parameter is, that it can be measured directly, so it is a fast way to determine the voltage range. However, as the voltage range is dependent on the cell age, this voltage range must be defined for the application in the second life. Then, based on the information gathered in Table 12, it can be said that the cells below 80 % need a wider range than the cells above. Even though the method was only tested in a certain voltage interval, one model with a high accuracy could be provided for cells below and above 80 % remaining capacity. In the example presented in Figure 20, the most frequent C-rate during the normal load cycle is 1.6 C, which is indicated with the green line. The tests with 1.6 C show that the voltage interval must be chosen even bigger than the one for 1 C. Based on this outcome, it is assumed that there would be an optimal charging length which considers not only the voltage range, also the ideal C-rate.

There are different ways to apply this method. However, in order to keep the battery as long as possible in the life cycle, it would make sense to apply it while the battery is still in the vehicle.An important requirement for the ICA method is, that the conditions are the same for every time the method is applied. This means, that the battery would have the same environmental conditions (i.e. temperature) and the same C-rate is used to charge the battery. To ensure a stable environment, it would make sense to apply the method in a workshop or in a garage and not while driving.

5 Conclusion

5.1 Findings

1. **Can the ICA method still deliver an estimation with a percentage error below the average estimation error of 5 %, if only a partial charging or discharging is performed?**

Based on the information gathered in chapter 4, it can be said, that it is possible to estimate the SoH accurately with only a partial charging procedure, also below 5 %. However, the voltage interval must be defined in such a way that the identification of the ICA peak can be obtained. In Table 12 the interval is presented. Based on the historical data, the red lines would have been wide enough, although considering the data from the experimental study, it had to be expanded to the green line. This leads to the assumption that the interval increases with increasing battery degradation. This method was only tested on the charging curve and not on the discharging curve.

2. **Is the ICA method applicable for batteries with a capacity below 80 %?**

Here as well a positive outcome was found. The ICA method is also applicable on batteries below 80 % remaining capacity, although the estimation error is depending on the training of the model. In this master thesis, training of the model with the experimental study gave the most accurate output for the older cells. This leads to the assumption, that a model only based on new RPTs could still deliver an accurate outcome to estimate the SoH. However, it must also be considered that the voltage interval increases with decreasing SoH.

3. **Which SoH indicator of the ICA method deliver the most accurate outcome for batteries with a capacity below 80 %?**

The validation of the model based on the feature “location” from scenario 2 is the only model which shows an estimation error of below 5 % for all battery cells used in this study. Therefore, the model in equation (11) is expected to be the most accurate for the cells below 80 % remaining capacity, where *Q* stands for the capacity and *U* for the peak location in volt.

$$Q = -49 * U + 123 \tag{11}$$

5.2 Future work

As the cell CYC13 did show some unexpected outcome, it is on one hand proposed to perform a post-mortem analysis, in order to be sure, where this behaviour is coming from. On the other hand, it is proposed to validate the model in equation (11) with another, independent LTO-cell, with the same nominal capacity but a remaining capacity of around 70 %. Given that the focus in this master thesis lies on battery cells below 80 % remaining capacity. Furthermore, the fresh battery cell did already deliver a good outcome.

Additionally, it shall be tested, if similar outcomes can be achieved, if this method is applied in a workshop and not under laboratory conditions. It shall also be verified, if there is a difference, if only the specified voltage interval is charged and measured, as in this study the interval was applied manually, after the measurement. The goal should be, that this method can be applied in every workshop or garage.

Another issue of this master thesis which needs further attention is the voltage interval, on which the method should be applied. This interval is dependent on the cell age and the current rate (C-rate), which is used to extract the current curve. It is proposed to find the ideal voltage interval for this cell technology and then to repeat the test with the new interval. For that however, one or more cells must be aged to the point where it would be ready for disposal. That way, it is known how wide the voltage interval could reach. However, studies have no common opinion about the very end of a battery. One study concludes that an Eo2ndL would be expected at around 60 % remaining capacity (Canals Casals et al., 2018), another one at 40 % remaining capacity (Montoya-Bedoya et al., 2020).

Bibliography

Berecibar, M., Gandiaga, I., Villarreal, I., Omar, N., Van Mierlo, J., & Van den Bossche, P. (2014). Critical review of state of health estimation methods of Li-ion batteries for real applications. *Elsevier*, *Renewableand Sustainable Energy Reviews*, 16. http://dx.doi.org/10.1016/j.rser.2015.11.042

Birkl, C. R., Roberts, M. R., McTurk, E., Bruce, P. G., & Howey, D. A. (2016). Degradation diagnostics for lithium ion cells. *Elsevier*, *Journal of Power Sources*, 14. http://dx.doi.org/10.1016/j.jpowsour.2016.12.011

BU-205: Types of Lithium-ion. (2020, March 12). Battery University. Accessed on 2020-10-10. https://batteryuniversity.com/learn/article/types_of_lithium_ion

Canals Casals, L., Amante Garcia, B., & Canal, C. (2018). Second life batteries lifespan: Rest of useful life and environmental analysis. *Elsevier*, *Journal of Environmental Management*, 10. https://doi.org/10.1016/j.jenvman.2018.11.046

Chiasserini, C.-F., & Rao, R. R. (2001). Improving Battery Performance by Using Traffic Shaping Techniques. *IEEE*, *Journal on selected areas in communications (19, No. z)*, 10. https://doi.org/S 0733-8716(01)04998-8

Dai, Q., Kelly, J. C., Gaines, L., & Wang, M. (2019). Life Cycle Analysis of Lithium-Ion Batteries for Automotive Applications. *Batteries*, 15. https://doi.org/10.3390/batteries5020048

Directive of the European Parlament and of the council on batteries and accumulators and waste batteries and accumulators (DIRECTIVE 2006/66/EC). (6. September 2006)., Pub. L. No. 2006L0066, 28 (2013).

Electrically propelled road vehicle—Test specification for lithium-ion traction battery packs and systems—Part 4: Performance testing, DS/ISO 12405-4:2018 82 (2018).

Dubarry, M., & Liaw, B. X. (2009). Identify capacity fading mechanism in a commercial LiFePO4 cell. *Elsevier*, *Journal of Power Sources*, 9. https://doi.org/doi:10.1016/j.jpowsour.2009.05.036

Eckert, M., Nieto, N., Käbitz, S., Schmalstieg, J., Blanke, H., Warnecke, A., & Sauer, D. U. (2013). Calendar and cycle life study of Li(NiMnCo)O2-based 18650 lithiumion batteries. *Elsevier*, *Journa of Power Sources*, 13. http://dx.doi.org/10.1016/j.jpowsour.2013.09.143

Eddahech, A., Briat, O., & Vinassa, J.-M. (2013). Lithium-ion battery performance improvement based on capacityrecovery exploitation. *Elsevier*, *Electrochimica Acta*, 8. http://dx.doi.org/10.1016/j.electacta.2013.10.101

Edström, K., & Perraud, S. (2019). *Inventing the batteries of the future—Research needs and future actions* (2nd ed.). Battery 2030+. https://battery2030.eu/digitalAssets/815/c_815818-l_1-k_battery-2030_roadmap-v2.1.pdf

Fischhaber, S., Regett, A., Schuster, S. F., & Dr. Hesse, H. (2016). *Second-Life-Konzepte für Lithium-Ionen-Batterien aus Elektrofahrzeugen Analyse von Nachnutzungsanwendungen, ökonomischen und ökologischen Potenzialen* (p. 156). Schaufenster Elektromobilität.

Fly, A., & Chen, R. (2020). Rate dependency of incremental capacity analysis (dQ/dV) as a diagnostic tool for lithium-ion batteries. *Elsevier*, *Journal of Energy Storage*, 13. https://doi.org/10.1016/j.est.2020.101329

Grandjean, T. R. B., Groenewald, J., McGordon, A., Widanage, W. D., & Marco, J. (2018). Accelerated Internal Resistance Measurements of Lithium-Ion Cells to Support Future End-of-Life Strategies for Electric Vehicles. *Batteries*, 17.

Han, X., Ouyang, M., Lu, L., & Li, J. (2014). Cycle Life of Commercial Lithium-Ion Batteries with Lithium Titanium Oxide Anodes in Electric Vehicles. *Energies*, 15. https://doi.org/10.3390/en7084895

Huang, K., Guo, Y.-F., Tseng, M.-L., Wu, K.-J., & Li, Z.-G. (2018). A Novel Health Factor to Predict the Battery's State-of-Health Using a Support Vector Machine Approach. *Applied Science*, 21. https://doi.org/10.3390/app8101803

Hustadt, D. (2018, September 19). *Second Life Batterien: Potential für Energiespeicher*. https://corporate.vattenfall.de/

IEA. (2019a, May). *Global EV Outlook*. International Energy Agency. Accessed on 2020-12-26. https://www.iea.org/reports/global-ev-outlook-2019

IEA. (2019b, November). *Change in final energy consumption by sector, 2000-2018, and by scenario to 2040*. International Energy Agency. Accessed on 2020-09-04. https://www.iea.org/data-and-statistics/charts/change-in-final-energy-consumption-by-sector-2000-2018-and-by-scenario-to-2040

Klotz, D., & Schönleber, M. (2010). *Kombinierten Messverfahrensfür Lithium-Ionen Batterien im Zeit-und Frequenzbereich* [Workshop].

Lee, H., Park, J., & Kim, J. (2019). Incremental Capacity Curve Peak Points-Based Regression Analysis for the State-of-Health Prediction of a Retired LiNiCoAlO2 Series/Parallel Configured Battery Pack. *Electronics*, 23. https://doi.org/10.3390/electronics8101118

Li, X., Yuan, C., Li, X., & Wang, Z. (2019). State of health estimation for Li-Ion battery using incremental capacity analysis and Gaussian process regression. *Elsevier*, *Energy*, 11. https://doi.org/10.1016/j.energy.2019.116467

Lin, C. P., Cabrera, J., Yu, D. Y. W., Yang, F., & Tsui, K. L. (2020). SOH Estimation and SOC Recalibration of Lithium-Ion Battery with Incremental Capacity Analysis & Cubic Smoothing Spline. *The Electrochemical Society*, 16. https://doi.org/10.1149/ 1945-7111/ab8f56

Liu, S., Winter, M., Lewerenz, M., Becker, J., Sauer, D. U., Ma, Z., & Jiang, J. (2019). Analysis of cyclic aging performance of commercial Li4Ti5O12-based batteries at room temperature. *Elsevier*, *Energy*, 13. https://doi.org/10.1016/j.energy.2019.02.150

Martinez-Laserna, E., Gandiaga, I., Sarasketa-Zabala, E., Badeda, J., Stroe, D.-I., Swierczynski, M., & Goikoetxea, A. (2018). Battery second life: Hype, hope or reality? A critical review of the state of the art. *Elsevier*, *Renewable and Sustainable Eergy Reviews*, 18. https://doi.org/10.1016/j.rser.2018.04.035

Meuser, C. (2011). *Physikalische und chemische Charakterisierung von Lithiumionenzellen* [Dissertation]. Fakultät Mathematik und Naturwissenschaften der Technischen Universität Dresden.

Montoya-Bedoya, S., Sabogal-Moncada, L. A., Garcia-Tamayo, E., & Martínez-Tejada, H. V. (2020). A Circular Economy of Electrochemical Energy Storage Systems: Critical Review of SOH/RUL Estimation Methods for Second-Life Batteries. *IntechOpen*, 22. http://dx.doi.org/10.5772/intechopen.91257

Nagpure, S. C., Downing, G., Bhushan, B., Babu, S. S., & Cao, L. (2011). Neutron depth profiling technique for studying aging in Li-ion batteries. *Elsvier*, *Electrochimica Acta*, 9. https://doi.org/10.1016/j.electacta.2011.02.037

Nemeth, T., Schröer, P., Kuipers, M., & Sauer, D. U. (2020). Lithium titanate oxide battery cells for high-power automotive applications—Electro-thermal properties, aging behavior and cost considerations. *Elsevier*, *Energy Storage*, 14. https://doi.org/10.1016/j.est.2020.101656

Pastor-Fernández, C., Fai Yu, T., Dhammika Widanagea, W., & Marcoa, J. (2019). Critical review of non-invasive diagnosis techniques for quantification of degradation modes in lithium-ion batteries. *Elsevier*, *Renewable and Sustainable Energy Reviews*, 22. https://doi.org/10.1016/j.rser.2019.03.060

Pillot, C. (2019, May 28). *The Rechargeable Battery Market and Main Trends* [Seminar]. Avicenne Energy, Paris, France.

Qu, S., Kang, Y., Gu, P., Zhang, C., & Duan, B. (2019). A Fast Online State of Health Estimation Method for Lithium-Ion Batteries Based on Incremental Capacity Analysis. *Energies*, 11. https://doi.org/10.3390/en12173333

Quinard, H., Redondo-Iglesia, E., Pelissier, S., & Venet, P. (2019). Fast Electrical Characterizations of High-Energy Second Life Lithium-Ion Batteries for Embedded and Stationary Applications. *Batteries*, 18. https://doi.org/10.3390/batteries5010033

Rahimzei, E., Sann, K., & Dr. Vogel, M. (2015). *Li-Ionen-Batterien* [Kompendium]. Verband der Elektrotechnik (VDE).

Reddy, T. B. (2011). *Linden's Handbook of Batteries* (4th ed.). The McGraw-Hill Companies.

Riviere, E., Sari, A., Venet, P., Meniere, F., & Bultel, Y. (2019). Innovative Incremental Capacity Analysis Implementation for C/LiFePO4 Cell State-of-Health Estimation in Electrical Vehicles. *Batteries*, 13. https://doi.org/10.3390/batteries5020037

Schalz, E., Stroe, D.-I., Noerregaad, K., Stenhoej Kofod, L., & Christensen, A. (2019). Incremental Capacity Analysis Applied on Electric Vehicles for Battery State-of-Health Estimation. *IEEE*, 6. Aalborg Universitetsbibliothek.

Sterner, M., & Stadler, I. (2014). *Energiespeicher – Bedarf, Technologien, Integration* (1st ed.). Springer Verlag.

Stolz, P. (2019, September 12). *Ökobilanz von Lithium-Ionen Batterien* [Seminar]. Second - Life Tagung, ETH, Zurich.

SUNBATT. (2015, December). Circe. Accessed on 2020-02-11. https://www.fcirce.es/en/smart-mobility-en-en/sunbatt-2

Tian, J., Xiong, R., & Shen, W. (2019). A review on state of health estimation for lithium ion batteries in photovoltaic systems. *Elsevier*, *eTransportation*, 53. https://doi.org/10.1016/j.etran.2019.100028.

Venugopal, P., & Vigneswaran, T. (2019). State-of-Health Estimation of Li-ion Batteries in Electric Vehicle Using IndRNN under Variable Load Condition. *Energies*, 29. https://doi.org/10.3390/en12224338

Wei, Z., Leng, F., He, Z., Zhang, W., & Li, K. (2018). Online State of Charge and State of Health Estimation for a Lithium-Ion Battery Based on a Data–Model Fusion Method. *Energies*, 16. https://doi.org/10.3390/en11071810

Xia, B., Chen, G., Zhou, J., Yang, Y., Huang, R., Wang, W., Lai, Y., Wang, M., & Wang, H. (2019). Online Parameter Identification and Joint Estimation of the State of Charge and the State of Health of Lithium-Ion Batteries Considering the Degree of Polarization. *Energies*, 13. https://doi.org/10.3390/en12152939

Zhao, L., Wang, Y., & Cheng, J. (2019). A Hybrid Method for Remaining Useful Life Estimation of Lithium-Ion Battery with Regeneration Phenomena. *Applied Science*, 15. https://doi.org/10.3390/app9091890

List of Figures

Figure 1 Market share of different battery types, where lithium-ions show the biggest market growth (Pillot, 2019). Lead Acid stands for Lead Acid batteries; NiCD stands for nickel-cadmium battery; NiMH stands for nickel-metal hybride battery; Li-ion stands for Lithium-ion batteries; others stands for all other batterie types as for example Flow batteries and NAS, which stands for Sodium-sulfur battery. The two arrows show the slope of the market growth. 9

Figure 2 Overview of the second life concept (Montoya-Bedoya et al., 2020). The dashed box indicates the importance of the state of health estimation. 11

Figure 3 Visualization of the most common SOH estimation methods, based on (Berecibar et al., 2014; Pastor-Fernández et al., 2019; Tian et al., 2019; Venugopal & Vigneswaran, 2019; Xia et al., 2019). The orange dashed lines indicate an indirect connection between the impedance-based and capacity-based method and the battery models. As well as the indirect connection between the battery models and the adaptive models. The different blue brightness indicates the level in the hierarchy. 13

Figure 4 Design and working principle of a commercial Lithium-ion battery (Reddy, 2011). $LiMO_2$-Electrode is also called LMO-electrode and means lithium-manganese-oxide-electrode, Li_xC is the graphite structure with inserted Lithium-ions. Li^+ stands for the positive Lithium-ions and e^- for the electrons. 17

Figure 5 Long term impact of temperature on capacity on the example of an LCO/graphite cell (Reddy, 2011, p. 869). 20

Figure 6 Long term impact of depth of discharge (DoD) on capacity (Eckert et al., 2013, p. 8). The green box highlights the DoD of the cell CYC13 and the orange box the DoD of cell CYC8. 20

Figure 7 Demonstrative incremental capacity analysis (ICA) procedure with a LTO/LNMC cell, where a) shows the CC charging current, b) the CC charging voltage, c) the capacity increase, d) the capacity vs. voltage and e) the capacity derived by the voltage, resulting in the ICA curve. The orange lines indicate the voltage level in the range between 2.2 and 2.4 V. The blue arrow indicates the time to measure the whole charging curve in order to create the ICA curve. The green arrow indicates the time needed for a partial charging. 22

Figure 8 Incremental capacity curve with same state of health (SoH) but different current rates (C-rate) (Riviere et al., 2019). Here at the example of a C/LFP cell. The red arrow indicates the change with increasing current rate. 23

Figure 9 Short term impact of the current rate (C-rate) on the capacity (Reddy, 2011, p. 867). The red arrow indicates the increase of the capacity with increasing current rate (C-rate). 23

Figure 10 ICA curve with the dependency of temperature (Riviere et al., 2019). Here at the example of a C/LFP cell. The red arrow indicates the change with increasing temperature. 24

Figure 11 Short term impact of the temperature on the capacity (Reddy, 2011, p. 868). The red arrow indicates the change with increasing temperature. 24

Figure 12 A partial ICA curve on an example of an LTO/LNMC cell, where the voltage interval between 2.2 and 2.4 V is chosen. The area [Ah] is indicated in blue; the peak amplitude [Ah/V] is indicated with the orange arrow and the peak location [V] is indicated with the green arrow. 25

Figure 13 Overview of the procedure in order to create a SoH estimation model. Green indicates an input, blue an output and grey stands for a process. The three different borders visualize in which chapter the processes are described in detail. *26*
Figure 14 Experimental study - the procedure was repeated four times. *27*
Figure 15 Organisation of the data collection. Light grey indicates the labeling of the data and dark blue indicates the procedure between two data sets. RPT stands for reference performance test; BoL stands for begin of life; EoL stands for end of life, where the number 1st, 2nd, 3d and 4th are added to it. *27*
Figure 16 ICA curves of the historical data from cell CYC8, conducted with 1 C. The red lines indicate the voltage interval. The green arrow indicated the ageing direction. *29*
Figure 17 ICA curves of the cell historical data from cell CYC13, conducted with 1 C. The red lines indicate the voltage interval, the green arrow indicated the ageing direction, the orange arrow highlights an outlier. *29*
Figure 18 Battery cell in thermal chamber connected to the battery cycler, which demands the specified load cycle from the battery cell and measures the voltage, the current and the temperature. *30*
Figure 19 Constant current (CC) and constant voltage (CV) procedure on the example of a LTO/LNMC cell. The red lines highlight the shift from CC to CV. *31*
Figure 20 Track profile used to age the batteries in the experimental study. *32*
Figure 21 Flowchart of the ICA method. Green indicates an input, blue an output and grey stand for a process. The three different borders visualize in which chapter the processes are described in detail. *33*
Figure 22 Flowchart describing the ICA algorithm. Dark blue shows the different steps which had to be considered while uploading the data and to prepare before creating the ICA curve. Dark green describes how the feature values were extracted. Yellow represents the model building procedure. *34*
Figure 23 ICA curves in a selected range to extract the feature values on the example of cell CYC13. .... *35*
Figure 24 State of health at each RPT, divided into the two battery cells CYC8 & CYC13 and also into historical data (H) and the data created in the experimental study (ES). The red line shows the 80 % SoH. *36*
Figure 25 Flowchart of the model validation. Green indicates an input, blue an output and grey stand for a process. The three different borders visualize in which chapter the processes are described in detail. *40*
Figure 26 Capacity development of the battery cell CYC8, CYC13 and the fresh cell. *41*

List of Tables

Table 1 Advantages and Disadvantages of the five defined SoH estimation categories based on literature research. *14*
Table 2 Overview of the most common lithium-ion technologies (BU-205: Types of Lithium-Ion, 2020; Meuser, 2011). LNMC stands for lithium-nickel-manganese-cobalt-oxide; LFP stands for lithium-iron-phosphate; LMO stands for lithium-manganese-oxide; LCO stands for lithium-cobalt-oxide; LNCA stands for lithium-nickel-cobalt-aluminum-oxide; C stands for graphite. *18*
Table 3 Stress factors for cell ageing (Sterner & Stadler, 2014). *19*
Table 4 Nominal information of LTO battery cells *28*

Table 5 Introduction of the battery cells under test. Cycle interval in State of charge (SoC), 2 C means that the throughput of the nominal capacity of 13.4 Ah is conducted twice as fast as nominal – in this case, in a half an hour. *29*
Table 6 Used equipment for the experimental study and its accuracy. *30*
Table 7 Pre-definitions in the ICA algorithm. *34*
Table 8 Definition of the scenarios, where H stands for the historical data and ES for the data established in the experimental study. *36*
Table 9 The data of the three different features plotted against the capacity in order to create a linear regression model. *37*
Table 10 Model diagnostic for Scenario 1 – Peak location *39*
Table 11 Capacity value in [Ah] and the SoH in [%] after each reference performance test (RPT) of the aged battery cells. *41*
Table 12 ICA curves of the output from the reference performance tests (RPT) in the experimental study. The red lines indicate the previous mentioned ideal voltage interval. The green lines indicate the adapted voltage range for the cell CYC13. .... *43*
Table 13 ICA models based on the different ICA features from scenario 1 .... *44*
Table 14 ICA models based on the different ICA features from scenario 2 .... *44*
Table 15 ICA models based on the different ICA features from scenario 3 .... *45*
Table 16 Average estimation error between the estimated capacity and the calculated remaining capacity. *45*
Table 17 Models according to the three scenarios. *61*
Table 18 Model diagnostic for Scenario 1 – Peak location *64*
Table 19 Model diagnostic for Scenario 1 – Peak amplitude *65*
Table 20 Model diagnostic for Scenario 1 – Area *66*
Table 21 Model diagnostic for Scenario 2 – Peak location *67*
Table 22 Model diagnostic for Scenario 2 – Peak amplitude *68*
Table 23 Model diagnostic for Scenario 2 – Area *69*
Table 24 Model diagnostic for Scenario 3 – Peak location *70*
Table 25 Model diagnostic for Scenario 3 – Peak amplitude *71*
Table 26 Model diagnostic for Scenario 3 – Area *72*
Table 27 Model output and estimation error of the feature "location". *73*
Table 28 Model output and estimation error of the feature "peak". *73*
Table 29 Model output and estimation error of the feature "area". *73*
Table 30 Model output and estimation error of the feature "location". *74*
Table 31 Model output and estimation error of the feature "peak". *74*
Table 32 Model output and estimation error of the feature "area". *74*
Table 33 Model output and estimation error of the feature "location". *75*
Table 34 Model output and estimation error of the feature "peak". *75*
Table 35 Model output and estimation error of the feature "area". *75*
Table 36 Model output and estimation error of the feature "location". *76*

Table 37 Model output and estimation error of the feature "peak". *76*
Table 38 Model output and estimation error of the feature "area". *76*
Table 39 Model output and estimation error of the feature "location". *77*
Table 40 Model output and estimation error of the feature "peak". *77*
Table 41 Model output and estimation error of the feature "area". *77*

Attachments

Attachment A: Declaration of plagiarism

Zürcher Hochschule für Angewandte Wissenschaften

Life Sciences und Facility Management

DECLARATION OF ORIGINALITY

Master's Thesis for the School of Life Sciences and Facility Management

By submitting this Master's thesis, the student attests of the fact that all the work included in the assignment is their own and was written without the help of a third party.

The student declares that all sources in the text (including Internet pages) and appendices have been correctly disclosed. This means that there has been no plagiarism, i.e. no sections have been partially or wholly taken from other texts and represented as the student's own work or included without being correctly referenced.

Any misconduct will be dealt with according to paragraphs 39 and 40 of the General Academic Regulations for Bachelor's and Master's Degree Courses at the Zurich University of Applied Sciences (dated 29 Januar 2008) and subject to the provisions for disciplinary action stipulated in the University regulations (Rahmenprüfungsordnung ZHAW (RPO)).

Town/City, Date: Aalborg DK, 2020-12-23

Signature: Kaja Mona Kristensen

The original signed and dated document (no copies) must be included in the appendix of the ZHAW version of all Master's theses submitted.

Zürcher Fachhochschule

Attachment B: Technical Data Sheets

In this attachment the technical data sheets are presented.

- MTCT 50-06-8(4) ME (multiple cell tester; 4x50A/0-6V, pre.f.8)

PC-Interface	BTS-600
Technology	ME
CE conformity	ja/yes/oui
Charge Current min.	0,05 A
Charge Current max.	50,0 A
Discharge Current min.	0,05 A
Discharge Current max.	50,0 A
Charge Voltage min.	0,00 V
Charge Voltage max.	6,00 V
Discharge Voltage min.	0,00 V
Discharge Voltage max.	6,00 V
Rise Time Current 10-90%	< 10 ms
Switchover from Charge to Discharge	10 ms
Accuracy in % of full scale	± 0,1 %
Resolution (U, I)	±15 bit
Data Acquisition Rate	20 ms

- PT100 Sensor

Sensor...Pt100 (100Ω at 0 °C)

Mounting of the element.......................2 or 3 wires

Linearization...EN60751, IEC 751

Current in the sensor...........................<1 mA

Measuring range..................................from -200 to +850 °C

Range by default..................................from 0 to 100 °C

Minimum measuring range...................25 °C

Influence of connection wires.............negligible with coupled wires

Speed conversion.................................2 measurements per second

Accuracy..from -100 to + 500 °C : ±0.1 °C
±0.1% of reading
beyond : ±0.2 °C ±0.2% of reading

Sensitivity to variations of feeding voltage..0.01 °C/°C

Sensitivity to variations of voltage supply..0.005% FC / Vdc

Storage temperature............................from -40 to +80 °C

Working temperature...........................from 0 to +70 °C

- Climatic Chamber

Temperature Range

- from -12 °C up to +60 °C
- temperature variation in time: < +/-0,1 °C (to DIN 12 880: 2007-05)
- temperature uniformity in chamber at 10 °C and 37 °C: < +/- 0.3 °C (to DIN 12 880: 2007-05)

Voltage / Power Rating

- 230 V (+/- 10%), 50 Hz
- ca. 700 W (during heating)

Packing Data

- net weight approx. 144 kg
- gross weight carton approx. 190 kg
- dimensions approx.:
  carton w x h x d: 108 x 153 x 82 cm
- the appliances must be transported upright

- LTO battery cell

Performance Characteristics	***Nominal Values***
Nominal Voltage	2.26 V
Nominal capacity (26 amp [2 C rate] at 25°C, CCCV charge)	13.4 Ah
Typical high rate capacity (120 amp [9.2 C rate] at 25°C, CCCV charge)	12.7 Ah
Typical energy (26 amp [2 C rate] at 25°C, CCCV charge)	29.7 Wh
Pulse power (130 Amp [10 C rate], 10 sec pulse, 50% SOC at 25°C) (Discharge/Charge)	260 W / 312 W
Pulse power (FreedomCar, 10 sec pulse, 50% SOC at 25°C) (Discharge/Charge)	644 W / 1,166 W
Energy density	146 Wh/l
Power density [1]	3,180 W/l
Specific energy	74 Wh/kg
Specific power [1]	1,611 W/kg
Internal charge impedance (10 sec DC pulse 50% SOC, at 25°C)	1.4 mΩ
Internal discharge impedance (10 sec DC pulse 50% SOC, at 25°C)	1.5 mΩ
Max continuous charge	130 A
Max continuous discharge	130 A
Pulse charge/discharge rate (10 sec pulse)	260 A max
Internal impedance (1 hertz AC, 10% SOC 25°C)	2.0 mΩ
Life Characteristics	
Cycle life at 2C charge & 2C discharge, 100% DOD, 25°C	>16,000 to 80% initial capacity
Cycle life at 2C charge & 2C discharge, 100% DOD, 55°C	> 4,000 to 80% initial capacity
Calendar life at 25°C	>25 years
Temperature Limits	
Operating and storage temperature range [2]	-40°C to +55°C cell temperature
Voltage Limits [3]	
Discharge cut off voltage at -40°C to +30°C	1.5 V
Discharge cut off voltage at +30°C to +55°C	1.8 V
Charge cut off voltage at +20°C to +55°C	2.8 V
Charge cut off voltage at -40°C to +20°C	2.9 V

Attachment C: Models according to the three scenarios

This attachment summarizes all models based on a linear regression between the ICA feature values and the capacity. The used training data is according to the three scenarios described in section 3.4.2.

Table 17 Models according to the three scenario 1.

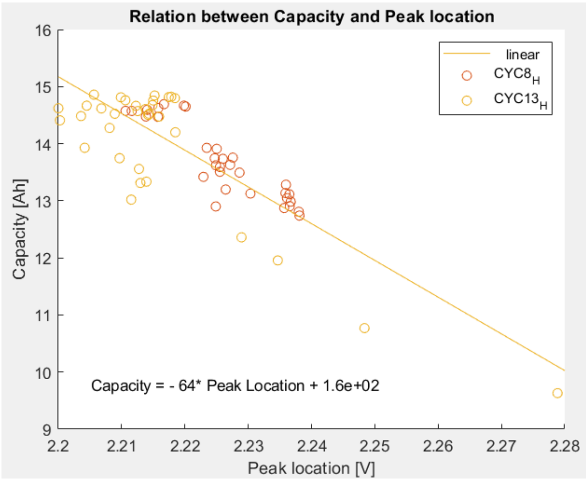

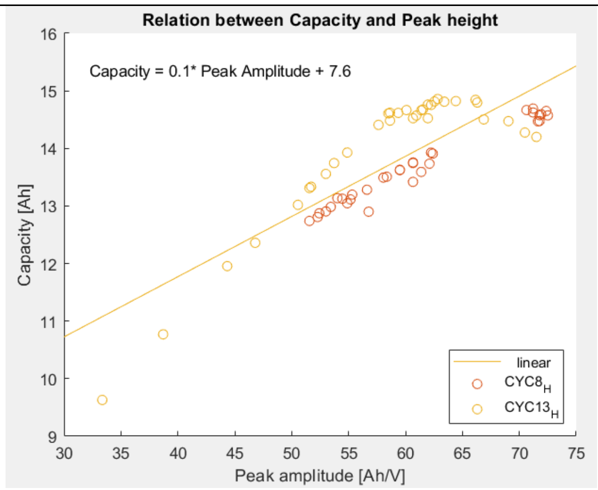

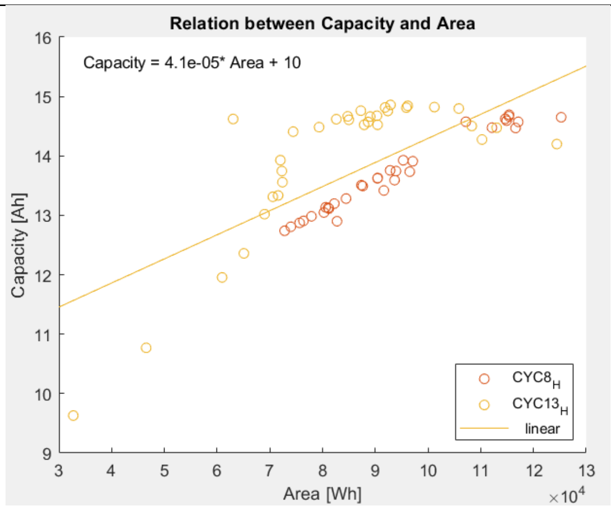

Table 18 Models according to the three scenario 2.

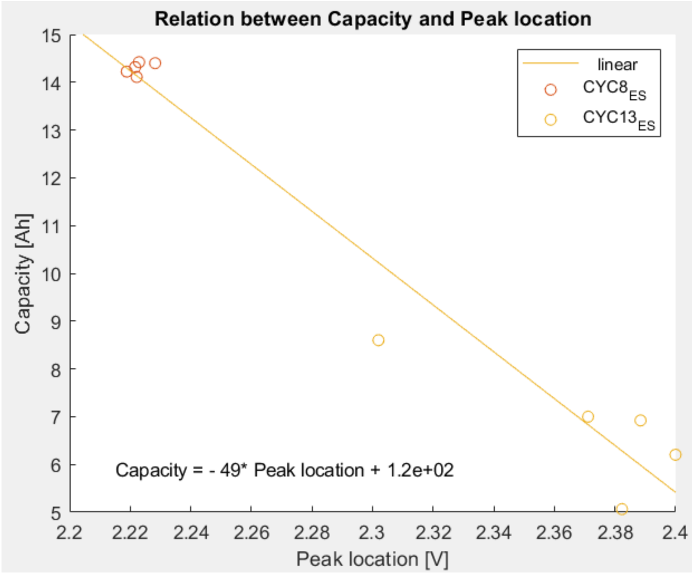

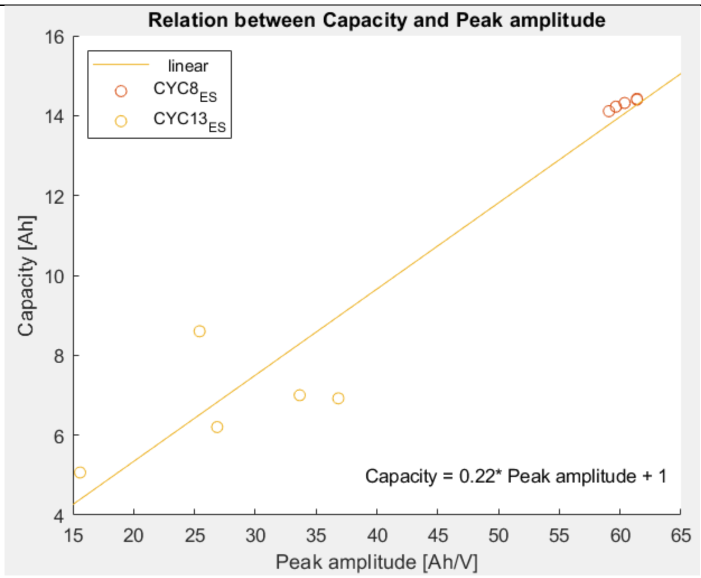

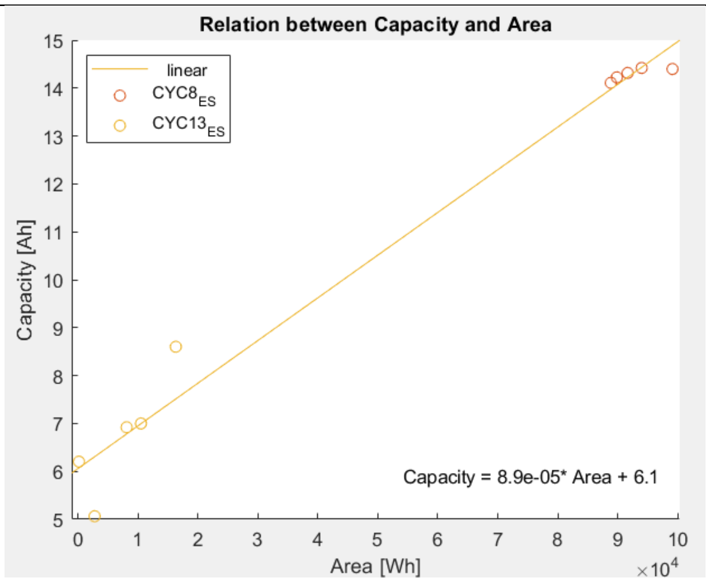

Table 19 Models according to the three scenario 3.

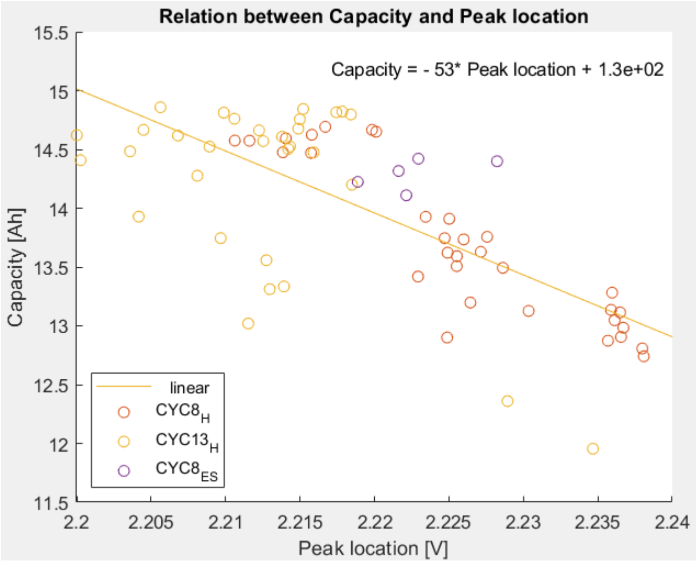

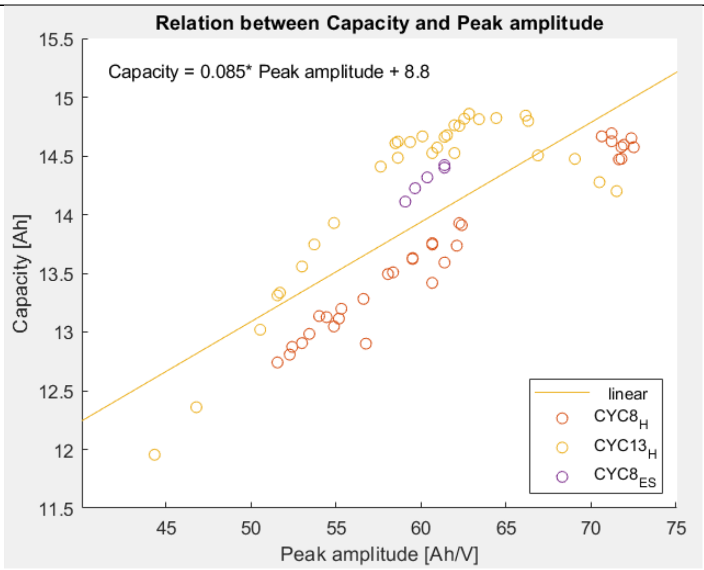

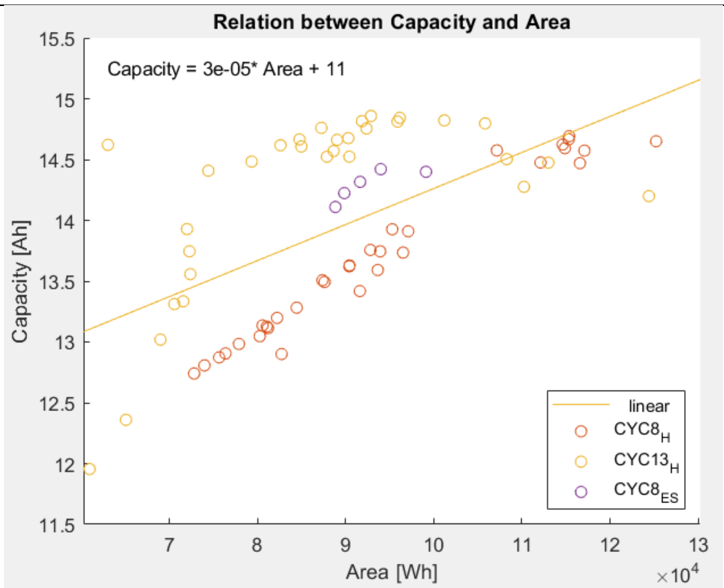

Attachment D: Model diagnostic

This attachment summarizes the model diagnostic based on the models presented in Attachment C: Models according to the three scenarios. The diagnostic procedure is explained in section 3.4.3, based on the example of Table 20.

Table 20 Model diagnostic for Scenario 1 – Peak location

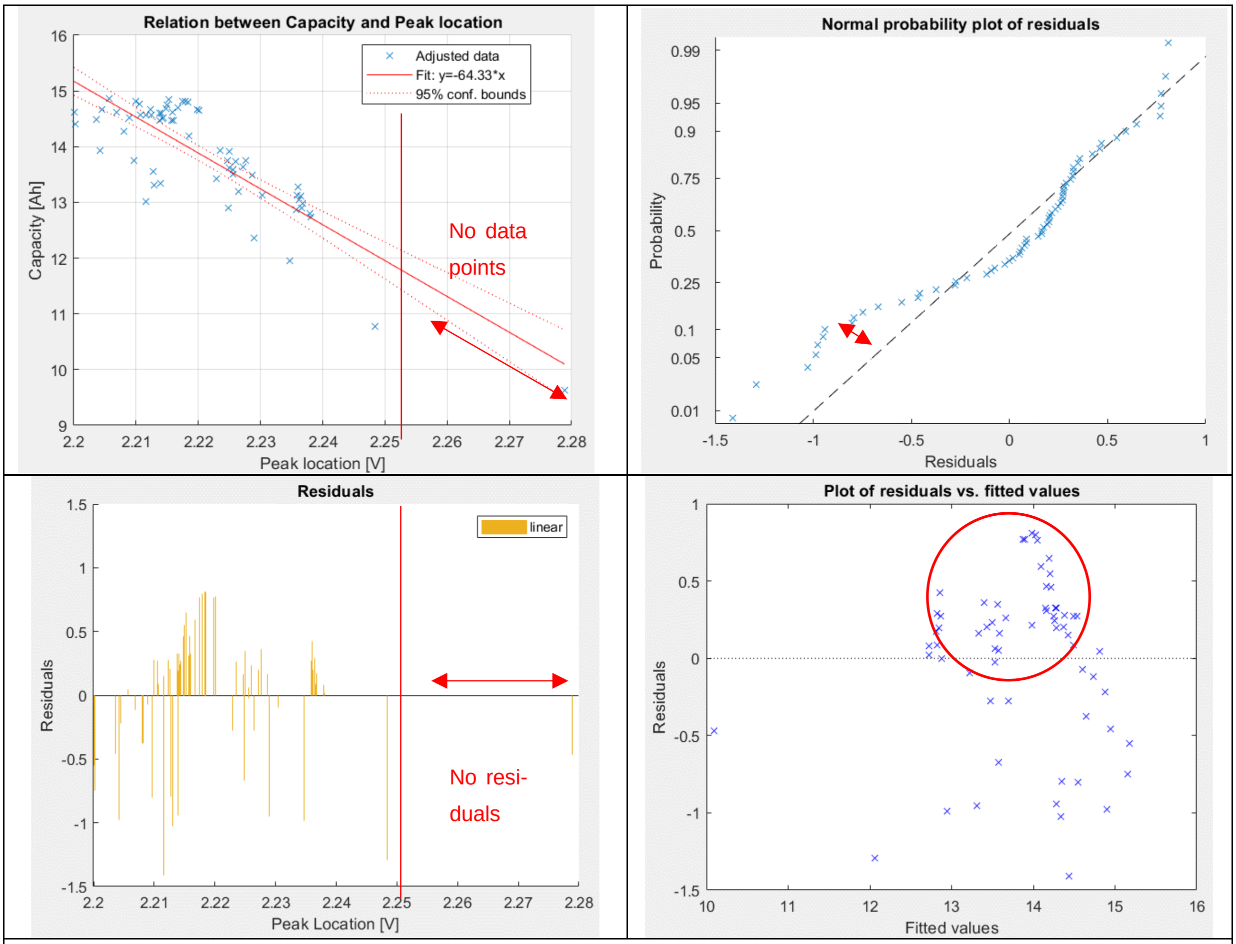

Location	Estimate	Standard error	t-value	p-value
Intercept	156.7	11.45	13.69	1.54e-20
Steepness	-64.33	5.16	-12.48	1.11e-18

Number of observations	65
Error degrees of freedom	63
Root Mean Squared Error	0.54
R-squares	**0.71**
Adjusted R-Squared	0.71
F-statistic vs. constant model	156
p-value	**1.11e-18**

Similar to the analysis in Table 20, this model is expected to have difficulties delivering accurate output at lower amplitudes, although it has more data pints than the feature “location”. Unfortunately, the number of residuals is increasing at higher amplitudes. It is expected that this is the reason for trend, which seems to be even bigger than the one from Table 20. However, the statistical data seems to be as good as for the feature “location”.

Table 21 Model diagnostic for Scenario 1 – Peak amplitude

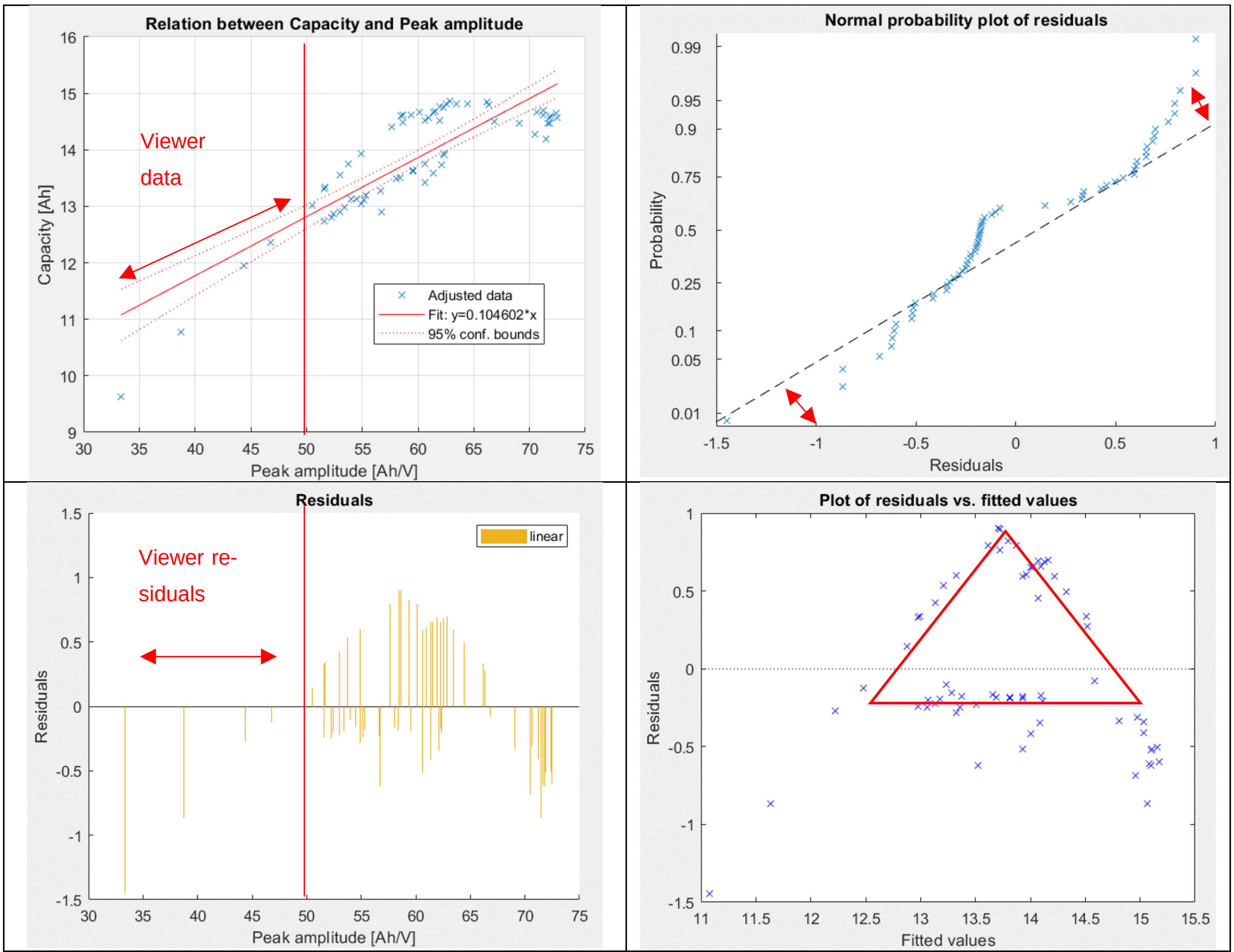

Amplitude	Estimate	Standard error	t-value	p-value
Intercept	7.59	0.49	15.17	1.03e-22
Steepness	0.10	0.008	12.62	6.67e-19

Number of observations	65
Error degrees of freedom	63
Root Mean Squared Error	0.53
R-squares	**0.72**
Adjusted R-Squared	0.71
F-statistic vs. constant model	159
p-value	**6.67e-19**

Also, here no surprises. The model has viewer data points when the area decreases. Here it is not the number of residuals which bothers, it is the discrepancy which reaches up to two. Besides the trend which the model shows, the statistical data are not promising at all.

Table 22 Model diagnostic for Scenario 1 – Area

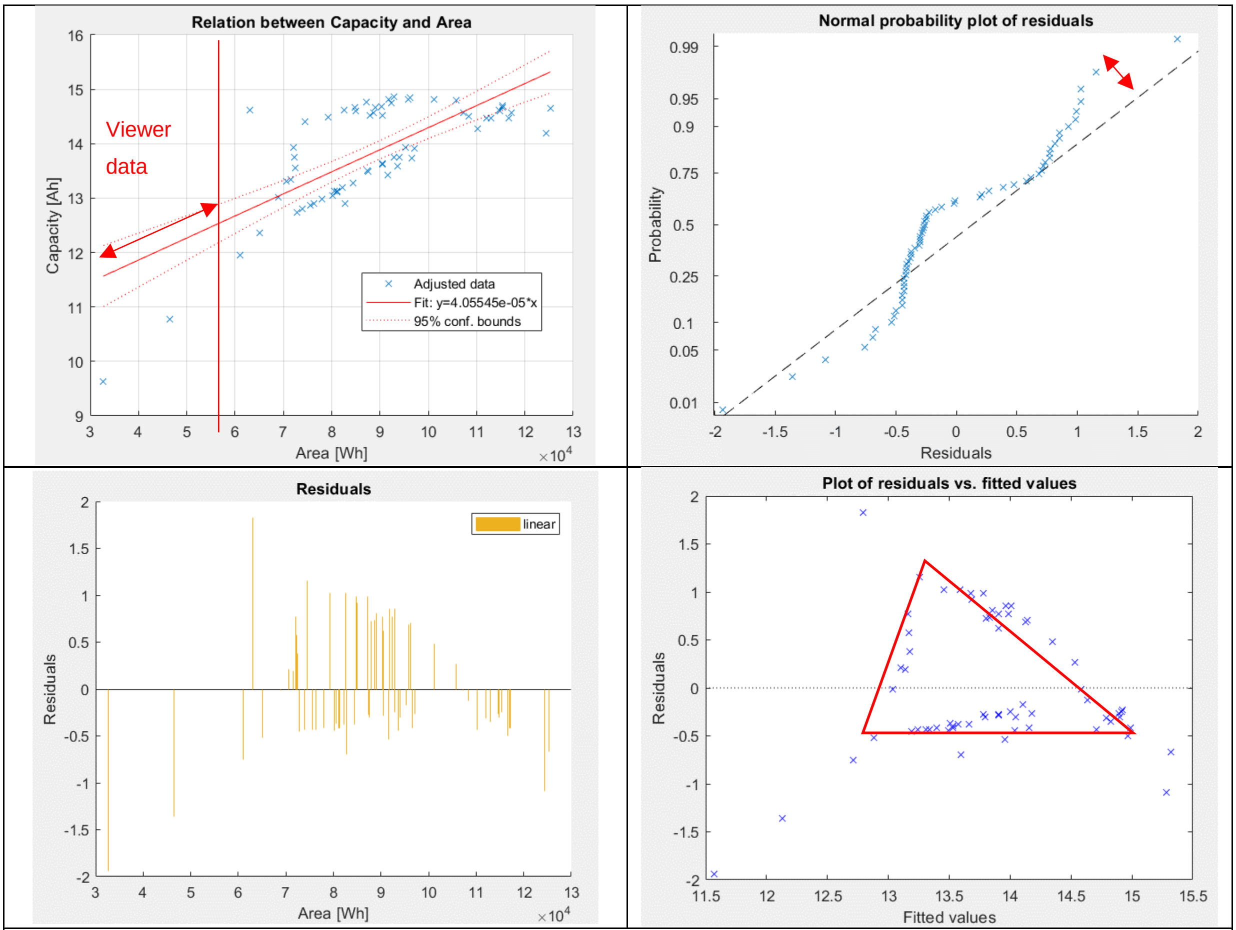

Area	Estimate	Standard error	t-value	p-value
Intercept	10.24	0.43	23.65	4.85e-33
Steepness	0.00004	4.78	8.48	5.07e-12

Number of observations	65
Error degrees of freedom	63
Root Mean Squared Error	0.68
R-squares	**0.53**
Adjusted R-Squared	0.53
F-statistic vs. constant model	72
p-value	**5.08e-12**

In scenario 2 is conspicuous that there are much less data points then for scenario 1. Nevertheless, they seem to be well distributed, so that no trend is occurring. There are only a few residuals which seem to reach the value of two. The statistical data seems to be very promising.

Table 23 Model diagnostic for Scenario 2 – Peak location

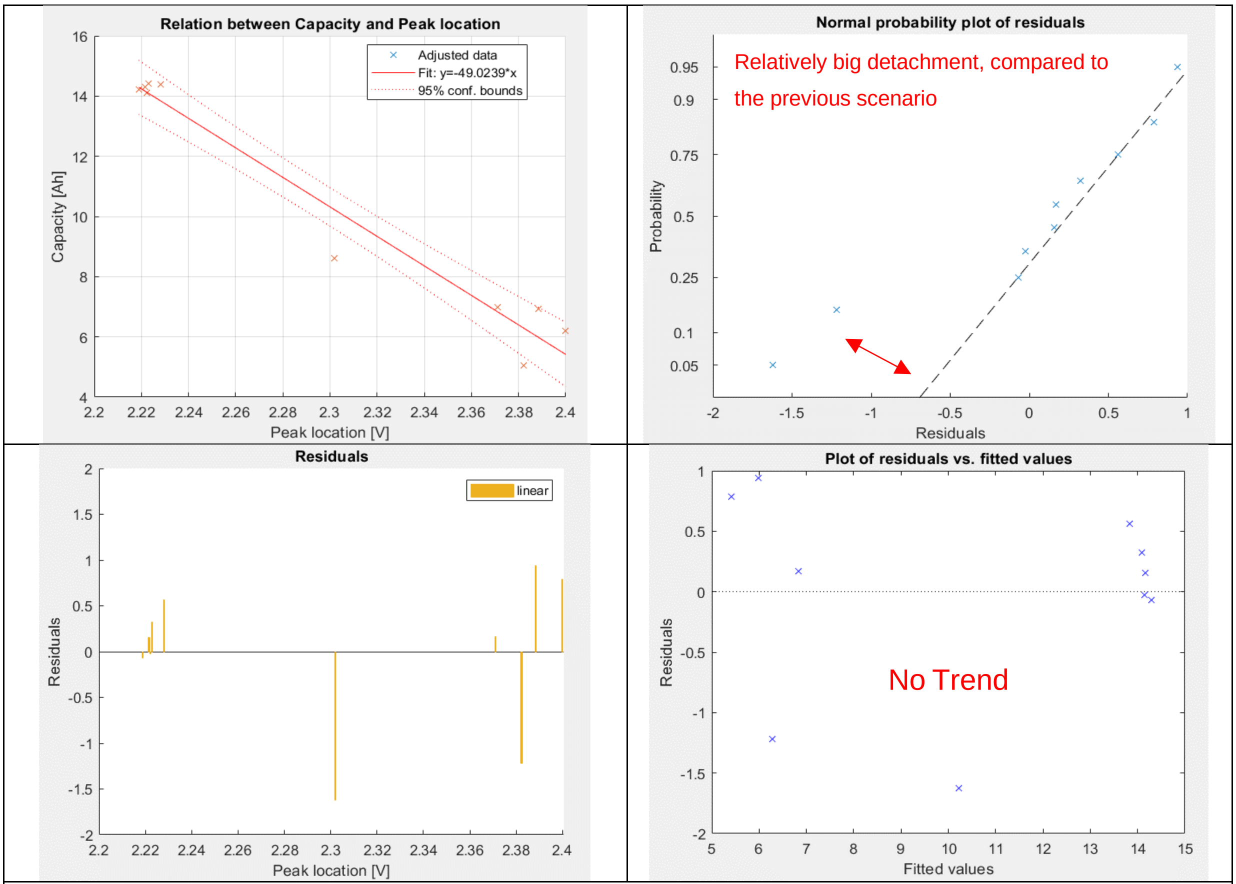

Location	Estimate	Standard error	t-value	p-value
Intercept	123.07	8.23	14.95	3.95e-07
Steepness	-49.02	3.58	-13.68	7.84e-07

Number of observations	10
Error degrees of freedom	8
Root Mean Squared Error	0.87
R-squares	**0.96**
Adjusted R-Squared	0.95
F-statistic vs. constant model	187
p-value	**7.84e-07**

Similar as in Table 23, the residuals seem to be well distributed, so that no trend is occurring. However, for this model, there seem to be residuals with a higher discrepancy, although this has not a huge impact on the statistical data, which seem to be still very promising.

Table 24 Model diagnostic for Scenario 2 – Peak amplitude

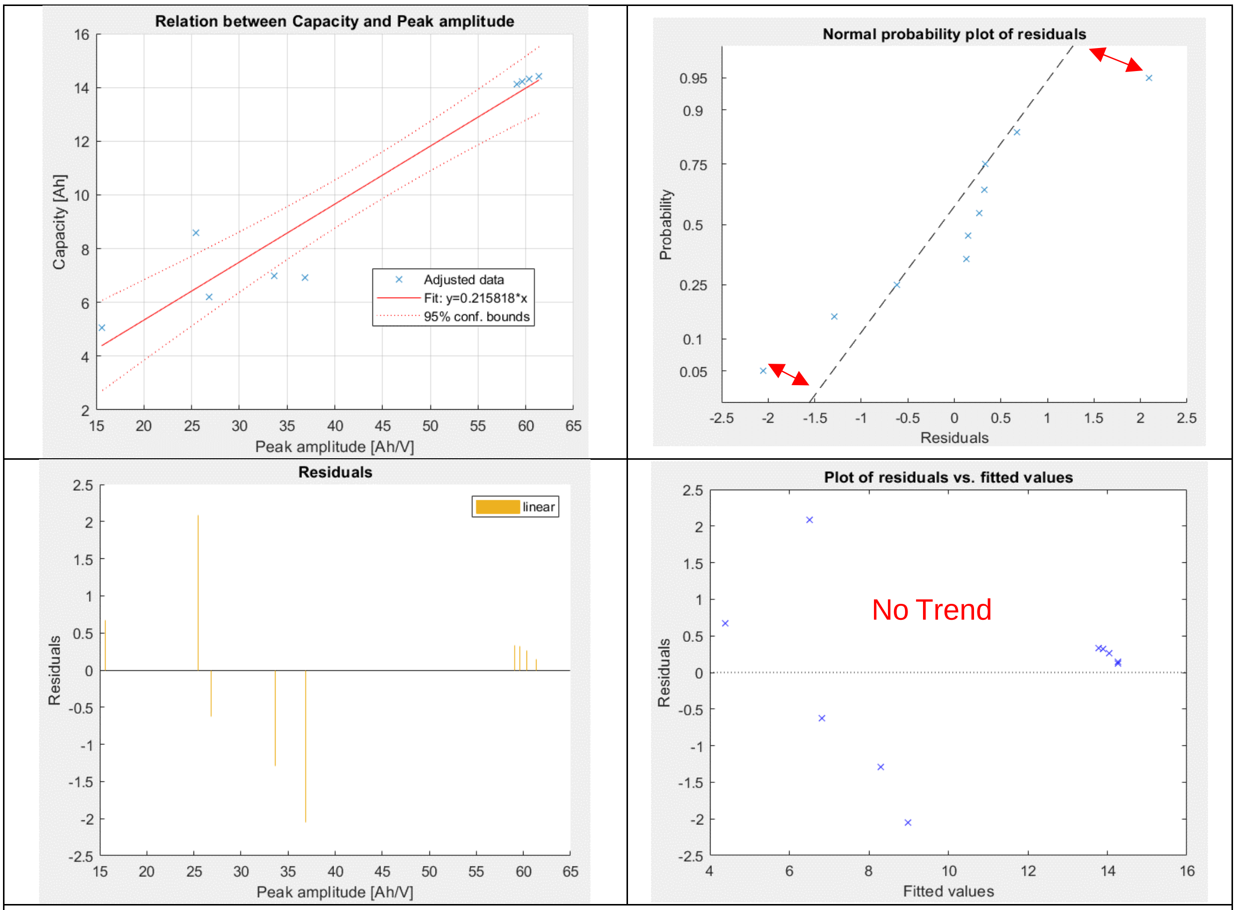

Amplitude	Estimate	Standard error	t-value	p-value
Intercept	1.03	1.04	0.99	0.35
Steepness	0.22	0.02	9.81	9.77e-06

Number of observations	10
Error degrees of freedom	8
Root Mean Squared Error	1.19
R-squares	**0.92**
Adjusted R-Squared	0.91
F-statistic vs. constant model	96.3
p-value	**9.77e-06**

This diagnostic does not differ much from the other two in scenario 2.

Table 25 Model diagnostic for Scenario 2 – Area

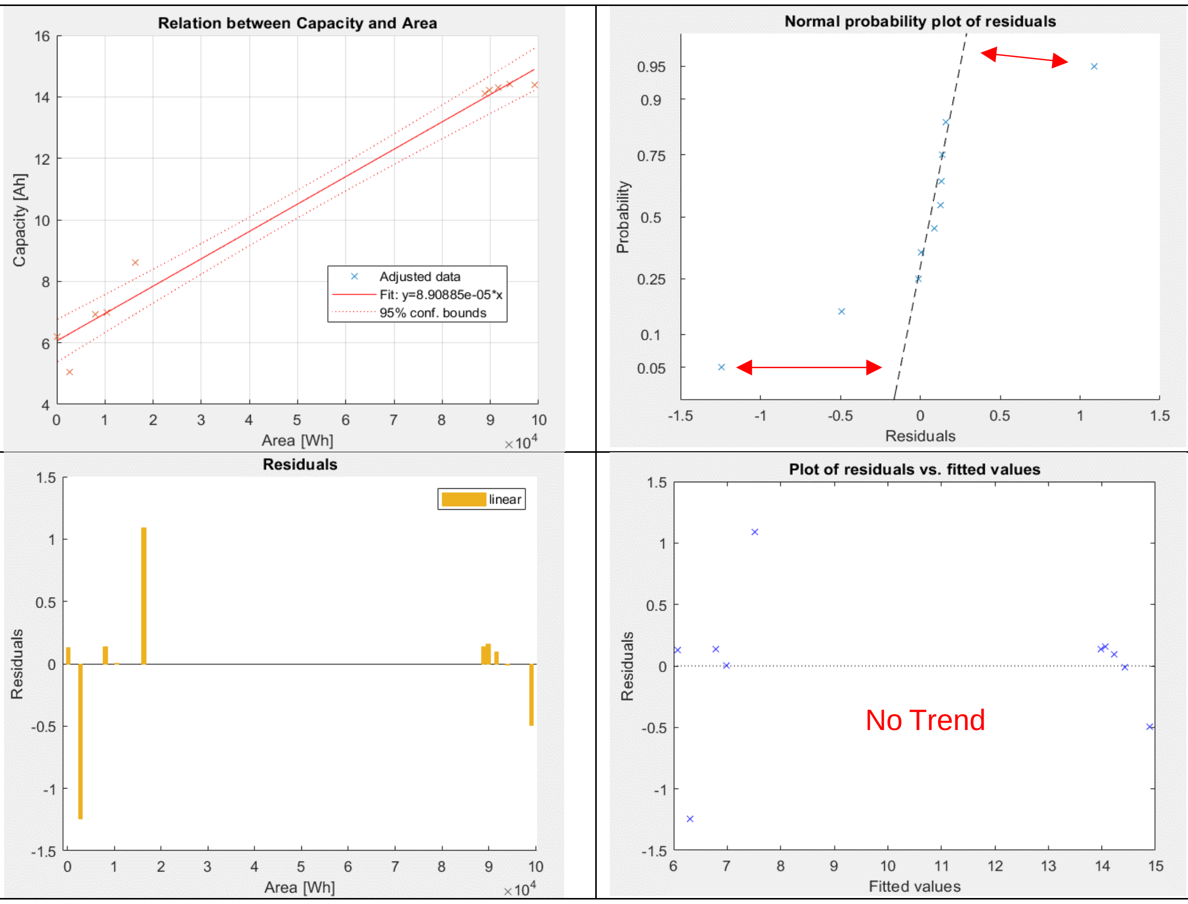

Area	Estimate	Standard error	t-value	p-value
Intercept	6.06	0.3	20.14	3.86e-08
Steepness	8.91e-05	4.56e-06	19.52	4.94e-08

Number of observations	10
Error degrees of freedom	8
Root Mean Squared Error	0.62
R-squares	**0.98**
Adjusted R-Squared	0.98
F-statistic vs. constant model	381
p-value	**4.94e-08**

At first sight, these diagnostic plots seem to be very promising. However, the statistical data does not support this first impression. The residuals seem to be well distributed, although according to the statistical data, a linear trend cannot be proven with this data set.

Table 26 Model diagnostic for Scenario 3 – Peak location

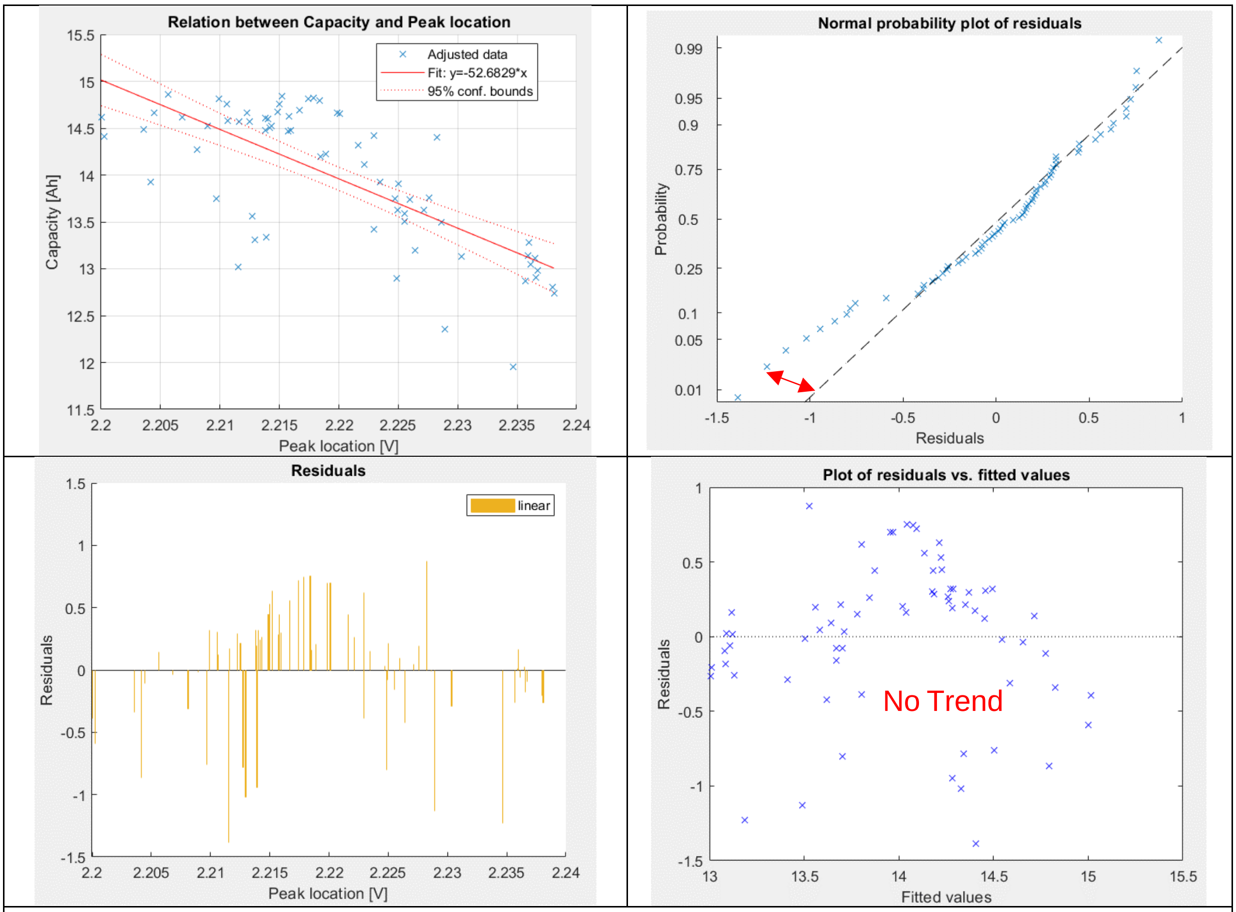

Location	Estimate	Standard error	t-value	p-value
Intercept	130.92	13.83	9.47	6.49e-14
Steepness	-52.68	6.23	-8.46	4.05e-12

Number of observations	68
Error degrees of freedom	66
Root Mean Squared Error	0.51
R-squares	**0.52**
Adjusted R-Squared	0.51
F-statistic vs. constant model	71.5
p-value	**4.05e-12**

The plots show a similar trend as in Table 26, although here the linearity is a but more significant.

Table 27 Model diagnostic for Scenario 3 – Peak amplitude

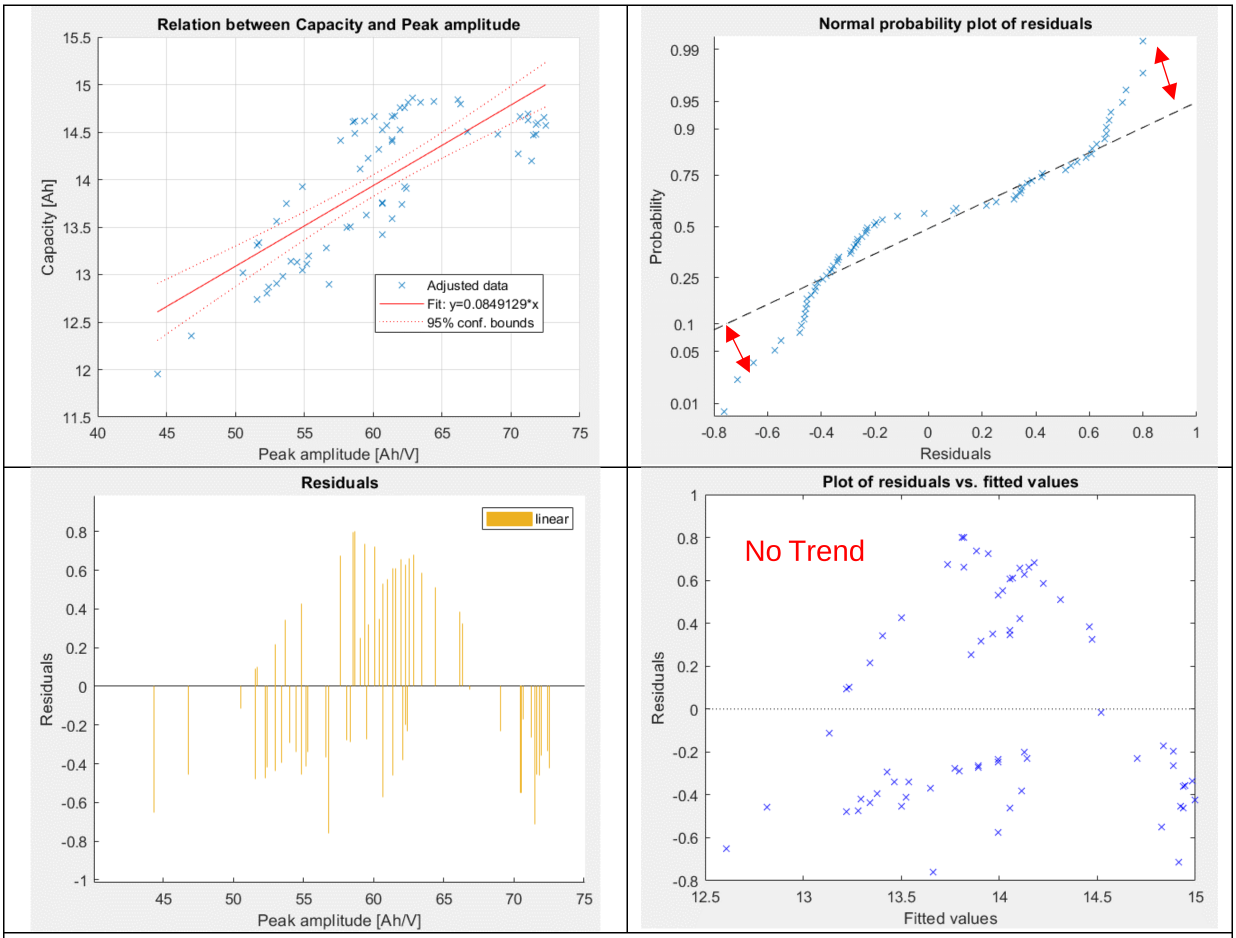

Amplitude	Estimate	Standard error	t-value	p-value
Intercept	8.84	0.52	16.91	1.10e-25
Steepness	0.08	0.0086	9.89	1.18e-14

Number of observations	68
Error degrees of freedom	66
Root Mean Squared Error	0.47
R-squares	**0.59**
Adjusted R-Squared	0.59
F-statistic vs. constant model	97.8
p-value	**1.17e-14**

This model diagnostic shows whether good plots, nor good statistical data.

Table 28 Model diagnostic for Scenario 3 – Area

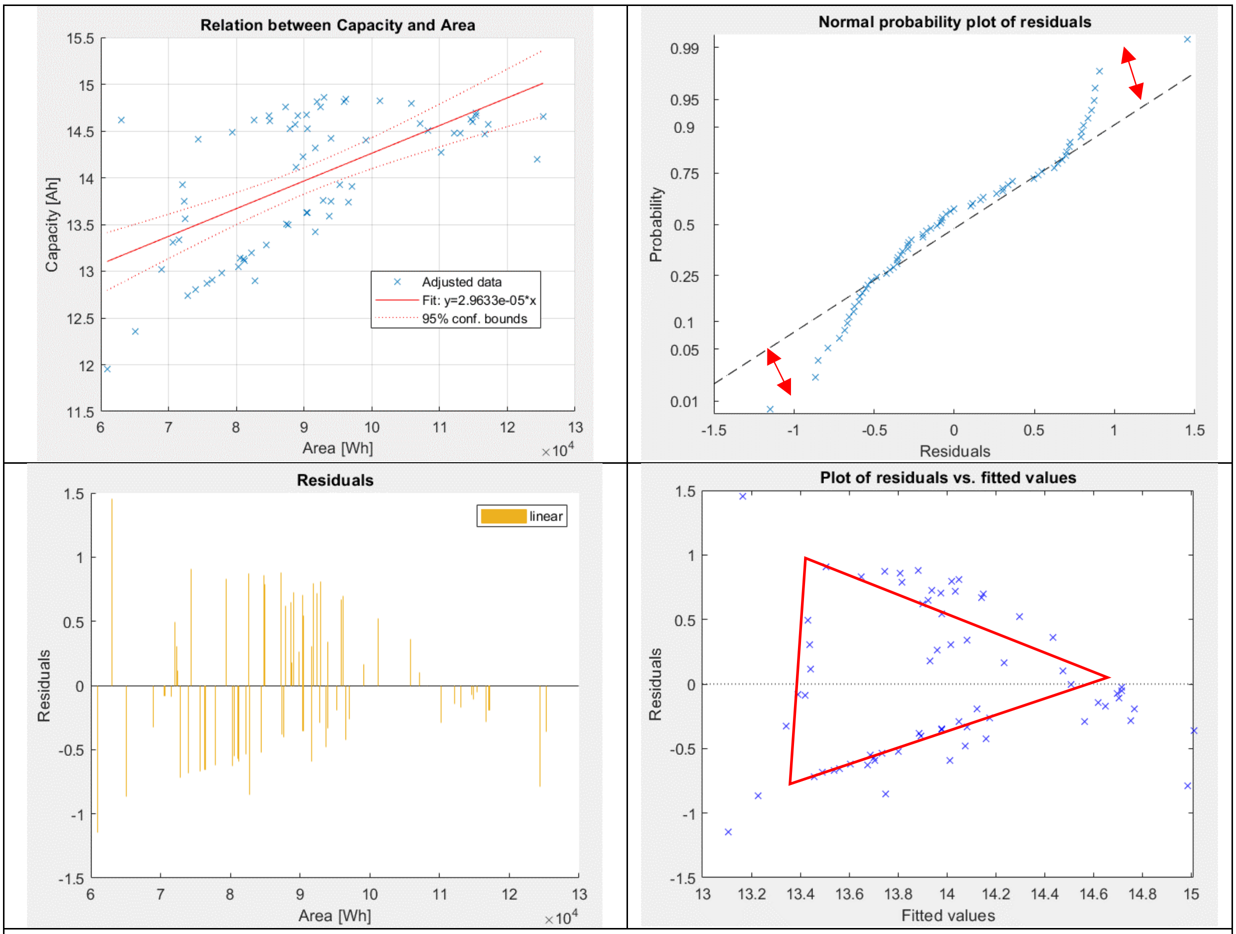

Area	Estimate	Standard error	t-value	p-value
Intercept	11.29	0.43	26.43	7.99e-37
Steepness	2.96e-05	4.66e-06	6.36	2.16e-08

Number of observations	68
Error degrees of freedom	66
Root Mean Squared Error	0.58
R-squares	**0.38**
Adjusted R-Squared	0.37
F-statistic vs. constant model	40.5
p-value	**21.16e-08**

Attachment E: Model validation

This attachment summarizes the interims results and also the average value of the model validation, ordered by the three scenarios. The validation is described in chapter 3.5. The average values of the most promising models, based on the diagnostic, are presented in section 4.2.2.

Validation with cell CYC8_ES in scenario 1

Table 29 Model output and estimation error of the feature "location".

RPT	Location (V)	Estimated capacity	Calculated capacity	Estimation error
BoL	2.23	13.36	14.4	7%
Eo1stL	2.22	13.69	14.42	5%
Eo2ndL	2.22	13.78	14.32	3%
Eo3dL	2.22	13.96	14.22	2%
Eo4thL	2.22	13.75	14.11	3%
Average				4%

Table 30 Model output and estimation error of the feature "peak".

RPT	Peak (Ah/V)	Estimated capacity	Calculated capacity	Estimation error
BoL	61.38	13.73	14.4	5%
Eo1stL	61.38	13.72	14.42	5%
Eo2ndL	60.37	13.63	14.32	5%
Eo3dL	59.65	13.55	14.22	5%
Eo4thL	59.08	13.49	14.11	4%
Average				5%

Table 31 Model output and estimation error of the feature "area".

RPT	Area (Ah)	Estimated capacity	Calculated capacity	Estimation error
BoL	99128	14.21	14.4	1%
Eo1stL	93999	14	14.42	3%
Eo2ndL	91650	13.91	14.32	3%
Eo3dL	89856	13.83	14.22	3%
Eo4thL	88845	13.79	14.11	2%
Average				2%

Validation with cell CYC13_ES in scenario 1

Table 32 Model output and estimation error of the feature "location".

RPT	Location (V)	Estimated capacity	Calculated capacity	Estimation error
BoL	2.3	8.62	8.6	0%
Eo1stL	2.38	3.45	5.06	32%
Eo2ndL	2.37	4.17	6.99	40%
Eo3dL	2.38	3.05	6.92	56%
Eo4thL	2.39	2.31	6.2	62%
Average				38%

Table 33 Model output and estimation error of the feature "peak".

RPT	Peak (Ah/V)	Estimated capacity	Calculated capacity	Estimation error
BoL	25.42	10.13	8.6	18%
Eo1stL	15.6	9.15	5.06	81%
Eo2ndL	33.65	10.95	6.99	56%
Eo3dL	36.83	11.27	6.92	63%
Eo4thL	26.87	10.27	6.2	66%
Average				57%

Table 34 Model output and estimation error of the feature "area".

RPT	Area (Ah)	Estimated capacity	Calculated capacity	Estimation error
BoL	16295	10.89	8.6	27%
Eo1stL	2759	10.35	5.06	104%
Eo2ndL	10484	10.66	6.99	52%
Eo3dL	8095	10.56	6.92	53%
Eo4thL	145.9	10.25	6.2	65%
Average				60%

Validation with cell CYC8_H in scenario 2

Table 35 Model output and estimation error of the feature "location".

RPT	Location (V)	Estimated capacity	Calculated capacity	Estimation error
6	2.23	13.95	13.73	2%
10	2.22	14.01	13.75	2%
13	2.23	13.87	13.76	1%
15	2.24	13.46	13.28	1%
17	2.23	13.93	13.20	6%
22	2.21	14.54	14.59	0%
25	2.22	14.01	12.90	9%
Average				3%

Table 36 Model output and estimation error of the feature "peak".

RPT	Peak (Ah/V)	Estimated capacity	Calculated capacity	Estimation error
6	62.11	14.69	13.73	7%
10	60.66	14.38	13.75	5%
13	60.66	14.38	13.76	5%
15	56.62	13.50	13.28	2%
17	55.32	13.19	13.20	0%
22	71.92	16.85	14.59	15%
25	56.76	13.52	12.90	5%
Average				5%

Table 37 Model output and estimation error of the feature "area".

RPT	Area (Ah)	Estimated capacity	Calculated capacity	Estimation error
6	96530	14.66	13.73	7%
10	93928	14.43	13.75	5%
13	92816	14.33	13.76	4%
15	84454	13.58	13.28	2%
17	82228	13.39	13.20	1%
22	114889	16.29	14.59	12%
25	82738	13.43	12.90	4%
Average				5%

Validation with cell CYC13_H in scenario 2

Table 38 Model output and estimation error of the feature "location".

RPT	Location (V)	Estimated capacity	Calculated capacity	Estimation error
1	2.22	14.32	14.20	1%
2	2.21	14.95	14.86	1%
3	2.21	14.83	14.28	4%
5	2.22	14.45	14.47	0%
7	2.22	14.32	14.80	3%
16	2.22	14.35	14.82	3%
31	2.23	13.53	11.95	13%
Average				4%

Table 39 Model output and estimation error of the feature "peak".

RPT	Peak (Ah/V)	Estimated capacity	Calculated capacity	Estimation error
1	71.50	16.76	14.20	18%
2	62.83	14.85	14.86	0%
3	70.49	16.54	14.28	16%
5	69.04	16.22	14.47	12%
7	66.30	15.62	14.80	6%
16	64.42	15.20	14.82	3%
31	44.34	10.79	11.95	9%
Average				9%

Table 40 Model output and estimation error of the feature "area".

RPT	Area (Ah)	Estimated capacity	Calculated capacity	Estimation error
1	124425	17.15	14.20	0.21
2	92888	14.34	14.86	0.04
3	110238	15.88	14.28	0.11
5	113017	16.13	14.47	0.11
7	105833	15.49	14.80	0.05
16	101210	15.08	14.82	0.02
31	60947	11.49	11.95	0.04
Average				8%

Validation with data > 80 % SoH in scenario 3

Table 41 Model output and estimation error of the feature "location".

RPT	Location (V)	Estimated capacity	Calculated capacity	Estimation error
BoL_ES	2.30	9.65	8.60	12%
Eo1stL_ES	2.38	5.42	5.06	7%
Eo2ndL_ES	2.37	6.01	6.99	14%
Eo3dL_ES	2.39	5.09	6.92	26%
Eo4thL_ES	2.39	4.48	6.20	27%
32_CYC13	2.24	12.92	11.42	13%
33_CYC13	2.26	11.71	10.43	12%
Average				16%

Table 42 Model output and estimation error of the feature "peak".

RPT	Peak (Ah/V)	Estimated capacity	Calculated capacity	Estimation error
BoL_ES	25.40	10.87	8.60	26%
Eo1stL_ES	15.60	10.08	5.06	99%
Eo2ndL_ES	33.66	11.53	6.99	65%
Eo3dL_ES	36.83	11.78	6.92	70%
Eo4thL_ES	26.86	10.99	6.20	77%
32_CYC13	41.89	12.19	11.42	7%
33_CYC13	38.27	11.90	10.43	14%
Average				51%

Table 43 Model output and estimation error of the feature "area".

RPT	Area (Ah)	Estimated capacity	Calculated capacity	Estimation error
BoL_ES	16295	11.77	8.60	37%
Eo1stL_ES	2760	11.37	5.06	125%
Eo2ndL_ES	10484	11.60	6.99	66%
Eo3dL_ES	8095	11.53	6.92	67%
Eo4thL_ES	146	11.29	6.20	82%
32_CYC13	53780	12.88	11.42	13%
33_CYC13	43129	12.56	10.43	20%
Average				59%

Attachment F: Overview historical data

Table 44 Historical data of the two cells CYC8 and CYC13. The green marking indicates the randomly chosen validation values.

Number	CYC8	CYC13
1	RPT0_odd_ANCyc8_TS002142	RPT0_odd_ANCyc13_TS002273
2	RPT1_even_ANCyc8_TS002355	RPT1_even_ANCyc13_TS002394
3	RPT2_odd_ANCyc8_TS002514	RPT2_odd_ANCyc13_TS002546
4	RPT3_even_ANCyc8_TS002582	RPT3_even_ANCyc13_TS002653
5	RPT4_odd_ANCyc8_TS002725	RPT4_odd_ANCyc13_TS002770
6	RPT5_even_ANCyc8_TS002827	RPT5_even_ANCyc13_TS002888
7	RPT6_odd_ANCyc8_TS002950	RPT6_odd_ANCyc13_TS003087
8	RPT7_even_ANCyc8_TS003063	RPT11_even_ANCyc13
9	RPT8_odd_ANCyc8_TS003278	RPT13_even_ANCyc13
10	RPT9_even_ANCyc8_TS003352	RPT15_even_ANCyc13
11	RPT10_odd_ANCyc8_TS003428	RPT16_odd_ANCyc13
12	RPT11_even_ANCyc8_TS003547	RPT18_even_ANCyc13
13	RPT12_odd_ANCyc8	RPT20_odd_ANCyc13
14	RPT13_even_ANCyc8	RPT22_even_ANCyc13
15	RPT14_odd_ANCyc8	RPT24_odd_ANCyc13
16	RPT15_even_ANCyc8	RPT26_even_ANCyc13
17	RPT16_odd_ANCyc8	RPT28_odd_ANCyc13
18	RPT17_even_ANCyc8	RPT32_odd_ANCyc13
19	RPT18_odd_ANCyc8	RPT42_even_ANCyc13
20	RPT19_even_ANCyc8	RPT46_even_ANCyc13
21	RPT20_odd_ANCyc8	RPT48_odd_ANCyc13
22	RPT22_even_ANCyc8	RPT50_even_ANCyc13
23	RPT24_odd_ANCyc8	RPT52_odd_ANCyc13
24	RPT26_even_ANCyc8	RPT56_odd_ANCyc13
25	RPT28_odd_ANCyc8	RPT58_even_ANCyc13
26	RPT30_even_ANCyc8	RPT60_odd_ANCyc13
27	RPT32_odd_ANCyc8	RPT62_even_ANCyc13
28	RPT34_even_ANCyc8	RPT64_odd_ANCyc13
29	RPT36_odd_ANCyc8	RPT66_even_ANCyc13
30	RPT38_even_ANCyc8	RPT70_odd_ANCyc13
31	RPT40_odd_ANCyc8	RPT72_even_ANCyc13
32	RPT42_even_ANCyc8	RPT76_even_ANCyc13
33		RPT78_odd_ANCyc13

Attachment G: Poster

Incremental Capacity Analysis (ICA) as a diagnostic tool for the State of Health (SoH) estimation of 2nd Life Batteries

Master Thesis of Kaja Mona Kristensen
Master in Environment and Natural Resources 2018
Field of Study: Renewable Energies

The results of the study have shown that an application of the ICA method on aged batteries is possible. Accurate results could be obtained with a deviation less than 5 %. In particular, the feature "peak location" (see green arrow in Figure 3) gave a promising result. Nonetheless, only a partial charging curve (from 2.2 to 2.4 V) was applied, as indicated in Figure 2 and 3.

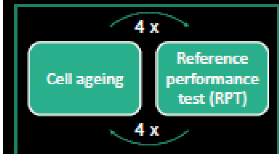

Figure 1 Experimental study - the procedure was repeated four times.

Experimental Study: In order to answer the research questions, the proposed ICA method was tested with two previously aged battery cells. In the beginning, a reference performance test (RPT) was performed to define the (remaining) capacity of the battery cells. This procedure includes the complete discharge and charge of the battery, which allows to determine the capacity of the cell by the Coulomb counting method. The RPT procedure was conducted with the constant current (CC) and constant voltage (CV) procedure. After the RPT, the battery was aged with a predefined load cycle. The whole procedure is repeated four times, as indicated in Figure 1. The cells were tested at 25°C but aged at 50°C, in order to age them faster.

The ICA method: Figure 2 visualizes the procedure of creating the ICA curve. The constant charging current a) and the charging voltage b) are used to create an ICA curve. The charging current curve is integrated by the time. This leads to the capacity curve presented in c). The capacity curve c) is then plotted against the voltage curve b), which results in the curve d). Thereafter, this curve is derived by the voltage, which then represents the characteristic ICA curve, as presented in e). As soon as the ICA curve is created, the three feature values "location", "amplitude" and "area" are extracted on a partial voltage interval (from 2.2 to 2.4 V), as visualized in Figure 3. This procedure is repeated for all RPTs (5 times). Each feature value is set in reference to the remaining capacity with a linear regression analysis, which is presented in Figure 4. This resulted in a linear model, which was validated with the historical data of the used cells. In order to compare the models, the estimation error was calculated.

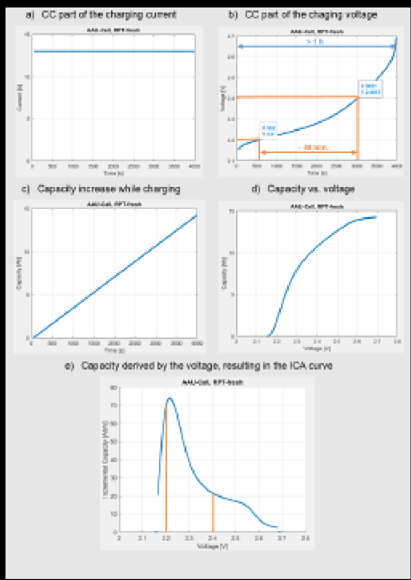

Figure 2 Demonstrative incremental capacity analysis (ICA) procedure with an LTO/LNMC cell, where a) shows the CC charging current, b) the CC charging voltage, c) the capacity increase, d) the capacity vs. voltage and e) the capacity derived by the voltage, resulting in the ICA curve. The orange lines indicate the voltage level in the range between 2.2 and 2.4 V. The blue arrow indicates the time to measure the whole charging curve in order to create the ICA curve. The blue arrow indicates the time needed for a partial charging.

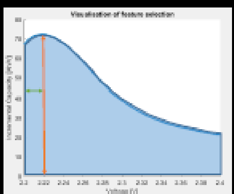

Figure 3 A partial ICA curve on an example of an LTO/LNMC cell, where the voltage interval between 2.2 and 2.4 V is chosen. The area [Ah] is indicated in blue; the peak amplitude [Ah/V] is indicated with the orange arrow and the peak location [V] is indicated with the green arrow.

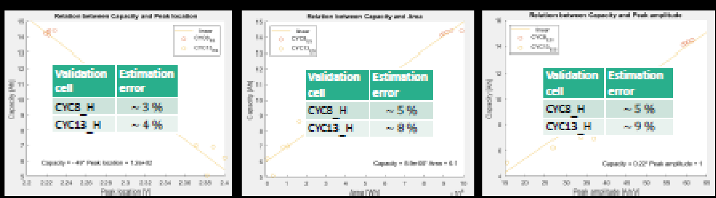

Figure 4 Three models based on the different feature values "location", "amplitude" and "area". For this battery chemistry 80% remaining capacity lies at 10.7 Ah. The feature "location" achieved an an average estimation error of ~3% for values above 80% remaining capacity and an average estimation error of ~4% for values below 80% remaining capacity. The feature "area" achieved ~5% for above 80% and an ~8% for below. The feature "amplitude" achieved ~5% and ~9% respectively.